ISTANBUL TECHNICAL UNIVERSITY ★ INSTITUTE OF SCIENCE AND TECHNOLOGY

APPLICATION OF DIFFERENT OPTIMIZATION TECHNIQUES TO PARAMETER ESTIMATION FROM INTERFERENCE WELL TEST DATA

M.Sc. Thesis by
Ahmet Ergün MENGEN, B.S.
505001553

Date of submission : 22 December 2003

Date of defence examination : 16 January 2004

Supervisor (Chairman) : Prof. Dr. Mustafa ONUR

Members of the Examining Committee : Prof.Dr. Abdurrahman SATMAN (ITU.)

Doç.Dr. Argun KOCAOĞLU (ITU.)

JANUARY 2004

İSTANBUL TEKNİK ÜNİVERSİTESİ ★ FEN BİLİMLERİ ENSTİTÜSÜ

GİRİŞİMLİ KUYU BASINÇ TESTİ VERİLERİNDEN FARKLI OPTİMİZASYON TEKNİKLERİNİN KULLANILMASIYLA PARAMETRE TAHMİNİ

YÜKSEK LİSANS TEZİ

Müh. Ahmet Ergün MENGEN

(505001553)

Tezin Enstitüye Verildiği Tarih : 22 Aralık 2003
Tezin Savunulduğu Tarih : 16 Ocak 2004

Tez Danışmanı : Prof.Dr. Mustafa ONUR
Diğer Jüri Üyeleri Prof.Dr. Abdurrahman SATMAN (İ.T.Ü.)
Doç.Dr. Argun KOCAOĞLU (İ.T.Ü.)

OCAK 2004

PREFACE

As known, interference well test data can be analyzed by using non-linear regression techniques. However, in literature there are not a lot of studies on comparisons of performances of different optimization techniques used to analyze interference well test data. The main purpose of this study is to construct the interference well test data numerically and to analyze them to obtain parameters of multi-layered reservoir and wellbore by using optimization techniques.

I would especially like to thank my research advisor Professor Mustafa ONUR who encouraged me to enter to the master program of ITU, for his constant support, suggestions, advice and encouragement to the completion of this work. It's the fact that this research study couldn't be completed without his contribution. Furthermore, I would like to thank Professor Abdurrahman SATMAN and Assoc. Professor Argun KOCAOĞLU who were members of the examining committee, because they evaluated and corrected my thesis. I would also like to thank my colleague and friend Mr. İhsan Murat GÖK for his suggestions and assistance especially implementation of LMDER1 source code to our problem on this research.

I would gratefully like to acknowledge the Department of Petroleum and Natural Gas Engineering and Istanbul Technical University for financial support. Most importantly, I wish to express my appreciation to my parents, brothers and sisters for their moral support, love, trust and encouragement throughout all my life.

16 January 2004 Ahmet Ergün Mengen

TABLE OF CONTENTS

LIST OF TABLES

LIST OF FIGURES

NOMENCLATURE

Symbol

C	:	wellbore storage constant, *RB / psi*
C_a	:	wellbore storage constant at the active well, *RB / psi*
C_o	:	wellbore storage constant at the observation well, *RB / psi*
c_i	:	step varying criterion for simulated annealing algorithm
c	:	centroid of the best n vertices $x_1, x_2, ..., x_n$ for polytope algorithm
c_r	:	porosity-thickness-compressibility ratio, defined by Eq. 2.8
c_t	:	system total compressibility, psi^{-1}
d_k	:	Gauss-Newton Direction, if λ_k is zero
E_1	:	exponential integral, defined by Eqs. 2.13 and 2.14
f_r	:	flow capacity ratio, defined by Eq 2.6
$f(x)$	:	function to be minimized by simulated annealing
$F(x)$	:	function to be minimized by polytope and/or Levenberg-Marquardt algorithms
h	:	total reservoir thickness, ft
h_j	:	layer j thickness, ft
$H(\vec{\beta}^{\infty})$	:	the sensitivity coefficient matrix
$J(\vec{\beta})$	:	objective function to be minimized defined by Eq.4.1
J_k	:	rank-deficient related Levenberg-Marquardt algorithm defined by 3.3
$J(x_k)$	:	jacobian matrix of $F(x_k)$ related L-M algorithm defined by 3.1
k	:	reservoir permeability, md
$\bar{k}$	:	thickness averaged permeability, md
N_d	:	number of observed pressure and sandface flow rate data
N_p	:	number of unknown parameters
N_S	:	step variation for simulated annealing algorithm
N_ε	:	number of successive temperature reductions to test for termination
$O(n^2)$	:	function evaluations required at each iteration defined by Eq. 3.3
p	:	pressure, psi
p_{oD}	:	dimensionless pressure drop at the observation well
p_{of}	:	bottomhole pressure at the observation well, psi
p_{wD}	:	dimensionless pressure drop at the active well
p_{wf}	:	bottomhole pressure at the active well, psi
p_{FCN}	:	rate normalized pressure drop for constant sandface rate production,

$psi / RB / day$

q_{sa} : total surface production flow rate from the active well, RB / day

q_{so} : total surface production flow rate from the observation well, RB / day

q_{aj} : sandface rate of production from layer j at the active well, RB / day

q_{oj} : sandface rate of production from layer j at the observation well, RB / day

q_{Daj} : dimensionless sandface rate at the active well, defined by Eq. C.1

q_{Doj} : dimensionless sandface rate at the observation well, defined by Eq.C.2

$Q(x)$: second-order term defined by Eq. 3.1

r : radial distance, ft

r_D : dimensionless distance between the active well and the observation well, defined by Eq.C.3

r_T : temperature reduction coefficient

r_w : wellbore radius, ft

r_{wa} : radius of the active well, ft

r_{wo} : radius of the observation well, ft

S : skin factor

S_{ai} : skin factor of layer j at the observation well

S_{oi} : skin factor of layer j at the observation well

t : time in hours or days

t_D : dimensionless time based on thickness averaged properties, defined by Eq.C.4

T_k : cooling temperature in simulated annealing

v_m : step vector in simulated annealing

x_i : randomly generated new point by simulated annealing

x_{opt} : randomly generated optimal point by simulated annealing

x_n : randomly generated new point by polytope annealing

Greek Symbol

β : expansion coefficient for polytope algorithm

β^{∞} : the estimate obtained by minimizing $J(\vec{\beta})$

β_i^{∞} : the estimate of i^{th} model parameter at the minimum

$\hat{\beta}_i$: the true, but unknown value of the model parameter

α : the reflection coefficient for polytope

γ : contraction coefficient for polytope algorithm

Δ : difference

λ_k : non-negative scalar related to Levenberg-Marquardt algorithm

Δ' : scalar related to λ_k defined by Eq. 3.2

ε	:	termination criteria
p_k	:	Gauss-Newton direction
$p_{LM}(\lambda_k)$	:	the solution of Eq. 3.1
$\bar{\phi}\,\bar{c}_t$	:	thickness averaged porosity compressibility product, psi^{-1}
ϕ_j	:	layer j porosity
η	:	diffusivity, $md - psi/cp$, $k/\phi c_t \mu$
$\bar{\eta}$	:	average diffusivity, $md - psi/cp$,defined by Eq. 2.3
η_j	:	diffusivity of layer j, $md - psi/cp$, defined by Eq. 2.5
η_r	:	diffusivity ratio, defined by Eq. 2.7
μ	:	viscosity, cp

Subscripts

a	:	active well
o	:	observation well
j	:	layer j
1	:	layer 1
2	:	layer 2
k	:	time index
D	:	dimensionless

Superscripts

A	:	analytical solution
N	:	numerical solution
$'$	:	derivative
-	:	average
T	:	transpose

TABLE OF SI AND METRIC CONVERSION FACTORS[1]

Field Units	Product Coefficients	SI Units
bbl (STB, RB)	× 1.589873 E-01	m^3
cp	× 1.0 E-03	Pa.s
ft	× 3.048 E-01	m
inch	× 2.54 E+00	cm
psi	× 6.894757 E+00	kPa
mD	× 9.869233 E-04	μm^2

APPLICATION OF DIFFERENT OPTIMIZATION TECHNIQUES TO PARAMETER ESTIMATION FROM INTERFERENCE WELL TEST DATA

SUMMARY

This study considers pressure interference testing in a two-well system in an infinite-acting, multi-layered commingled reservoir where the layers are in communication only through the wellbore. The first well is an active well which is produced at a specified surface flow rate history, and the second well is an observation well which is shut-in for all times during the test. Wellbore storage and individual layer skins in both wells are considered. The results are described in two parts. In the first part, the effects of reservoir parameters such as layer permeabilities, layer skin factors and wellbore storage effects (in both wells) on the active/ observation wellbore pressures and layer sandfaces rates were examined through forward computations carried out by a semi-analytical model developed during the course of this study. The semi-analytical model developed is based on the assumption of line-source wells and is quite general in the sense that it can be used to simulate interference tests in a reservoir sytem consisting of N layers. In the first part, different case studies about evaluation of interference tests in single and multi-layer commingled reservoirs are given to show the effects of wellbore storage/skin and cross-flow among the layers in both wells on pressure responses and sandface flow rates at both wells. The results in the first part indicate that conventional type-curve matching based on the well-known Theis curve and semilog straight-line analysis methods are not feasible to determine individual layer parameters from pressure interference tests in multi-layer commingled systems with wellbore and skin effects in both wells.

In the second part, nonlinear parameter estimation methods are used to determine layer parameters from pressure and/or sandface flow rate data obtained from two-well interference tests in single and multi-layered commingled systems. Since parameter estimation is an inverse problem, its solution needs to be found by optimization techniques. Both gradient and non-gradient based optimization algorithms are considered to identify which optimization methods can be effective and efficient in terms of uniqness and computation for the problem considered in this study. Due to its popular use, only the Levenberg-Marquardt method is considered as a gradient-based algorithm. Simulated annealing and ploytope methods are considered as two non-gradient based methods in the study. It is shown that the Levenberg-Marquardt algorithm uses gradient (or derivative) information and thus converges to the global minimum of the objective function faster than simulated annealing and polytope methods. However, it has a problem related to sticking at local minima, particularly when the number of parameters to be estimated is quite large. Although it is a global optimizer method, simulated annealing does not appear to be a feasible optimization method to be used for the parameter estimation problem considered in this study due to its computational inefficiency. Because the computation of gradients from the forward solutions, particularly in cases where the

number of layers is large and pressure and sandface flow rates at both wells are matched simultaneously, introduces a heavy computational overhead for the gradient based Levenberg-Marquardt method, polytope algorithm appears to be more efficient than the Levenberg-Marquardt method in such cases.

GİRİŞİMLİ KUYU BASINÇ TESTİ VERİLERİNDEN FARKLI OPTİMİZASYON TEKNİKLERİNİN KULLANILMASIYLA PARAMETRE TAHMİNİ

ÖZET

Bu çalışmada, çok tabakalı, tabakalar arasında geçirimsiz arayüzeylerin bulunduğu ve tabakalar arası iletişimin sadece kuyuiçi boyunca söz konusu olduğu ve tamamıyla üretime açık iki kuyulu bir rezervuar sisteminde basınç girişim testi ele alınmaktadır. Birinci kuyu, sabit veya değişken debide üretim yapan aktif kuyudur ve ikinci kuyu da test boyunca tüm zamanlarda kapalı tutulan gözlem kuyusudur. Her iki kuyuda da kuyuiçi depolama etkilerinin hesaba katılmasının yanısıra, her tabaka için farklı zar faktörü değerlerinin olabileceği varsayılmaktadır. Sonuçlar iki ayrı kısımda tanımlanmaktadır. İlk kısımda, tabakalara ait geçirgenlik, gözeneklilik, zar faktörü ve her iki kuyudaki kuyu içi depolama katsayıları gibi rezervuar parametrelerinin aktif ve/veya gözlem kuyusu basınç sinyali ve tüm tabakalara ait formasyon debileri üzerindeki etkileri, bu çalışma esnasında geliştirilen yarı analitik bir model ile incelenmiştir. Geliştirilen yarı analitik model çizgi kaynak kuyular varsayımına dayanmaktadır ve N tabakadan oluşan bir rezervuar sisteminde girişim testlerinin simülasyonunda kullanılabilecek tarzda geneldir. İlk kısımda, tek ve çok tabakalı ve tabakalar arasında geçirimsiz arayüzeylerin bulunduğu rezervuarlarda girişim testlerinin değerlendirilmesi hakkında bilgi edinmek amacı ile göz önünde bulundurulmuştur. Bu durumlarda iki kuyudaki kuyuiçi depolama katsayıları, zar faktörleri ve tabakalar arası oluşan karşılıklı akışın her iki kuyudaki basınç sinyali ve tabakalara ait formasyon debileri üzerindeki etkileri gösterilmiştir. İlk kısımdaki sonuçlar, iyi bilinen Theis eğrisi (veya Çizgi Kaynak Çözümü) ve yarı log doğru analizi yöntemlerine dayanan geleneksel tipte eğri çakıştırmanın, her iki kuyuda kuyu içi depolama ve zar faktörlerinin bulunduğu arayüzeyleri geçirimsiz çok tabakalı rezervuarlarda basınç girişim testlerinden bireysel tabaka özelliklerinin belirlenebilmesinin makul olmadığını göstermiştir.

İkinci kısımda, doğrusal olmayan parametre tahmini yöntemleri, tek ve çok tabakalı (tabaka arayüzeyleri geçirimsiz) rezervuarlarda iki kuyulu girişim testlerinden elde edilen basınç ve/veya tabakalara ait formasyon debi verilerinden tabakalara ait parametreleri belirlemek için kullanılmaktadırlar. Parametre tahmini ters bir problem olduğu için çözümü optimizasyon tekniklerinin kullanılmasını gerekli kılar. Bu çalışmada düşünülen problem için sonuçların tekil olarak elde edilip edilemeyeceği ve hesaplama zamanı bakımından araştırmak amacıyla hem gradyent kökenli ve hem de gradyent kökenli olmayan optimizasyon algoritmaları göz önünde bulundurulmuştur. Yaygın kullanımı nedeniyle, sadece bir gradyent kökenli algoritma (Levenberg-Marquardt yöntemi) bu çalışmada düşünülmüştür. Bu çalışmada ayrıca gradyent kökenli olmayan iki farklı yöntem olarak, simulated annealing ve polytope yöntemleri düşünülmüştür. Levenberg-Marquardt algoritması türev bilgisini kullandığı için hedef fonksiyonun "global" minimumuna simulated annealing ve polytope yöntemlerinden çok daha hızlı yakınsadığı görülmüştür.

Ancak, özellikle tahmin edilecek parametre sayısının oldukça fazla olduğu durumlarda, Levenberg-Marquardt algoritması lokal minimumlara takılma problemi ile karşılaşmaktadır. Simulated annealing bir global optimizasyon yöntemi olmasına rağmen, hesaplama süresi verimsizliği yüzünden, bu çalışmada düşünülen parametre tahmini problemi için kullanılabilecek makul bir optimizasyon yöntemi olmadığı anlaşılmıştır. Her iki kuyudaki basınç ve formasyon debi verilerine eşzamanlı bir şekilde çakıştırma yapılması ve de özellikle tabaka sayısının fazla olduğu durumlarda ileri (forward) çözümlerden türevlerin hesaplanması Levenberg-Marquardt yöntemi için ağır bir hesaplama yükü getirdiği için, böyle durumlarda polytope algoritmasının Levenberg-Marquardt algoritmasına alternatif olarak kullanılabileceği görülmüştür.

CHAPTER I

INTRODUCTION

In this study, we consider a two-well problem in an infinite acting multi-layered commingled reservoir. One well (the active well) is produced at a specified total surface rate, and the second well (the observation well or interference well) is shut-in for all times. The layers are commingled; that is, they communicate only through the wellbore, and no crossflow between layers occurs within the reservoir. Such reservoir systems are quite common in real reservoir systems, where the layers are separated by impermeable barriers such as shales, and thus their pressure behavior has attracted attentions of many researchers in the literature (Lefkovits [2], Larsen [3,4], Onur [5], etc.).

This work focuses on the observation and active well pressure and sandface rate responses in a multi-layered reservoir system. It examines in detail the causes and effects of crossflow through the observation and active wells and presents results regarding pressure changes, pressure-derivative and sandface flow rates data at both wells.

The first major objective of this study is to develop a semi-analytical procedure for obtaining the pressure responses and individual layer flow rates at both wells. The semi-analytical procedure for generating solutions can be used for any number of layers and allows consideration of individual layer skin factors as well as wellbore storage in both wells. The semi-analytical procedure uses the well-known Duhamel principle and superposition in space, which enables to model production/injection with different surface flow rates at active and observation wells. The semi-analytical model used in the study is similar to that of given by Onur [5]. The model developed in this study can also be used for studying two-well interference tests in single layered reservoir systems including wellbore storage and skin effects in both wells. We utilize the skin concept of Van Everdingen [6] and Hurst [7]. The wellbore storage effects are modeled by using

the ideas presented by Ogbe and Brigham [8], who investigated the influence of wellbore-storage and skin effects at both wells on interference pressure response in a single-layer system in their work. They concluded that when wellbore storage was present in both wells, it was not possible to define a single, equivalent wellbore storage factor because the pressure response is different in shape from the single wellbore storage case. For the case where wellbore storage presents only in the active well, Jargon [9] indicated that neglecting the effect of wellbore storage at the active well could cause an underestimation of transmissivity (kh/μ) and an overestimation of storativity ($\phi c_t h$) when analyzing an interference test by Theis's type curve. Onur [5] studied the interference tests in a two layer commingled system, but did not consider wellbore storage effects in both wells in their analysis. They concluded that it would be extremely difficult to determine individual layer permeabilities, porosities and skin factors from pressure data at active and observation well alone unless individual sandface flow rates are measured and used in the analysis. The parameter estimation from two-well interference tests in multi-layered commingled systems with wellbore storage and skin in both wells has not been investigated in detail in the literature. Thus, the second major objective of this work is to investigate the use of both gradient and non-gradient nonlinear parameter estimation methods to determine layer parameters from pressure and/or sandface flow rate data obtained from two-well interference tests in single and multi-layered commingled systems. Levenberg-Marquardt as a gradient method, and simulated annealing and polytope as two non-gradient optimization methods are considered to achieve the second objective.

There are five chapters in this thesis. In chapter II, we give the development of semi-analytical solution used to compute pressure drops and sandface flow rates at active and observation wells. The specific results computed for a two-layered reservoir case were compared with analytical and other numerical solutions computed by Onur [5] to verify the semi-analytical model developed in this study. In this chapter, it is also shown and discussed that a lot of study cases related to effects of wellbore storage and skin terms on active and observation well pressure and sandface flow rates for single and multi-layered reservoirs.

Chapter III presents parameter estimation by using different optimization algorithms. In this study, the second objective which was focused on especially based on inverse problem. Parameters such as permeability, porosity, skin and wellbore storage coefficients are estimated for a reservoir system whose model behavior is known mathematically by using interference well test data. For this purpose, gradient-based and non-gradient optimization techniques are used in this study. Since derivative information is used by gradient-based methods (we only used the Levenberg-Marquardt method in this study), parameter estimation can be carried out in a very short time by reaching global minimum of non-linear functions needed to be optimized. However, if smart initial guesses are not given in non-convex problems, gradient-based methods can get stuck in local minima. To exceed this problem, non-gradient methods (we used both Simulated Annealing and Polytope algorithms in this study) are also considered alternatively to gradient-based Levenberg-Marquardt method. Menekse [10] studied the analysis of well test data belonging to naturally fractured reservoir by using non-linear regression analysis. He used Levenberg-Marquardt algorithm to analyze the well test data. He concluded and focused on that more realistic initial guesses should be used to reach more accurate results and to shorten the duration of regression analysis.

Since the simulated annealing method does not use gradient (derivative) information and it is a statistically random search method, it is possible that it can reach the global minimum of the objective function even if time cost and number of function evaluations are higher than that in gradient-based techniques. Press et al [11] expressed that the simulated annealing technique has recently attracted significant attention as suitable for optimization problems of very large scale. Yoshida et al [12] used simulated annealing algorithm to analyze interference test in fractured reservoir. They developed a method for analyzing for interference well test data by using simulated annealing. Model data of interference well test were analyzed by them for four kinds of reservoir parameters to examine the effects of cooling coefficient (r_T) on estimates of the parameters and computational time. They achieved good estimates and acceptable computational time when $r_T = 0.999$ is given. However, they did not report and compare the computational efficiency of the simulated annealing with a gradient-based method. Goktas [13] used simulated annealing to do an automated well test

interpretation in horizontal wells. He concluded that results and plots of the final match of all the cases considered in his study show that the simulated annealing is highly reliable. As a second non-gradient method, we consider polytope algorithm. It was firstly introduced by Nelder and Mead [14] . The polytope method which is a typically direct search method is usually named as "Simplex" method. However, Philip et al [15] preferred not to use the latter name, to avoid confusion with the better-known simplex method for linear programming. They modified polytope method to improve its performance considerably. Leitão and Schiozer [16] used polytope algorithm, direct search method, in automatic history matching for reservoir characterization. Since polytope algorithm reduces total number of function evaluations in these kinds of optimization problems and it is very robust technique too, they suggested that this kind of optimization techniques must be used to estimate parameters for reservoir characterization.

In Chapter IV, applications about parameter estimation are presented by considering several synthetic cases. This chapter also includes performance and cpu time comparisons of optimization algorithms used in this study.

Chapter V gives conclusions and recommendations withdrawn from this study.

CHAPTER II

MATHEMATICAL FORMULATION AND CASE STUDIES

In this chapter, we give the relevant equations which describe the problem of interest and present a computational procedure for generating the layer sandface flow rates and wellbore pressures at the active and observation wells. We also show that our computational procedure gives accurate results by comparing our results with analytical solutions presented previously by Onur [5] in the literature.

2.1 Definitions

All definitions are given in oil field units and assume single phase flow of a slightly compressible liquid of constant viscosity. Unless specifically stated otherwise, all rates refer to sandface flow rates and are in RB/day. The subscripts "a" and "o" refer to the active well and the observation well, respectively. The symbols, $\bar{k}$, $\overline{\eta}$ and η_j used in this study represent respectively the thickness-averaged value of permeability, the average diffusivity and the diffusivity of layer j. The thickness averaged permeability is defined by

$$\bar{k} = \frac{1}{h}\sum_{j=1}^{l} k_j h_j \tag{2.1}$$

where l is the number of layers and h is the sum of the individual layer thickness; that is, the total reservoir thickness given by

$$h = \sum_{j=1}^{l} h_j \tag{2.2}$$

The average diffusivity is defined by

$$\overline{\eta} = \frac{\bar{k}}{\bar{\phi} c_t \mu} \tag{2.3}$$

where $\bar{\phi}c_t$ represents the thickness-averaged porosity-compressibility product and is given by

$$\bar{\phi}c_t = \frac{1}{h}\sum_{j=1}^{l}\phi_j c_{tj} h_j \tag{2.4}$$

The diffusivity of layer j is given by

$$\eta_j = \frac{k_j}{\phi_j c_{tj}\mu} \tag{2.5}$$

The subscript j in Eqs. 2.1-2.5 refers to the layer index and ϕ_j, k_j, c_{tj} and h_j represent respectively porosity, permeability, compressibility and thickness of layer j. Also l represents the total number of layers.

When we consider a two-layer commingled reservoir for convenience, we let f_r, η_r and c_r, respectively, represent the flow capacity ratio, the diffusivity ratio, and the porosity-compressibility-thickness ratio defined, respectively by

$$f_r = \frac{k_1 h_1}{k_2 h_2} \tag{2.6}$$

$$\eta_r = \frac{\eta_1}{\eta_2} \tag{2.7}$$

and

$$c_r = \frac{\phi_1 c_{t1} h_1}{\phi_2 c_{t2} h_2}. \tag{2.8}$$

2.2 Mathematical Model and Solutions

The model used in this study is based on the application of Duhamel's principle and superposition in space. We consider the single phase flow of a slightly compressible fluid of constant viscosity in a multi-layered reservoir. We consider only infinite-acting behavior. We assume that each layer is homogeneous. We neglect gravitational effects and assume that the initial prssure is the same in all layers. We also assume that only two wells exist in the reservoir and they are fully penetrating. The active well is produced at a constant total surface sandface flow rate

and the observation well is shut-in all times. A shematic diagram of a two-layer system is shown in Figure 2.1. In Figure 2.1, k denotes permeability (horizontal), ϕ porosity, c_t system compressibility, h thickness, q_a sandface flow rate at the active well, q_o sandface flow rate at the observation well and r distance between the wells. The subscripts 1 and 2 refer to layer 1 and 2, respectively.

We begin with a single-layer problem. Duhamel's principle and superposition in space give the pressure drop at any point for a two-well problem in an infinite reservoir as :

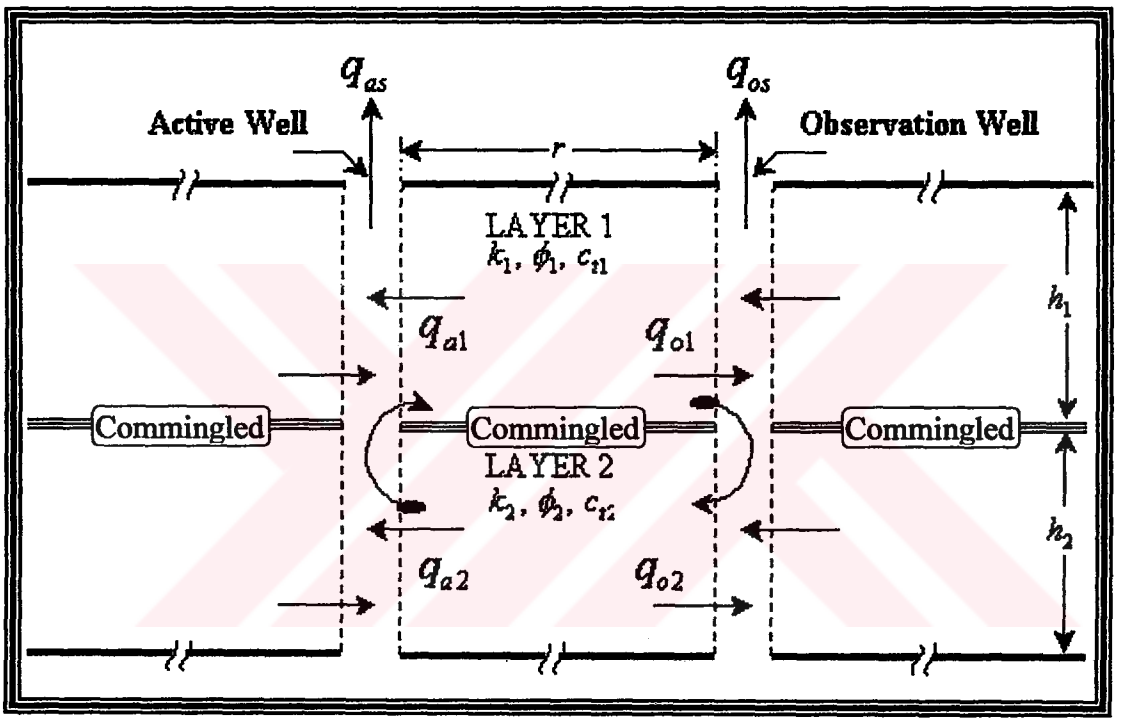

Figure 2.1 Two-layered reservoir geometry.

$$\Delta p_{wf}(t) = \int_0^t q_a(\tau) p'_{FCN}(r_{wa}, t-\tau) d\tau + \int_0^t q_o(\tau) p'_{FCN}(r, t-\tau) d\tau \qquad (2.9)$$

$$\Delta p_{of}(t) = \int_0^t q_a(\tau) p'_{FCN}(r, t-\tau) d\tau + \int_0^t q_o(\tau) p'_{FCN}(r_{wo}, t-\tau) d\tau . \qquad (2.10)$$

Recall that q_a and q_o in Eqs. 2.9 and 2.10 represent the sandface (at the formation/wellbore face) flow rates in RB/day at the active and observation wells, respectively. p_{FCN} represents the rate normalized pressure drop that would be

obtained if production were at a constant sandface flow rate, and p'_{FCN} denotes the derivative of p_{FCN} with respect to time. The expressions for flow rates are given by

$$q_a(t) = q_{sa}(t) - 24C_a \frac{d\Delta p_{wf}}{dt} \tag{2.11}$$

and

$$q_o(t) = q_{so}(t) - 24C_o \frac{d\Delta p_{of}}{dt} \tag{2.12}$$

where q_{sa} and q_{so}, respectively, denote the surface rates at the active and observation wells. Note that if the observation well is shut-in at surface, then we set $q_{so}(t) = 0$ for all t during the test time. We wrote Eqs. 2.11 and 2.12 in a general way so that we can consider variable surface rate production at the active (or even observation) well. In Eqs. 2.9-2.12, $\Delta p_{wf}(t) = p_i - p_{wf}(t)$ and $\Delta p_{of}(t) = p_i - p_{of}(t)$. Furthermore, p_{FCN} functions in Eqs. 1 and 2 are given by

$$p_{FCN}(r,t) = \frac{141.2\mu}{kh}\left[\frac{1}{2}E_1\left(\frac{r^2}{4(2.637x10^{-4})\eta t}\right)\right], \text{ for } r > r_{wa} \text{ or } r > r_{wo} \tag{2.13}$$

$$P_{FCN}(r_w,t) = \frac{141.2\mu}{k_j h_j}\left\{-\frac{1}{2}E_1\left[\frac{-r_w^2}{4(2.637x10^{-4})\eta t}\right] + S_{mj}\right\} \tag{2.14}$$

and

$$\begin{aligned} r_w = r_{wa} \quad &\Rightarrow \quad S_{mj} = S_a \\ r_w = r_{wo} \quad &\Rightarrow \quad S_{mj} = S_o \end{aligned} \tag{2.15}$$

Note that we consider that active and observation wells can have different well radii. Also, the skin factor at both wells can be different as defined by S_a and S_o, which represent the skin factors at the active and observation wells, respectively.

We wish to write Eqs.(2.9-2.10) in a discrete form. To do so, we will partition the time interval $(0,t)$ into discrete time points, as defined by

$$0 = t_0 < t_1 < t_2 < \ldots < t_n < t_{n+1} = t\,. \tag{2.16}$$

Note that $t_0 = 0$ and $t_{n+1} = t$. Using the partition given by Eq. 2.16, we can rewrite Eqs. 2.9 and 2.10, respectively, as

$$\Delta p_{wf}(t_{n+1}) = \sum_{k=0}^{n} \int_{t_k}^{t_{k+1}} q_a(\tau) p'_{FCN}(r_{wa}, t_{n+1} - \tau) d\tau + \sum_{k=0}^{n} \int_{t_k}^{t_{k+1}} q_o(\tau) p'_{FCN}(r, t_{n+1} - \tau) d\tau \tag{2.17}$$

and

$$\Delta p_{of}(t_{n+1}) = \sum_{k=0}^{n} \int_{t_k}^{t_{k+1}} q_a(\tau) p'_{FCN}(r, t_{n+1} - \tau) d\tau + \sum_{k=0}^{n} \int_{t_k}^{t_{k+1}} q_o(\tau) p'_{FCN}(r_{wo}, t_{n+1} - \tau) d\tau\,. \tag{2.18}$$

Now, we will approximate the integrals in Eqs. 2.17 and 2.18. We will show how we do it only for the first integral term in Eq. 2.17. The other integrals are similarly approximated. Let's rewrite the first sum of integrals given in Eq. 2.17, which is

$$\sum_{k=0}^{n} \int_{t_k}^{t_{k+1}} q_a(\tau) p'_{FCN}(r_{wa}, t_{n+1} - \tau) d\tau\,. \tag{2.19}$$

There are several methods to numerically approximate an integral. For our purposes, it is convenient to use rectangular rule for the flow rate q_a, i.e., in the interval from t_k to t_{k+1}, we approximate $q_a(\tau) = q_a(t_{k+1})$ in Eq. 2.19 so we can take it out of the integral in Eq. 2.19. Thus, we can approximate Eq. 2.19 as :

$$\sum_{k=0}^{n} q_a(t_{k+1}) \int_{t_k}^{t_{k+1}} p'_{FCN}(r_{wa}, t_{n+1} - \tau) d\tau \tag{2.20}$$

Now recall that $p'_{FCN}(r_{wa}, t - \tau)$ in Eq. 2.20 is noting more than

$$p'_{FCN}(r_{wa}, t_{n+1} - \tau) = \frac{dp_{FCN}(r_{wa}, t_{n+1} - \tau)}{d\tau}\,. \tag{2.21}$$

Using Eq. 2.21 in Eq. 2.20 and performing the integration gives

$$\sum_{k=0}^{n} q_a(t_{k+1}) \int_{t_k}^{t_{k+1}} p'_{FCN}(r_{wa}, t_{n+1} - \tau) d\tau = \sum_{k=0}^{n} q_a(t_{k+1}) \left[- p_{FCN}(r_{wa}, t_{n+1} - \tau) \right]_{t_k}^{t_{k+1}}$$
$$= \sum_{k=0}^{n} q_a(t_{k+1}) \left[p_{FCN}(r_{wa}, t_{n+1} - t_k) - p_{FCN}(r_{wa}, t_{n+1} - t_{k+1}) \right] \quad (2.22)$$

We would like to write Eq. 2.22 in a more conveniet structure for computational purposes. To do so, first let's see the structure by taking $n = 3$ in Eq. 2.22. Thus, $t_{n+1} = t_4$.

$$\begin{aligned} &\sum_{k=0}^{3} q_a(t_{k+1}) \left[p_{FCN}(r_{wa}, t_{n+1} - t_k) - p_{FCN}(r_{wa}, t_{n+1} - t_{k+1}) \right] \\ &= q_a(t_1) \left[p_{FCN}(r_{wa}, t_4 - t_0) - p_{FCN}(r_{wa}, t_4 - t_1) \right] \\ &+ q_a(t_2) \left[p_{FCN}(r_{wa}, t_4 - t_1) - p_{FCN}(r_{wa}, t_4 - t_2) \right] \\ &+ q_a(t_3) \left[p_{FCN}(r_{wa}, t_4 - t_2) - p_{FCN}(r_{wa}, t_4 - t_3) \right] \\ &+ q_a(t_4) \left[p_{FCN}(r_{wa}, t_4 - t_3) - p_{FCN}(r_{wa}, t_4 - t_4) \right] \end{aligned} \quad (2.23)$$

Because $t_0 = 0$ and $p_{FCN}(r_{wa}, t_4 - t_4) = p_{FCN}(r_{wa}, 0) = 0$ (note that this is true regardless of skin factor; i.e., it is zero even if we have S_a is not zero. At first glance, this may appear a contradiction what is given by Eq. 2.14 (or Eq. 2.15 for the observation well). It is not really, because skin becomes effective when $t = 0^+$ (given by Onur [17]), then we can rewrite Eq. 2.23 as

$$\begin{aligned} &\sum_{k=0}^{3} q_a(t_{k+1}) \left[p_{FCN}(r_{wa}, t_{n+1} - t_k) - p_{FCN}(r_{wa}, t_{n+1} - t_{k+1}) \right] \\ &= q_a(t_1) \left[p_{FCN}(r_{wa}, t_4 - t_0) - p_{FCN}(r_{wa}, t_4 - t_1) \right] \\ &+ q_a(t_2) \left[p_{FCN}(r_{wa}, t_4 - t_1) - p_{FCN}(r_{wa}, t_4 - t_2) \right] \\ &+ q_a(t_3) \left[p_{FCN}(r_{wa}, t_4 - t_2) - p_{FCN}(r_{wa}, t_4 - t_3) \right] \\ &+ q_a(t_4) \left[p_{FCN}(r_{wa}, t_4 - t_3) \right] \end{aligned} \quad (2.24)$$

Because $q_a(t_0) = q_a(0) = 0$ and note that $t_0 = 0$, we can rewrite Eq. 2.24 as

$$\sum_{k=0}^{3} q_a(t_{k+1})[p_{FCN}(r_{wa}, t_{n+1}-t_k) - p_{FCN}(r_{wa}, t_{n+1}-t_{k+1})]$$
$$= [q_a(t_1)-q_a(t_0)]p_{FCN}(r_{wa}, t_4-t_0) + [q_a(t_2)-q_a(t_1)]p_{FCN}(r_{wa}, t_4-t_1) \quad (2.25)$$
$$+ [q_a(t_3)-q_a(t_2)]p_{FCN}(r_{wa}, t_4-t_2) + [q_a(t_4)-q_a(t_3)]p_{FCN}(r_{wa}, t_4-t_3)$$

which can be generalized as

$$\sum_{k=0}^{n} q_a(t_{k+1})[p_{FCN}(r_{wa}, t_{n+1}-t_k) - p_{FCN}(r_{wa}, t_{n+1}-t_{k+1})]$$
$$= \sum_{j=0}^{n} [q_a(t_{k+1})-q_a(t_k)]p_{FCN}(r_{wa}, t_{n+1}-t_k), \quad (2.26)$$

where in the right-hand side, $t_0 = 0$ and $q_a(t_0) = q_a(0) = 0$.

Now, we are going to replace all the integrals appearing in Eqs. 2.17 and 2.18 with their approximations similar to those given in the form of Eq. 2.26. Doing so, we can approximate Eqs. 9 and 10, respectively, as

$$\Delta p_{wf}(t_{n+1}) = \sum_{k=0}^{n} [q_a(t_{k+1})-q_a(t_k)]p_{FCN}(r_{wa}, t_{n+1}-t_k)$$
$$+ \sum_{k=0}^{n} [q_o(t_{k+1})-q_o(t_k)]p_{FCN}(r, t_{n+1}-t_k) \quad (2.27)$$

and

$$\Delta p_{of}(t_{n+1}) = \sum_{k=0}^{n} [q_a(t_{k+1})-q_a(t_k)]p_{FCN}(r, t_{n+1}-t_k)$$
$$+ \sum_{k=0}^{n} [q_o(t_{k+1})-q_o(t_k)]p_{FCN}(r_{wo}, t_{n+1}-t_k) \quad (2.28)$$

These are two main equations to be used. The other two equations are obtained by approximating flow rate equations given by Eqs. 2.11 and 2.12 as, respectively,

$$\frac{24C_a}{t_{n+1}-t_n}\Delta p_{wf}(t_{n+1}) + q_a(t_{n+1}) = q_{sa}(t_{n+1}) + \frac{24C_a}{t_{n+1}-t_n}\Delta p_{wf}(t_n) \quad (2.29)$$

and

$$\frac{24C_o}{t_{n+1}-t_n}\Delta p_{of}(t_{n+1})+q_o(t_{n+1})=q_{so}(t_{n+1})+\frac{24C_o}{t_{n+1}-t_n}\Delta p_{of}(t_n) \tag{2.30}$$

(of course, if the observation well is shut-in for all times, then we set $q_{so}(t_{n+1})=0$ for t_{n+1}).

Let's investigate our system of equations in terms of implementation in computing pressure drops and flow rates at the active and observation wells as a function of time. We start with $n=0$, here the objective is to compute pressure drops and sandface flow rates at t_1. For, $n=0$, Eq. 2.27 can be written as

$$\begin{aligned}\Delta p_{wf}(t_1)&=\sum_{k=0}^{0}[q_a(t_{k+1})-q_a(t_k)]p_{FCN}(r_{wa},t_1-t_k)\\&\quad+\sum_{k=0}^{n}[q_o(t_{k+1})-q_o(t_k)]p_{FCN}(r,t_1-t_k)\\&=[q_a(t_1)-q_a(t_0)]p_{FCN}(r_{wa},t_1-t_0)\\&\quad+[q_o(t_1)-q_o(t_0)]p_{FCN}(r,t_1-t_0)\end{aligned} \tag{2.31}$$

Because $q_a(t_0)=q_a(0)=0$ and $t_0=0$, then Eq. 2.31 can be rewritten as

$$\Delta p_{wf}(t_1)=q_a(t_1)p_{FCN}(r_{wa},t_1)+q_o(t_1)p_{FCN}(r,t_1)$$

or can be rearranged as

$$\Delta p_{wf}(t_1)-q_a(t_1)p_{FCN}(r_{wa},t_1)-q_o(t_1)p_{FCN}(r,t_1)=0 \tag{2.32}$$

Similarly, for $n=0$, Eq. 2.28 can be written as

$$\Delta p_{of}(t_1)=q_a(t_1)p_{FCN}(r,t_1)+q_o(t_1)p_{FCN}(r_{wo},t_1)$$

or can be rearranged as

$$\Delta p_{of}(t_1)-q_a(t_1)p_{FCN}(r,t_1)-q_o(t_1)p_{FCN}(r_{wo},t_1)=0\,. \tag{2.33}$$

For $n=0$, Eqs. 2.29 and 2.30 become

$$\frac{24C_a}{t_1-t_0}\Delta p_{wf}(t_1)+q_a(t_1)=q_{sa}(t_1)+\frac{24C_a}{t_1-t_0}\Delta p_{wf}(t_0) \tag{2.34}$$

and

$$\frac{24C_o}{t_1-t_0}\Delta p_{of}(t_1)+q_o(t_1)=q_{so}(t_1)+\frac{24C_o}{t_1-t_0}\Delta p_{of}(t_0) \tag{2.35}$$

Note that $t_0=0$ and $\Delta p_{of}(t_0)=\Delta p_{of}(0)=0, \Delta p_{wf}(t_0)=\Delta p_{wf}(0)=0$. We take pressure drops at the wells at $t_0=0$ to be zero but they can be treated different from initial pressure. However, for our applications, we set them to zero as done here. So, Eqs. 2.34 and 2.35 become

$$\frac{24C_a}{t_1}\Delta p_{wf}(t_1)+q_a(t_1)=q_{sa}(t_1) \tag{2.36}$$

and

$$\frac{24C_o}{t_1}\Delta p_{of}(t_1)+q_o(t_1)=q_{so}(t_1). \tag{2.37}$$

Thus, the system of equations by Eqs. 2.32, 2.33, 2.36 and 2.37 for pressure drops and sand face rates at time t_1.

For $n=1$, Eq. 2.27 becomes

$$\begin{aligned}\Delta p_{wf}(t_2)=&\sum_{k=0}^{1}\left[q_a(t_{k+1})-q_a(t_k)\right]p_{FCN}(r_{wa},t_2-t_k)\\&+\sum_{k=0}^{1}\left[q_o(t_{k+1})-q_o(t_k)\right]p_{FCN}(r,t_2-t_k)\end{aligned} \tag{2.38}$$

or

$$\begin{aligned}\Delta p_{wf}(t_2)=&\left[q_a(t_1)-q_a(t_0)\right]p_{FCN}(r_{wa},t_2-t_0)\\&+\left[q_a(t_2)-q_a(t_1)\right]p_{FCN}(r_{wa},t_2-t_1)\\&+\left[q_o(t_1)-q_o(t_0)\right]p_{FCN}(r,t_2-t_0)\\&+\left[q_o(t_2)-q_o(t_1)\right]p_{FCN}(r,t_2-t_1)\end{aligned} \tag{2.39}$$

or can be rearranged as

$$\begin{aligned}&\Delta p_{wf}(t_2)-q_a(t_2)p_{FCN}(r_{wa},t_2-t_1)-q_o(t_2)p_{FCN}(r,t_2-t_1)=\\&[q_a(t_1)-q_a(t_0)]p_{FCN}(r_{wa},t_2-t_0)+[-q_a(t_1)]p_{FCN}(r_{wa},t_2-t_1).\\&+[q_o(t_1)-q_o(t_0)]p_{FCN}(r,t_2-t_0)+[-q_o(t_1)]p_{FCN}(r,t_2-t_1)\end{aligned} \tag{2.40}$$

Similarly, for $n=1$, Eq. 2.28 can be written as

$$\begin{aligned}&\Delta p_{of}(t_2)-q_a(t_2)p_{FCN}(r,t_2-t_1)-q_o(t_2)p_{FCN}(r_{wo},t_2-t_1)=\\&[q_a(t_1)-q_a(t_0)]p_{FCN}(r,t_2-t_0)+[-q_a(t_1)]p_{FCN}(r,t_2-t_1)\\&+[q_o(t_1)-q_o(t_0)]p_{FCN}(r_{wo},t_2-t_0)+[-q_o(t_1)]p_{FCN}(r_{wo},t_2-t_1)\end{aligned} \tag{2.41}$$

For $n=1$, Eqs. 2.29 and 2.30 can be written as, respectively,

$$\frac{24C_a}{t_2-t_1}\Delta p_{wf}(t_2)+q_a(t_2)=q_{sa}(t_2)+\frac{24C_a}{t_2-t_1}\Delta p_{wf}(t_1) \tag{2.42}$$

and

$$\frac{24C_o}{t_2-t_1}\Delta p_{of}(t_2)+q_o(t_2)=q_{so}(t_2)+\frac{24C_o}{t_2-t_1}\Delta p_{of}(t_1). \tag{2.43}$$

Now, we can solve the system of equations given by 2.40-2.42 for pressure drops and sandface flow rates at time t_2 because pressure drops and flow rates at time t_1 are known because they were computed at the time level at $n=0$.

Now we consider the time level at $n=2$, then Eq. 2.27 becomes

$$\begin{aligned}\Delta p_{wf}(t_3)=&\sum_{k=0}^{2}[q_a(t_{k+1})-q_a(t_k)]p_{FCN}(r_{wa},t_3-t_k)\\&+\sum_{k=0}^{2}[q_o(t_{k+1})-q_o(t_k)]p_{FCN}(r,t_3-t_k)\end{aligned} \tag{2.44}$$

or

$$\begin{aligned}\Delta p_{wf}(t_3)=&[q_a(t_1)-q_a(t_0)]p_{FCN}(r_{wa},t_3-t_0)+[q_a(t_2)-q_a(t_1)]p_{FCN}(r_{wa},t_3-t_1)\\&+[q_a(t_3)-q_a(t_2)]p_{FCN}(r_{wa},t_3-t_2)\\&+[q_o(t_1)-q_o(t_0)]p_{FCN}(r,t_3-t_0)+[q_o(t_2)-q_o(t_1)]p_{FCN}(r,t_3-t_1)\\&+[q_o(t_3)-q_o(t_2)]p_{FCN}(r,t_3-t_2)\end{aligned}$$

which can be rearranged as

$$\begin{aligned}
&\Delta p_{wf}(t_3)-q_a(t_3)p_{FCN}(r_{wa},t_3-t_2)-q_o(t_3)p_{FCN}(r,t_3-t_2)\\
&=[q_a(t_1)-q_a(t_0)]p_{FCN}(r_{wa},t_3-t_0)+[q_a(t_2)-q_a(t_1)]p_{FCN}(r_{wa},t_3-t_1)\\
&+[-q_a(t_2)]p_{FCN}(r_{wa},t_3-t_2)\\
&+[q_o(t_1)-q_o(t_0)]p_{FCN}(r,t_3-t_0)+[q_o(t_2)-q_o(t_1)]p_{FCN}(r,t_3-t_1)\\
&+[-q_o(t_2)]p_{FCN}(r,t_3-t_2)
\end{aligned} \quad . \tag{2.44}$$

Similarly, for $n=2$, Eq. 2.28 can be rearranged as

$$\begin{aligned}
&\Delta p_{of}(t_3)-q_a(t_3)p_{FCN}(r,t_3-t_2)-q_o(t_3)p_{FCN}(r_{wo},t_3-t_2)\\
&=[q_a(t_1)-q_a(t_0)]p_{FCN}(r,t_3-t_0)+[q_a(t_2)-q_a(t_1)]p_{FCN}(r,t_3-t_1)\\
&+[-q_a(t_2)]p_{FCN}(r,t_3-t_2)\\
&+[q_o(t_1)-q_o(t_0)]p_{FCN}(r_{wo},t_3-t_0)+[q_o(t_2)-q_o(t_1)]p_{FCN}(r_{wo},t_3-t_1)\\
&+[-q_o(t_2)]p_{FCN}(r_{wo},t_3-t_2)
\end{aligned} \quad . \tag{2.45}$$

For $n=2$, Eqs. 2.29 and 2.30 can be written as, respectively,

$$\frac{24C_a}{t_3-t_2}\Delta p_{wf}(t_3)+q_a(t_3)=q_{sa}(t_3)+\frac{24C_a}{t_3-t_2}\Delta p_{wf}(t_2) \tag{2.46}$$

and

$$\frac{24C_o}{t_3-t_2}\Delta p_{of}(t_3)+q_o(t_3)=q_{so}(t_3)+\frac{24C_o}{t_3-t_2}\Delta p_{of}(t_2). \tag{2.47}$$

Now, we can solve the system of equations given by Eqs. 2.44-2.47 for pressure drops at t_3. The system of equations to be solved for the active and observation wells at time level n can be generalized by the following equations :

$$\begin{aligned}
&\Delta p_{wf}(t_{n+1})-q_a(t_{n+1})p_{FCN}(r_{wa},t_{n+1}-t_n)-q_o(t_{n+1})p_{FCN}(r,t_{n+1}-t_n)\\
&=\sum_{k=0}^{n-1}[q_a(t_{k+1})-q_a(t_k)]p_{FCN}(r_{wa},t_{n+1}-t_k)-q_a(t_n)p_{FCN}(r_{wa},t_{n+1}-t_n)\\
&+\sum_{k=0}^{n-1}[q_o(t_{k+1})-q_o(t_k)]p_{FCN}(r,t_{n+1}-t_k)-q_o(t_n)p_{FCN}(r,t_{n+1}-t_n)
\end{aligned} \tag{2.48}$$

$$\Delta p_{of}(t_{n+1}) - q_a(t_{n+1})p_{FCN}(r, t_{n+1} - t_n) - q_o(t_{n+1})p_{FCN}(r_{wo}, t_{n+1} - t_n)$$
$$= \sum_{k=0}^{n-1} [q_a(t_{k+1}) - q_a(t_k)]p_{FCN}(r, t_{n+1} - t_k) - q_a(t_n)p_{FCN}(r, t_{n+1} - t_n) \quad (2.49)$$
$$+ \sum_{k=0}^{n-1} [q_o(t_{k+1}) - q_o(t_k)]p_{FCN}(r_{wo}, t_{n+1} - t_k) - q_o(t_n)p_{FCN}(r_{wo}, t_{n+1} - t_n)$$

and the flow rate equations are given by Eqs. 2.29 and 2.30.

Eqs. 2.48 and 2.49 can be easily extended to l -layered system by introducing a layer index j in flow rates and p_{FCN} terms in Eqs. 2.48 and 2.49. Then the resulting equations represent $2l$ equations in $2l+2$ unknowns, Δp_{wf}, Δp_{of}, q_{aj} and q_{oj}, $j = 1, 2, \ldots l$. We need two more equations to solve the problem. The two necessary equations are the wellbore flow rate conditions as given by :

$$\sum_{j=1}^{l} q_{aj}(t) = q_{sa}(t) - 24C_a \frac{d\Delta p_{wf}}{dt} \quad (2.50)$$

and

$$\sum_{j=1}^{l} q_{oj}(t) = q_{so}(t) - 24C_o \frac{d\Delta p_{of}}{dt}, \quad (2.51)$$

In our applications given in thesis study, we consider observation well is shut-in for all times so $q_{so}(t) = 0$ in Eq. 2.51.

The system of equations, Eqs. 2.48 and 2.51, can be written in matrix form as :

$$A\vec{x} = \vec{b} \quad (2.52)$$

The structure of the coefficient matrix A, and column vectors are given in Table 2.1. Note that A is a real symmetric matrix. In Table 2.1, b_j, c_j, d_j and e_j are given by the mathematical expressions in Appendix A.

Table 2.1: Matrix representation of the problem with storage and skin.

$$A=\begin{bmatrix}
d_1 & 0 & . & . & 0 & b_1 & 0 & . & . & 0 & 1 & 0 \\
0 & d_2 & . & . & . & 0 & b_2 & . & . & . & 1 & 0 \\
. & . & . & . & . & . & . & . & . & . & . & . \\
. & . & . & . & 0 & . & . & . & . & 0 & . & . \\
0 & . & . & 0 & d_l & 0 & . & . & 0 & b_l & 1 & 0 \\
b_1 & 0 & . & . & 0 & e_1 & 0 & . & . & 0 & 0 & 1 \\
0 & b_2 & . & . & . & 0 & e_2 & . & . & . & 0 & 1 \\
. & . & . & . & . & . & . & . & . & . & . & . \\
. & . & . & . & 0 & . & . & . & . & 0 & . & . \\
0 & . & . & 0 & b_l & 0 & . & . & 0 & e_l & 0 & 1 \\
1 & 1 & . & . & 1 & 0 & 0 & . & . & 0 & f_1 & 0 \\
0 & 0 & . & . & 0 & 1 & 1 & . & . & 1 & 0 & f_2
\end{bmatrix}$$

$$\vec{x}=\begin{bmatrix}
q_{a1} \\ q_{a2} \\ . \\ . \\ q_{al} \\ q_{o1} \\ q_{o2} \\ . \\ . \\ q_{ol} \\ \Delta p_{wf} \\ \Delta p_{of}
\end{bmatrix} \qquad \vec{b}=\begin{bmatrix}
c_1 \\ c_2 \\ . \\ . \\ c_l \\ c_{l+1} \\ c_{l+2} \\ . \\ . \\ c_{2l} \\ q_{as}+g_1 \\ q_{os}+g_2
\end{bmatrix}$$

2.3 Accuracy Study About Number of Time Points per Log Cycle :

In this study, computations were done by using 3, 5, 8, 10, 15, 20, 30, 40, 50, 80, 100 numbers in turn as a number of time points per log cycle. Scenario used in these computations takes into account existence of wellbore storage and skin effects at both active and observation wells ($C_a = C_o = 0.5$ and $S_a = S_o = 5$).

Table 2.2 Reservoir properties.

Parameters	Values
μ, cp (viscosity)	1.0
k, md (permeability)	100
ϕ (porosity)	0.15
c_t, psi^{-1} (compressibility)	10^{-5}
h, ft (layer thickness)	50
r_{wa} *and* r_{wo}, ft (radii of wells)	0.33
r, ft (distance between both wells)	200

Numerical values in Table 2.2 were used in this accuracy study. To decide how many number of time points per log cycle need, results of the study are shown by graphs given below .

As seen in Figures 2.2-2.3, while pressure change, pressure-derivative and sandface flow rate curves were constructed in forward computation, firstly 3 time points on each log cycle were used to do accuracy analysis. Although computation time decreases when we use a few time points on each log cycle, accurate and sensitive results cannot be obtained in computing of pressures and sandface flow rates at both active and observation well. When we increase number of time points on each log cycle like 50 or 100 time points, very much accurate and sensitive results can be obtained, but computation time increases in forward problem. Therefore, optimum number of time points on each log cycle needs to be used to reach optimum accuracy and computation time. When we look at graphs and tables beginning from Figure 2.2 and Table 2.3 (many of them are in Appendix A section), it will be seen that computation accuracy doesn't change after 20 time points on each log cycle, though termination time continues increasing in forward computation.

In Table 2.3, dimensionless sandface flow rates in 2^{nd} layer at active well were computed by using analytical and numerical methods. These analytical and numerical results are compared with results obtained by this study. In Table 2.4, results in Table 2.3 were recomputed by using different number of time points on each log cycle. It is appeared that more accurate and sensitive results can be obtained when number of time points on each log cycle increases in forward computation. In

these figures, f_r denotes flow capacity ratio, η_r denotes diffusivity ratio, r_D denotes dimensionless distance between the active well and the observation well, S_{an} denotes skin factor at n^{th} layer at active well and S_{on} denotes skin factor at n^{th} layer at observation well. Other comparison figures and tables are given in Appendix A section. Furthermore, mathematical expressions of dimensionless layer rates q_D and pressure changes P_D are given in Appendix C section.

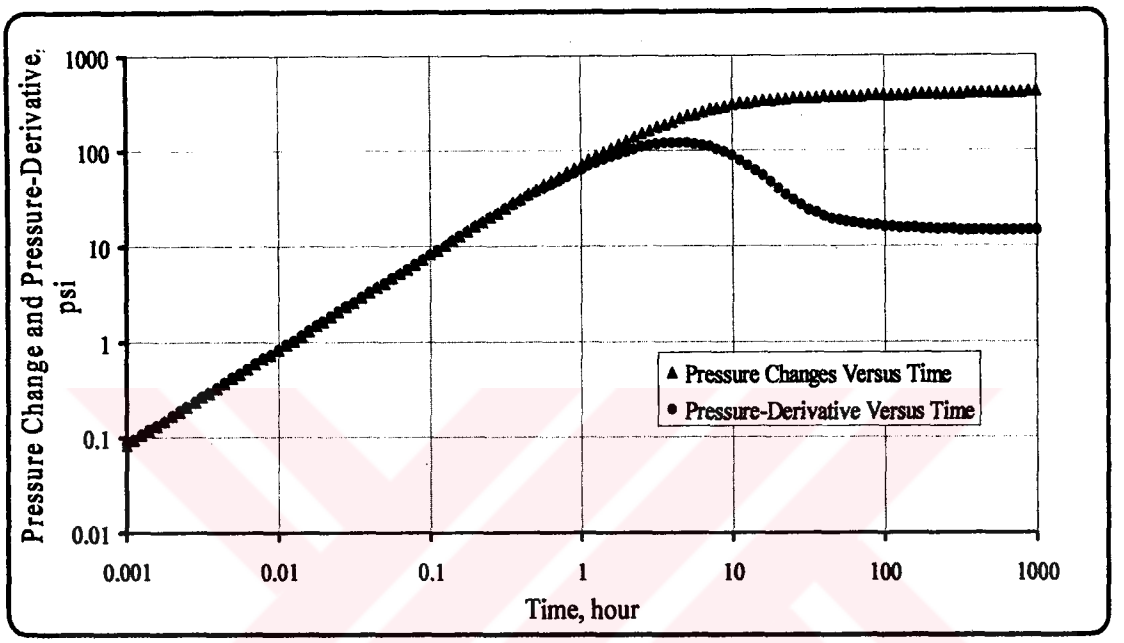

Figure 2.2 Pressure change and pressure-derivative versus time at the active well which consists of 20 points on each log cycle.

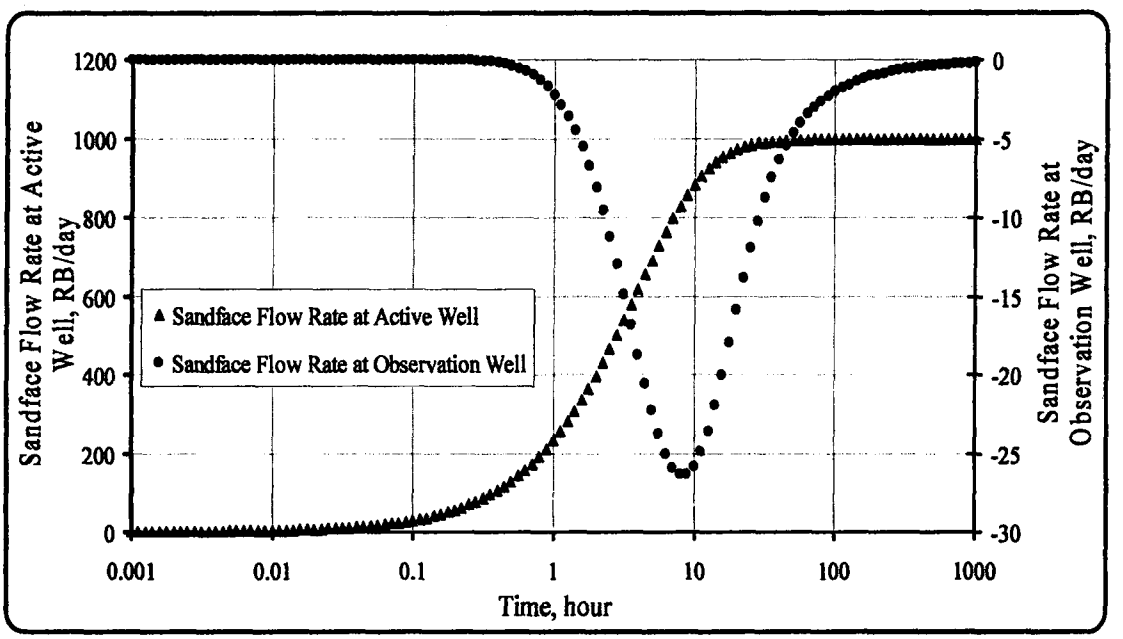

Figure 2.3 Sandface flow rates versus time at both wells which consists of 20 points on each log cycle.

Table 2.3 Comparison of analytical and numerical solutions; dimensionless layer rate q_{Da2}. ($f_r = 1.0$, $\eta_r = 100$, $r_D = 1000$ *and* $s_{a1} = s_{a2} = s_{o1} = s_{o2} = 0$)

	Onur's Analytical	**This Study**
t_D/r_D^2	q_{Da2}	q_{Da2} (N=10)
0.01	0.59748	0.59868
0.05	0.58417	0.58481
0.08	0.58059	0.5809
0.1	0.57882	0.57906
0.5	0.56648	0.56679
0.7	0.56407	0.5643
1	0.56163	0.56183
2	0.55725	0.5575
6	0.55137	0.5517
10	0.54906	0.54931
20	0.54627	0.5465
50	0.54307	0.54328
80	0.5416	0.54177
100	0.54094	0.54107

Table 2.4 Comparison of analytical and numerical solutions in terms of number of time points on each log cycle; dimensionless layer rate q_{Da2}.

($f_r = 1.0$, $\eta_r = 100$, $r_D = 1000$ *and* $s_{a1} = s_{a2} = s_{o1} = s_{o2} = 0$)

This Study % Deviation (N=10)	**This Study % Deviation (N=20)**	**This Study % Deviation (N=30)**	**This Study % Deviation (N=50)**
0.201	**0.030**	0.022	**0.015**
0.110	**0.050**	0.046	**0.042**
0.053	**0.016**	0.013	**0.009**
0.041	**0.014**	0.011	**0.008**
0.055	**0.013**	0.010	**0.006**
0.041	**0.015**	0.011	**0.008**
0.036	**0.014**	0.010	**0.007**
0.045	**0.013**	0.009	**0.005**
0.060	**0.014**	0.010	**0.007**
0.046	**0.013**	0.009	**0.006**
0.042	**0.011**	0.008	**0.005**
0.039	**0.009**	0.007	**0.004**
0.031	**0.009**	0.007	**0.005**
0.024	**0.009**	0.006	**0.005**

2.4 Case Studies

In this section, pressure change, pressure-derivative and sandface flow rate data are investigated for both wells and plotted on graphs. Wellbore storage and/or skin factor effects over these data are investigated in this case study section. Therefore Theis's line source solution which does not consider wellbore storage and skin terms is used to comparison with other case with wellbore storage/skin terms.

$$\Delta p_a = \frac{70.6 q_{sa} B\mu}{kh} E_1\left[\frac{948\phi c_t \mu r_{wa}^2}{kt}\right] + \frac{70.6 q_{so} B\mu}{kh} E_1\left[\frac{948\phi c_t \mu r^2}{kt}\right] \tag{2.53}$$

$$\Delta p_o = \frac{70.6 q_{so} B\mu}{kh} E_1\left[\frac{948\phi c_t \mu r_{wo}^2}{kt}\right] + \frac{70.6 q_{sa} B\mu}{kh} E_1\left[\frac{948\phi c_t \mu r^2}{kt}\right] \tag{2.54}$$

We accept that formation volume factor equals to one and observation well is shut-in all times in this thesis study. So we can rewrite Eqs.(2.53-2.54) as given below.

$$\Delta p_a = \frac{70.6 q_{sa} \mu}{kh} E_1\left[\frac{948\phi c_t \mu r_{wa}^2}{kt}\right] \tag{2.55}$$

$$\Delta p_o = \frac{70.6 q_{sa} \mu}{kh} E_1\left[\frac{948\phi c_t \mu r^2}{kt}\right] \tag{2.56}$$

we should use average permeability and storativity $(\phi c_t h)$ for multi-layered reservoir as given below:

$$\bar{k} = \frac{k_1 h_1 + k_2 h_2 + \ldots + k_l h_l}{h_1 + h_2 + \ldots + h_l} \tag{2.57}$$

$$\bar{\phi}\,\bar{c}_t \bar{h} = \phi_1 c_{t1} h_1 + \phi_2 c_{t2} h_2 + \ldots + \phi_l c_{tl} h_l \tag{2.58}$$

where subscript l refers to number of layers.

2.4.1 Single-Layered System 1 : This case study considers single layer system with an active well and an observation well. The active well is produced at a specified surface flow rate with $q_{as} = 1000\,RB/day$, and the second well (the observation well or interference well) is shut-in for all times. Using information below, sandface flow rate, pressure and pressure derivative values versus time were computed in each well and then their graphics were plotted here. The objective of this case is

considering study interference test pressure behavior in a single layer system for various cases.

Table 2.5 Wellbore data for different cases (1).

	Active Well		**Observation Well**	
Cases	C_a, *RB/psi*	S_a	C_o, *RB/psi*	S_o
1.1	**0**	**0**	**0**	**0**
1.2	**0**	**2**	**0**	**0**
1.3	**0.1**	**2**	**0**	**0**
1.4	**0**	**0**	**0**	**2**
1.5	**0**	**0**	**0.1**	**2**
1.6	**0.1**	**2**	**0**	**2**
1.7	**0.1**	**2**	**0.1**	**2**

Other parameters for reservoir are given in Table 2.2 (except for $C_t = 10^{-4}\ psi^{-1}$) :

In Figure 2.4, log-log plots of pressure change and pressure-derivative versus time for the active well. As can be seen from Figure 2.4, skin factor at the active well affects pressure response at the active well. However, skin factor at the observation well (Case 1.4) does not affect pressure response at the active well, because there is no production available at the observation well. In the same manner, skin factor at the active well does not affect pressure change at the observation well. Skin factor at the observation well does not vary pressure change at the observation well either as can be seen from Figure 2.5. Therefore pressure response for the cases 1.1-1.4 matches with Theis' line source solution.

In Figures 2.6-2.7, sandface flow rate changes are shown for both wells. Apparently, surface rate at the active well changes sandface flow rate at the active well, but surface rate at the active well does not affect sandface flow rate at the

observation well, because there is no any wellbore storage/skin effects at the observation well.

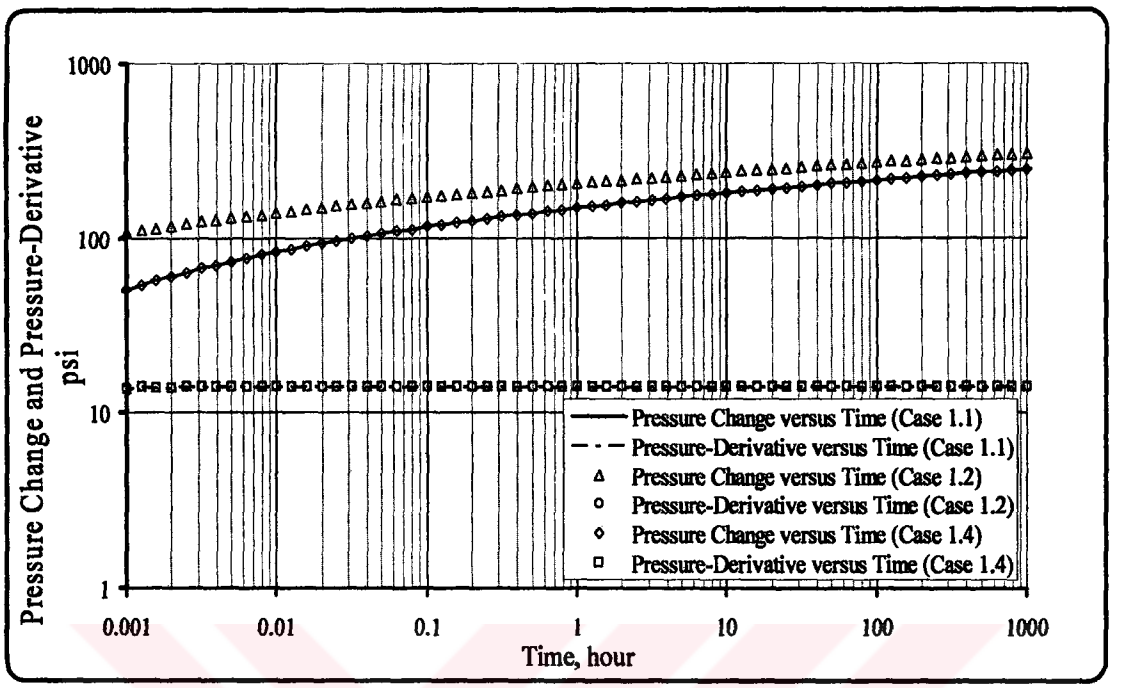

Figure 2.4 Pressure change and pressure-derivative versus time at the active well for Cases 1.1-1.2-1.4.

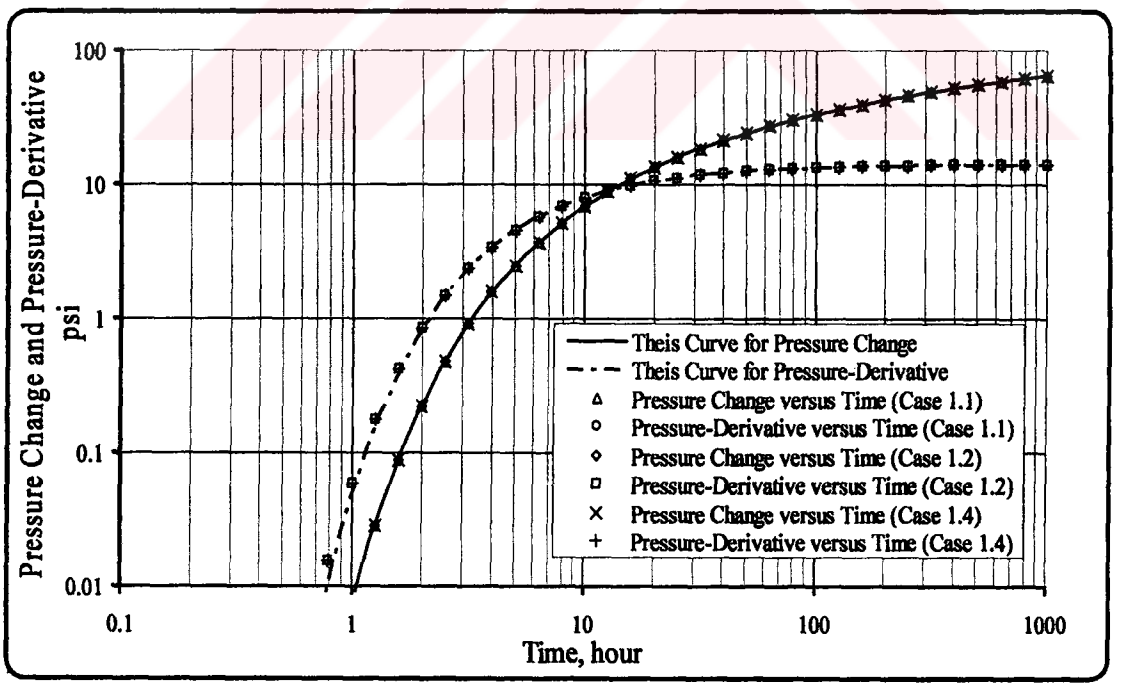

Figure 2.5 Pressure change and pressure-derivative versus time at the observation well for Cases 1.1-1.2-1.4.

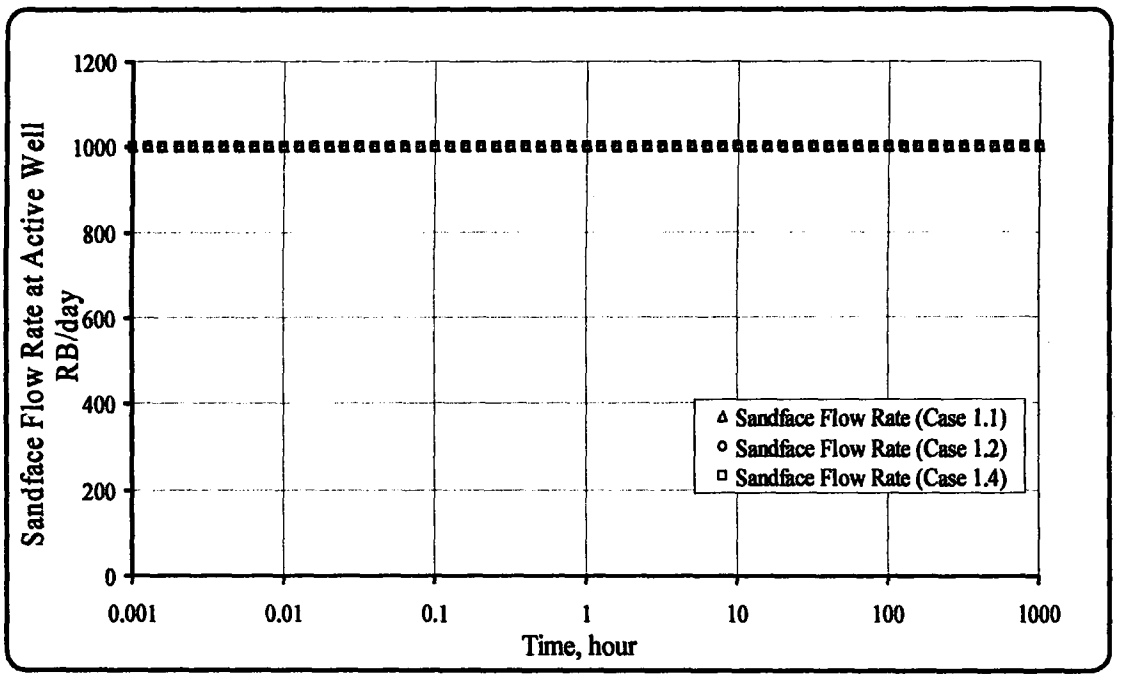

Figure 2.6 Sandface flow rate versus time at the active well for Cases 1.1-1.2-1.4.

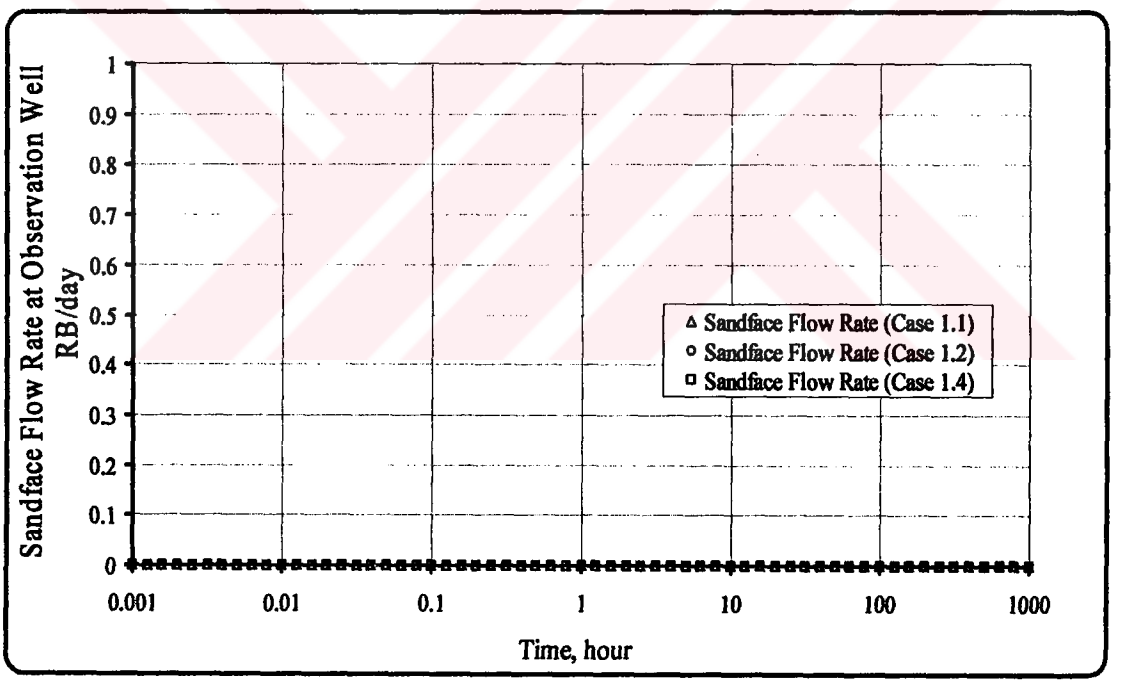

Figure 2.7 Sandface flow rate versus time at the observation well for Cases 1.1-1.2-1.4.

Figure 2.8 shows effects of wellbore storage and skin factor over pressure change and its derivative information at the active well. As you can see in Figure 2.8, wellbore storage and skin factor at the active well affect the pressure response at the active well. However, there is no any effect of wellbore storage and skin factor at the observation well over pressure signal over the active well.

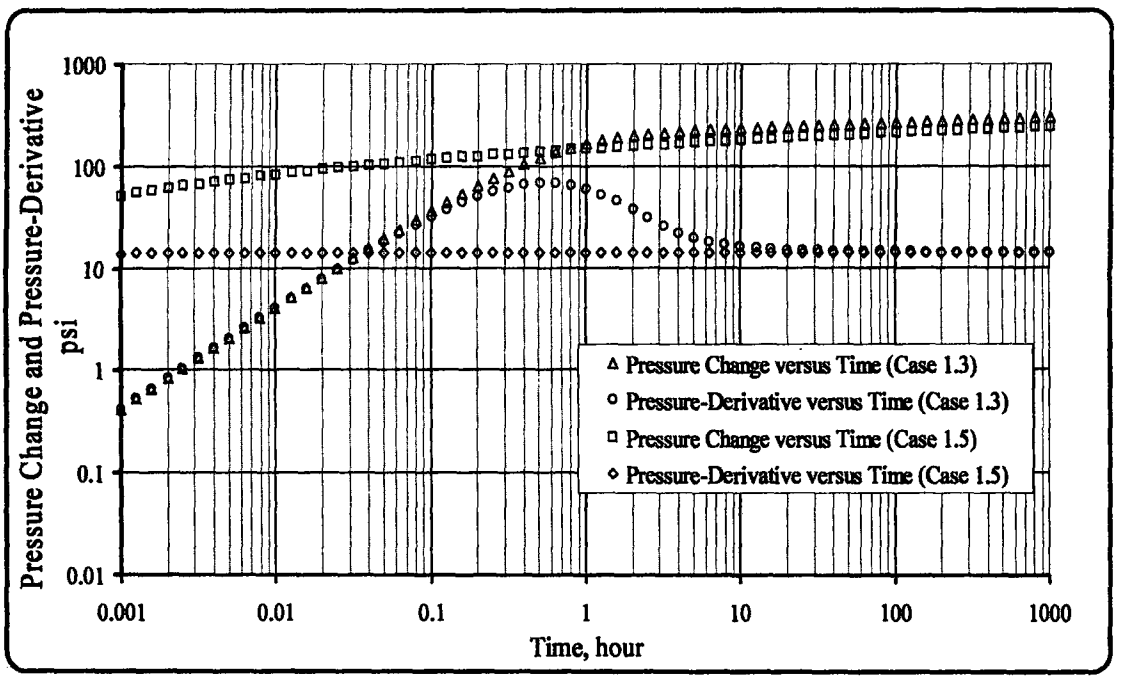

Figure 2.8 Pressure change and pressure-derivative versus time at the active well for Cases 1.3-1.5.

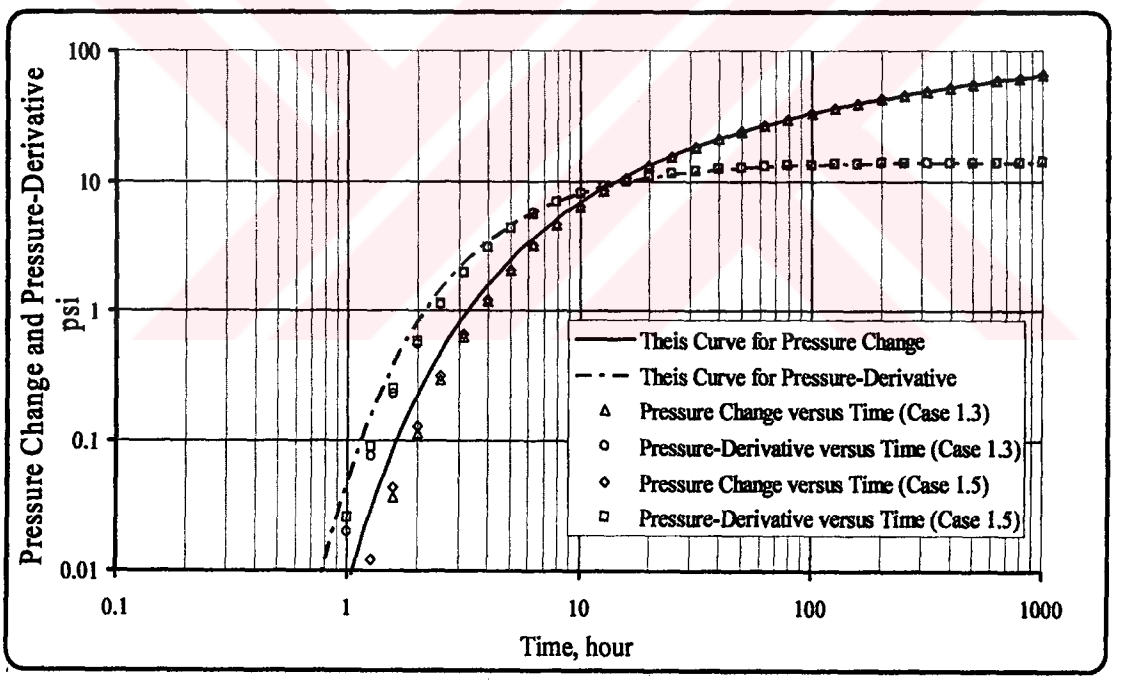

Figure 2.9 Pressure change and pressure-derivative versus time at the observation well for Cases 1.3-1.5.

Figure 2.9 shows effects of wellbore storage and skin factor for both wells over pressure response at the observation well. Apparently, at early times wellbore storage and skin term for cases 1.3-1.5 affects pressure signal at the observation well. As you can remember from Figure 2.5, only skin term at the observation well does not affect pressure signal at the observation well. However, in cases of existence of

both wellbore storage and skin factor at the observation well, it can be seen effect of wellbore storage and skin factor over pressure response at the observation well. We can also see that wellbore storage and skin factor at only active well affect pressure change at the observation well, even if there is no wellbore storage and skin factor available at the observation well. But when the wellbore storage effects disappear at late times, all pressure data match with the Theis curve.

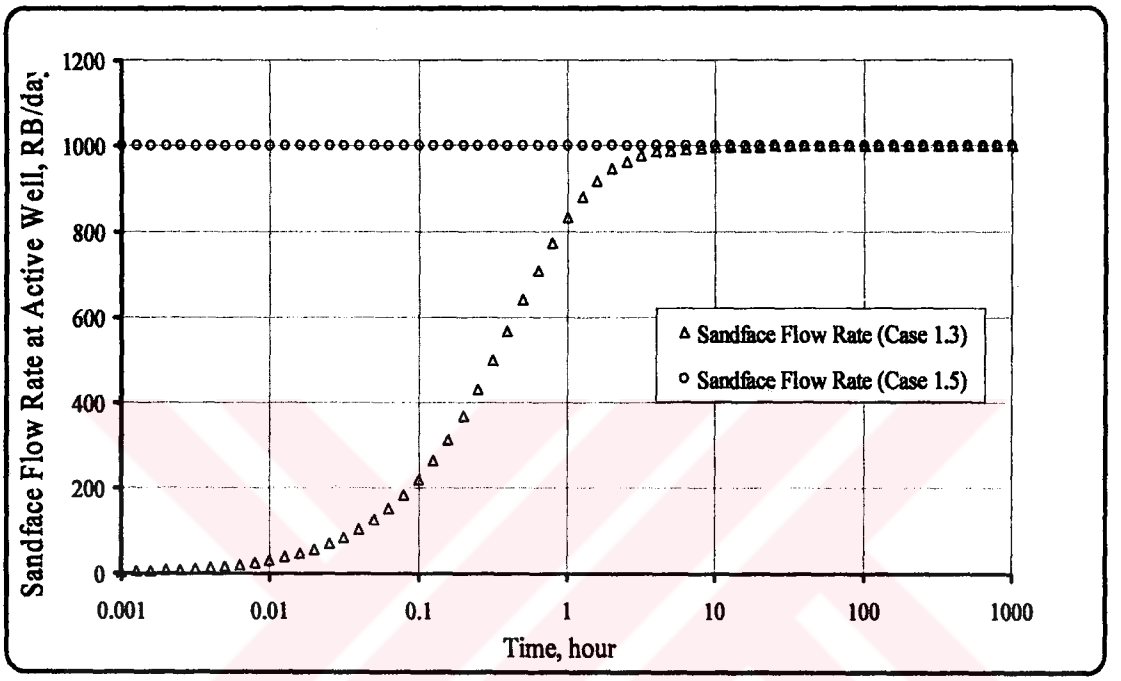

Figure 2.10 Sandface flow rate versus time at the active well for Cases 1.3-1.5.

Figure 2.10 illustrates sandface flow rate changes at the active well. Nonexistence of wellbore storage and skin factor (Case 1.5) at the active well causes that sandface flow rate remains constant. Moreover existence of wellbore storage and skin factor at the observation well does not cause to change sandface flow rate at the active well, due to the fact that there is no production from surface at the observation well. However, when wellbore storage and skin factor exist in the active well (Case 1.3), sandface flow rate changes from zero to surface production rate at the active well until wellbore storage effects dissappear at the active well.

Figure 2.11 shows sandface flow rate changes at the observation well. Since wellbore storage and skin factor does not exist in the observation well (Case 1.3), sandface flow rate does not change in terms of time at the observation well even if wellbore storage and skin factor exist in the active well. However, in case of existence of wellbore storage and skin factor at the observation well (Case 1.5),

injection fron wellbore through layer occurs at the active well. Sandface flow rate decreases from zero to -2.1 RB/day (minus means injection) sharply after 1 hour production time and then sandface flow rate begins to increase after 10^{th} hour from -2.1 RB/day toward zero gradually, because of wellbore storage at the observation well, though there is no available surface flow rate at the observation well. Injection occurs between 1 and 10 hours by expanding fluid volume in the wellbore at the observation well and then injection from the wellbore through the layer begins decreasing from 2.1 RB/day to zero, because fluid in the wellbore cannot expand any more at the observation well.

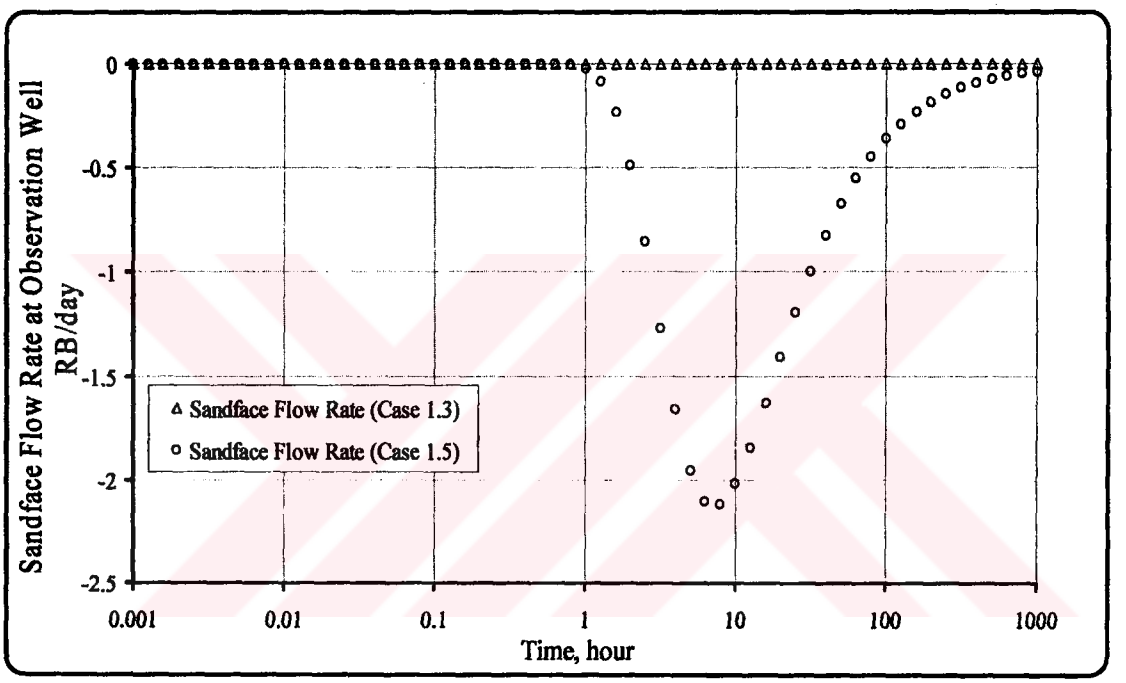

Figure 2.11 Sandface flow rate versus time at the observation well for Cases 1.3-1.5.

Figure 2.12 shows log-log plots of pressure change and pressure-derivative versus time for the active well. Since wellbore storage and skin factor exist in the active well for each cases 1.3-1.6-1.7, a unit-sloped line occurs at early times till about 18 minutes. Wellbore storage and/or skin factor at the observation well does not affect pressure change and its derivative at the active well, because of nonexistence of surface production rate at the observation well.

Figure 2.13 illustrate log-log plots of pressure change and its derivative versus time at the observation well. Wellbore storage and skin factor at the active well (Case 1.3) affect pressure signal at the observation well, even if there is no wellbore storage and skin factor at the observation well. Only skin factor but not

wellbore storage at the observation well (Case 1.6) does not affect pressure change and its derivative at the observation well. However, both wellbore storage and skin factor at the observation well (Case 1.7) affect pressure change and its derivative at the observation well.

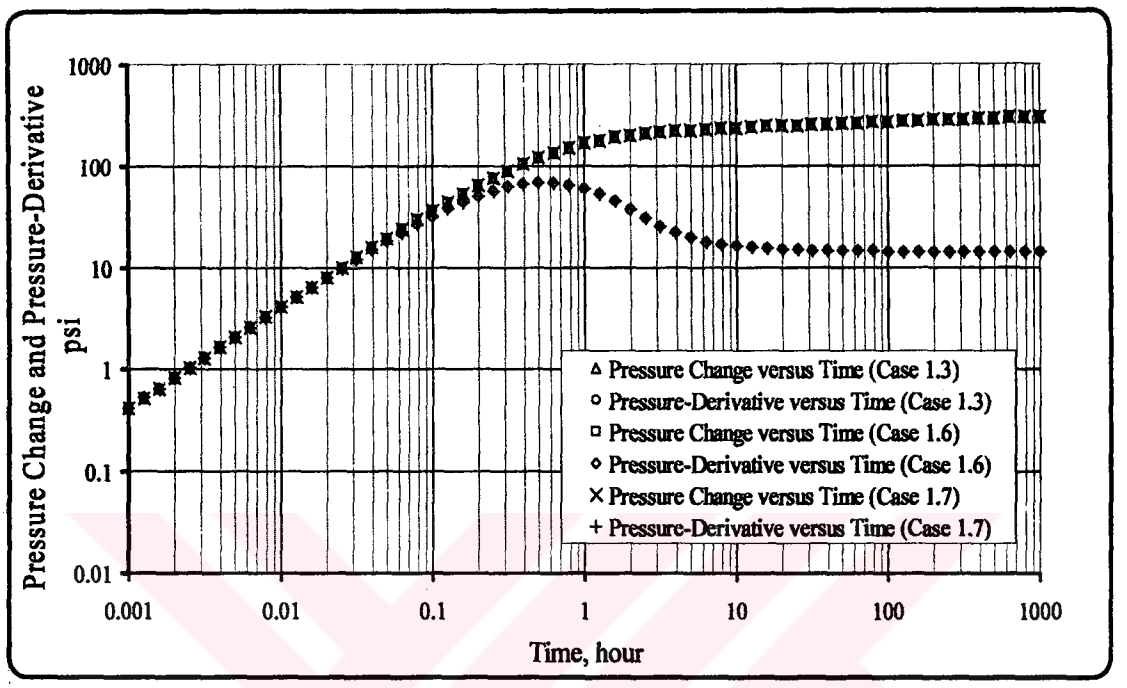

Figure 2.12 Pressure change and pressure-derivative versus time at the active well for Cases 1.3-1.6-1.7.

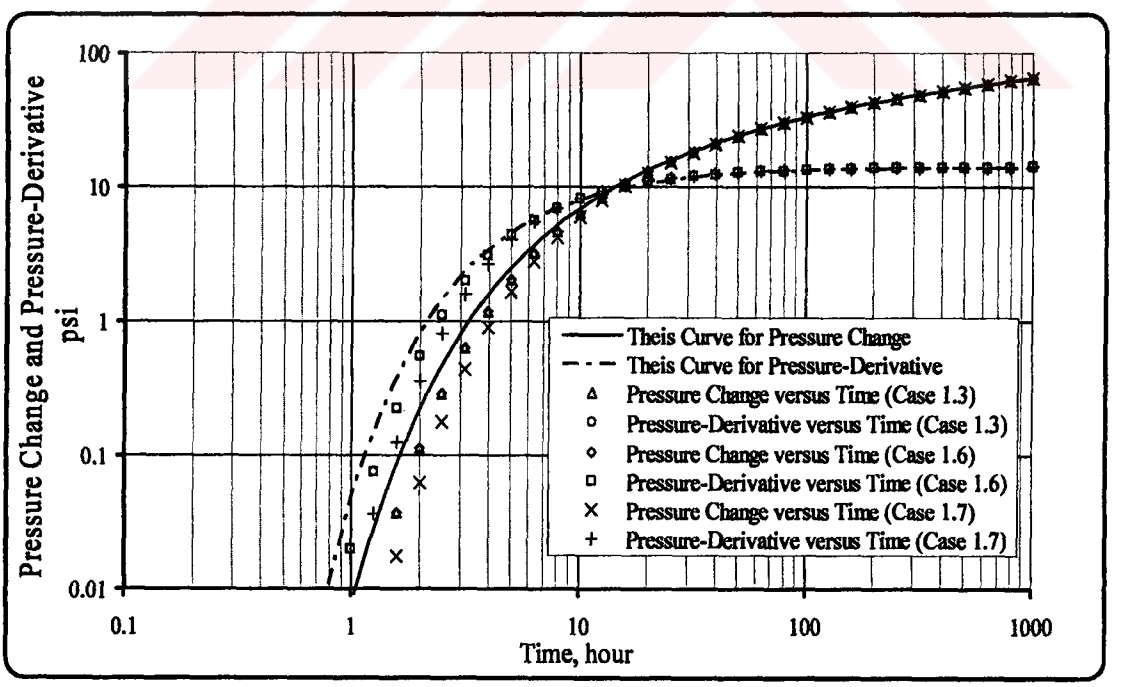

Figure 2.13 Pressure change and pressure-derivative versus time at the observation well for Cases 1.3-1.6-1.7.

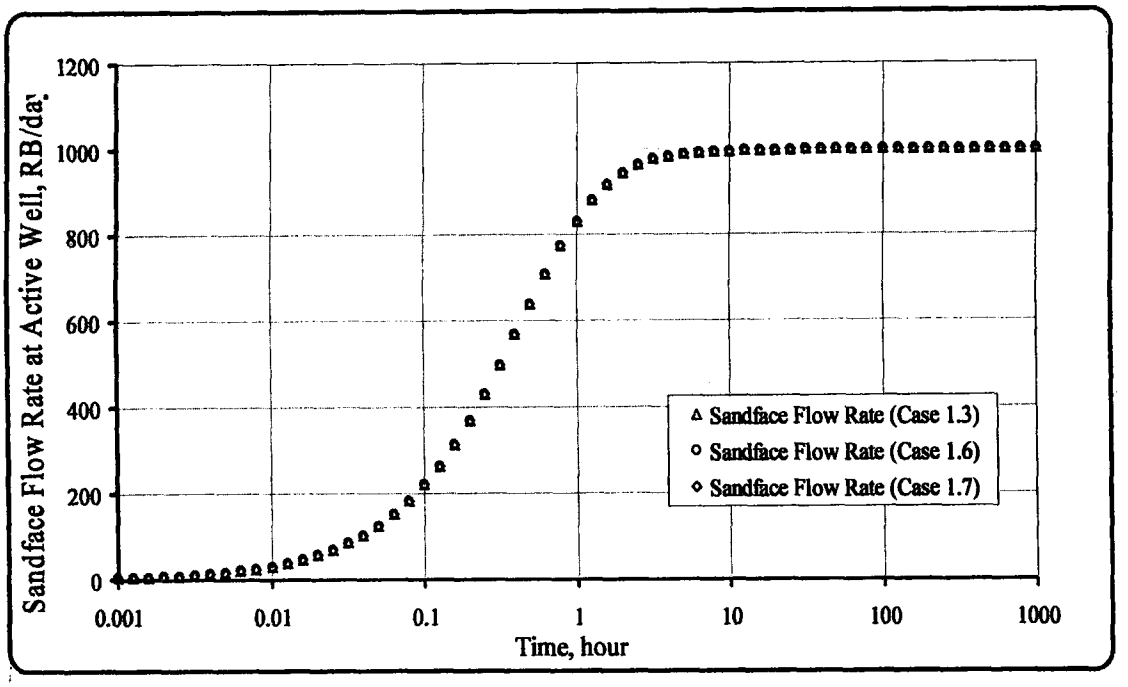

Figure 2.14 Sandface flow rate versus time at the active well for Cases 1.3-1.6-1.7.

Figure 2.14 shows plots of sandface flow rate versus time at the active well for each cases 1.3-1.6-1.7. Since wellbore storage for each cases 1.3-1.6-1.7 exists in the active well, active well produces fluid at early times from wellbore instead of reservoir due to expanding volume of fluid in the active well. After 10 hours, wellbore storage effects at the active well begin decrasing and then the active well begins producing fluid truly from reservoir. In the same manner, Figure 2.15 shows plots of sandface flow rate versus time at the observation well for each cases 1.3-1.6-1.7. In cases 1.3-1.6, since wellbore storage does not exist in the observation well, sandface flow rate at the observation well remains zero, though there is a skin factor available at the observation well. Moreover, wellbore storage and skin factor (Case 1.6) at the active well does not affect sandface flow rate at the observation well, because of nonexistence of wellbore storage at the observation well. However, when both wellbore storage and skin factor exist in the observation well, injection occurs from the wellbore at the observation well thtough the reservoir. Injection occurs between 1 and 10 hours by expanding fluid volume in the wellbore at the observation well and after 10 hours injection from the wellbore through the reservoir begins decreasing from 2.1 RB/day to zero, because fluid in the wellbore cannot expand any more at the observation well.

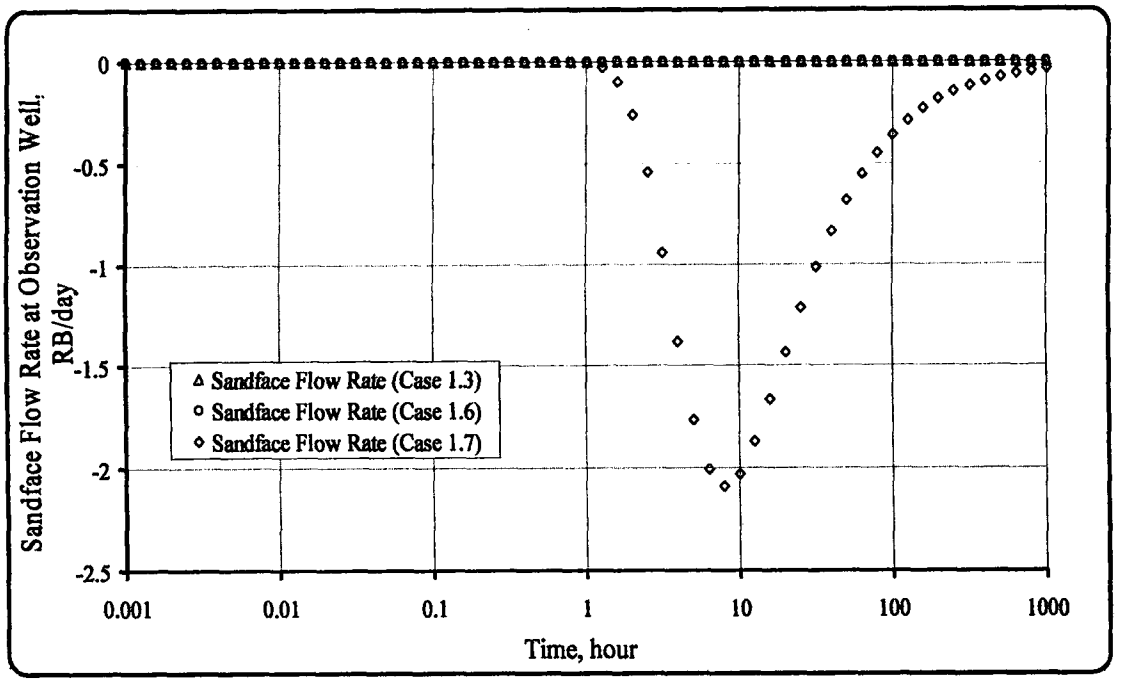

Figure 2.15 Sandface flow rate versus time at the observation well for Cases 1.3-1.6-1.7.

2.4.2 Single-Layered System 2 : This case study considers again single layer system with an active well and an observation well.

Table 2.6 Wellbore data for different cases (2).

	Active Well		**Observation Well**	
Cases	C_a, *RB/psi*	S_a	C_o, *RB/psi*	S_o
2.1	**0.5**	**0**	**5**	**0**
2.2	**0.5**	**0.5**	**5**	**5**

The active well is produced at a specified surface flow rate with $q_{as} = 1000\, RB/day$, and the second well (the observation well or interference well) is shut-in for all times. Using information above, sandface flow rate, pressure and pressure derivative values versus time were computed in each well and then their graphics were plotted here. The objective of this case is considering study interference test pressure behavior in a single layer system for various cases. Reservoir properties are given in Table 2.2 and other parameters such as wellbore storage and skin factor are given above in Table 2.6.

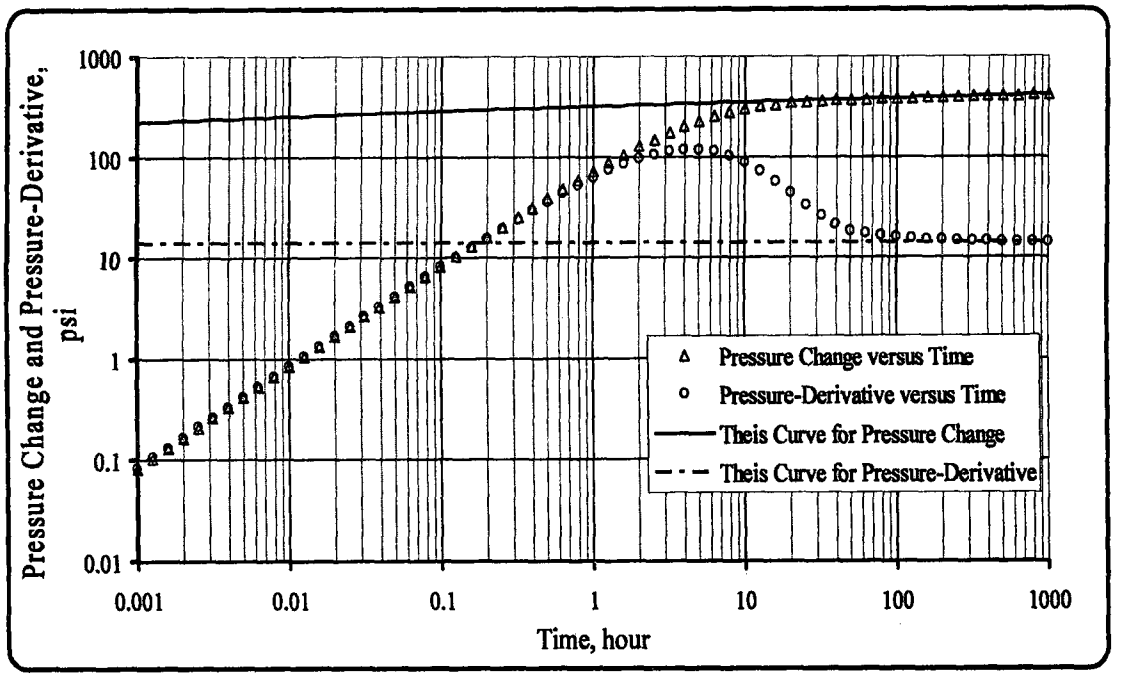

Figure 2.16 Pressure change and pressure-derivative versus time at the active well for Case 2.1.

As can be seen from Figure 2.16, pressure change and pressure-derivative are shown on the same graph. A unit-sloped line is seen at early times till approximately 1 hour, because of existence of wellbore storage effect. After 1 hour, pressure-derivative curve starts separating from pressure changes curve, due to the fact that there is wellbore storage and skin effects at the active well. Size of hump seen after approximately 100 hours is controlled by wellbore storage at the active well. In Figure 2.17, pressure change and pressure-derivative are shown at the observation well. Wellbore storage at the active well causes to a small hump among 10 and 100 hours. In both Figure 2.16 and Figure 2.17, radial flow is seen after about 100 hours. In Figure 2.18, sandface flow rates are shown at both active and observation wells. Since active well has wellbore storage effect, production at surface is done from wellbore until about 50 hours. Since observation well shuts-in at all production time and there is no wellbore storage and skin effects, sandface flow rate at observation well equals to zero at all times.

As can be seen from Figure 2.19, pressure change and pressure-derivative at the active well are shown on the same graph. A unit-sloped line is seen at early times till approximately 1 hour, because of existence of wellbore storage effect as been in Figure 2.16. Differently from Case 2.1, size of hump in Figure 2.20 is greater than

that in Figure 2.17, because there is wellbore storage and skin effects at observation well though there is no surface production.

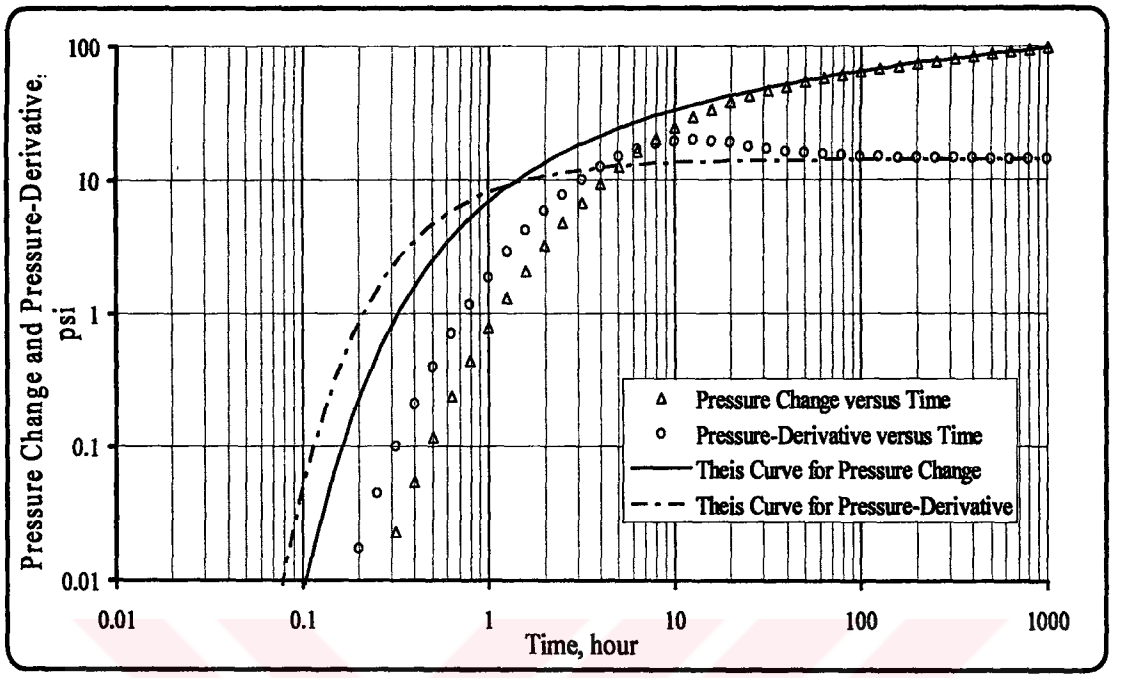

Figure 2.17 Pressure change and pressure-derivative versus time at the observation well for Case 2.1.

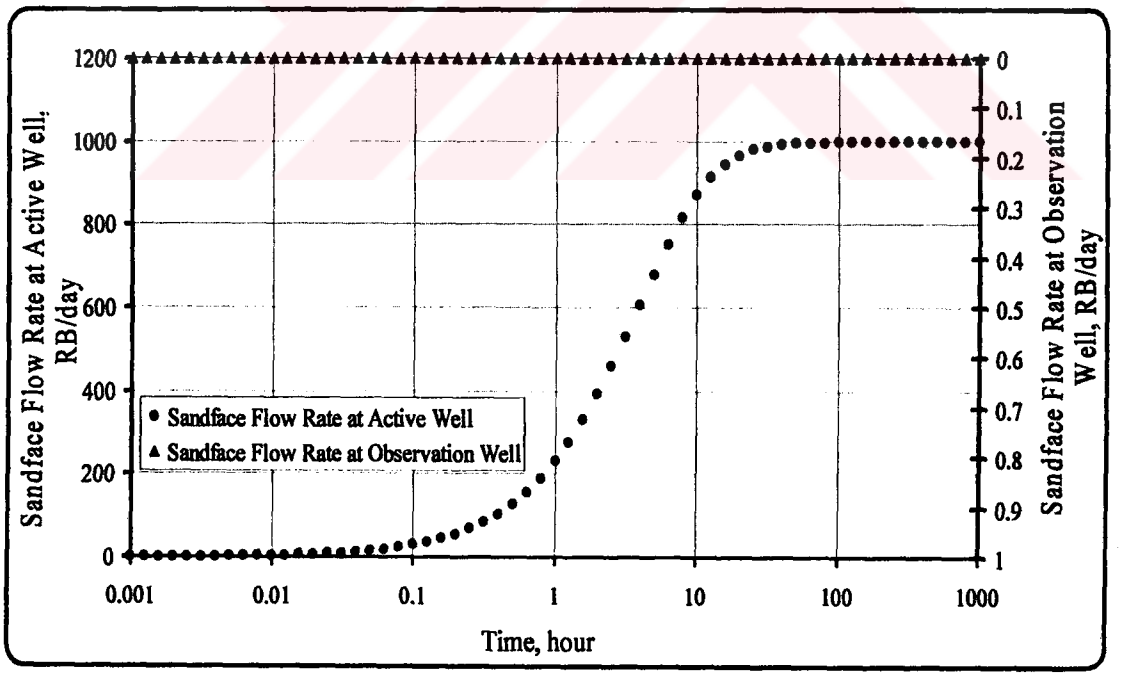

Figure 2.18 Sandface flow rates versus time at the active and observation wells for Case 2.1.

In Figure 2.21, sandface flow rates are shown at the active and observation wells. Since the active well has wellbore storage effect, production at surface is done

from wellbore until about 50 hours. Since the observation well has wellbore storage and skin effects though there is no surface production, sandface flow rate toward reservoir increases among 0.8 and 10 hours, because of expanding of fluid volume in wellbore. After 10 hours, the active well produces from surroundings observation well, because fluid in wellbore of observation well couldn't expand any more. Therefore, injection from observation well to active well starts decreasing after about 10 hours.

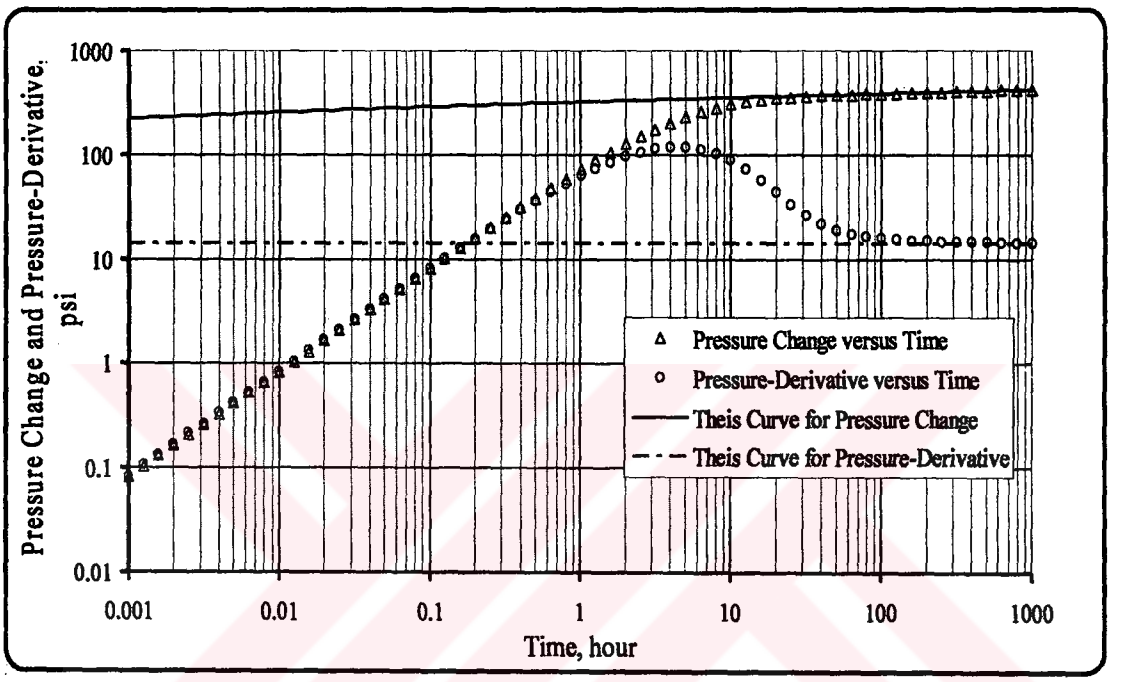

Figure 2.19 Pressure change and pressure-derivative versus time at the active well for Case 2.2.

In Figure 2.22, pressure changes and pressure-derivative curves in Case 2.1 and Case 2.2 are shown on the same graph. Although wellbore storage and skin effects are different from each other in both cases, pressure changes and pressure-derivative curves matches at late times. Namely, effects of wellbore storage and skin factor don't appear over pressure changes and pressure-derivative curves.

In Figure 2.23, sandface flow rate curves at the active well and observation well are shown on the same graph. Existence of wellbore storage and skin effects at the observation well doesn't affect sandface flow rate at the active well. However, existence of wellbore storage at observation well affect sandface flow rate at observation well.

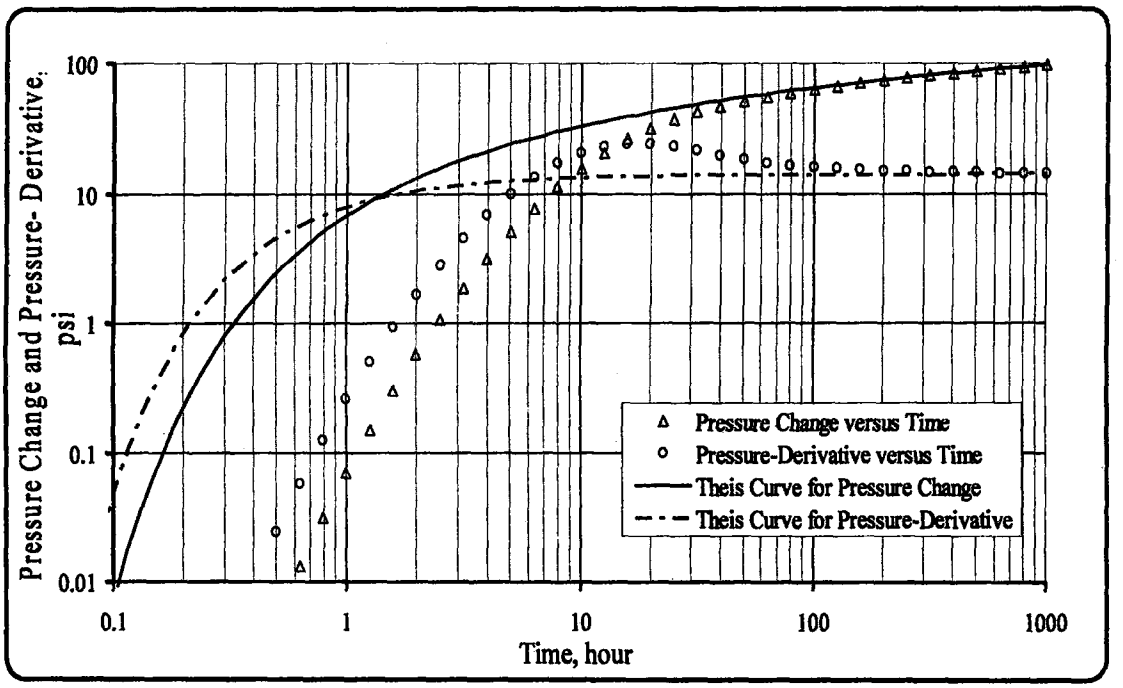

Figure 2.20 Pressure change and pressure-derivative versus time at the observation well for Case 2.2.

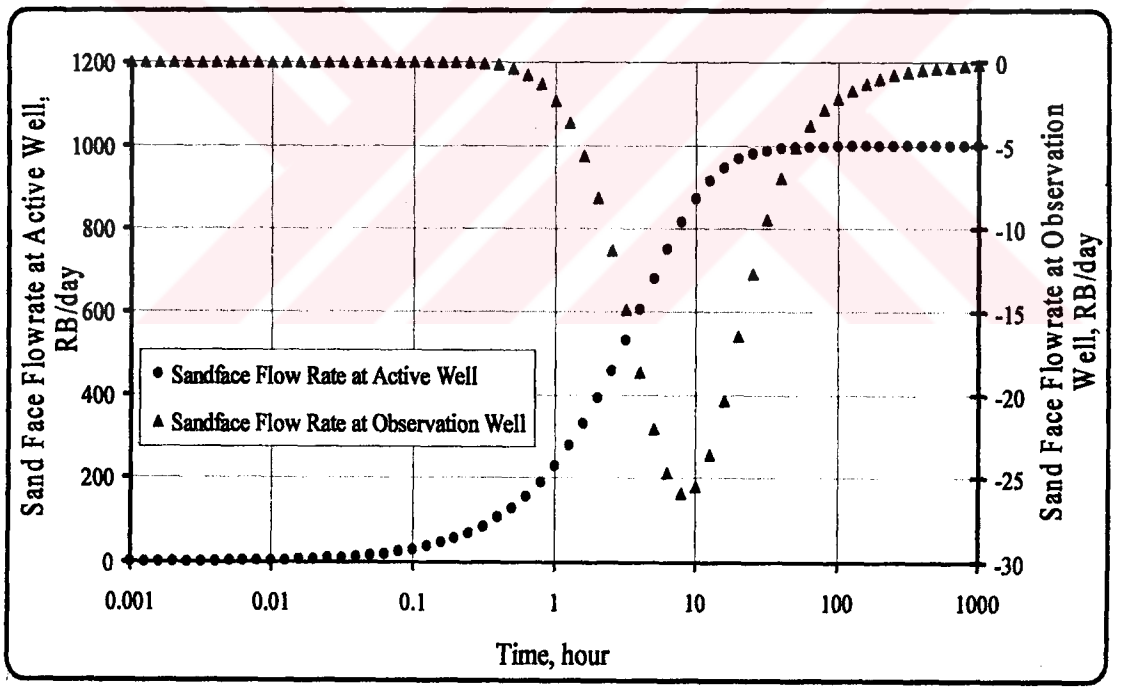

Figure 2.21 Sandface flow rates versus time at the active and observation wells for Case 2.2.

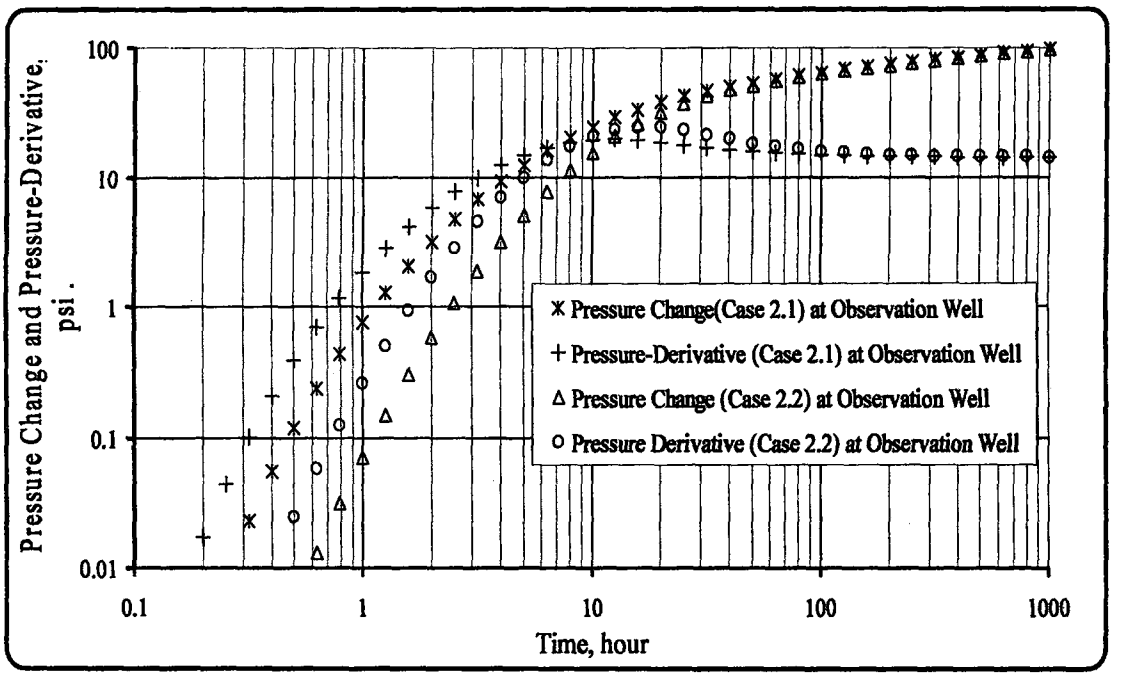

Figure 2.22 Pressure change and pressure-derivative versus time at the observation well for Case 2.3.

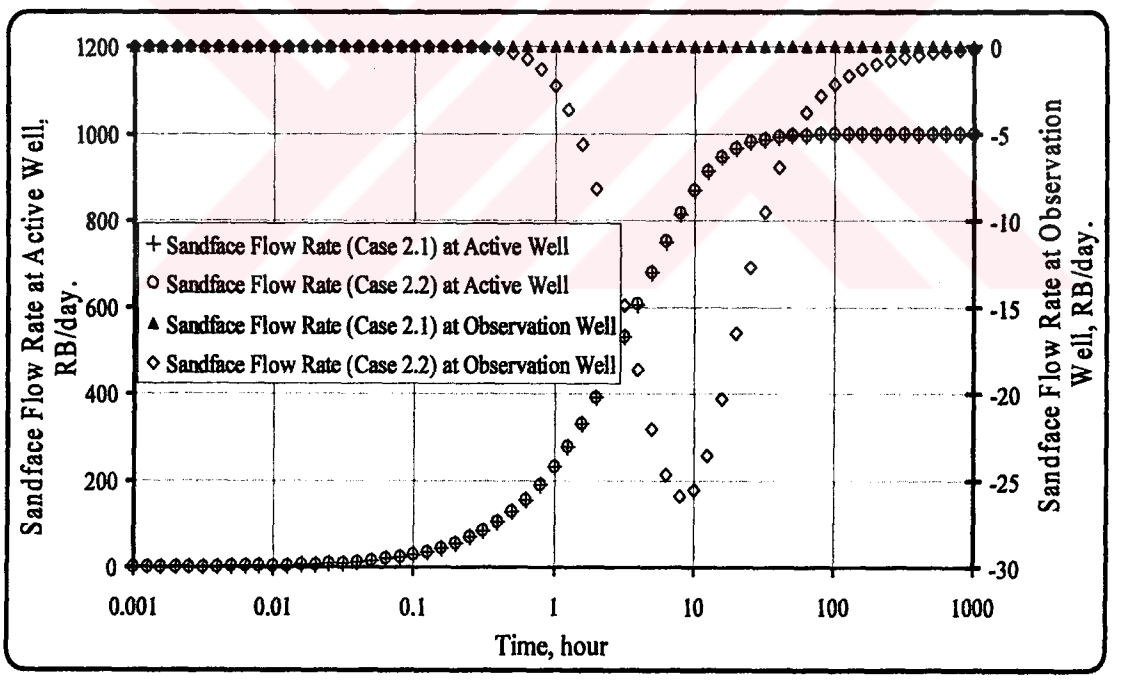

Figure 2.23 Sandface flow rates versus time at the active and observation wells for Case 2.3.

2.4.3 Single-Layered System 3 : In this application study, there are seven different substudies related to how distance between active and observation wells, wellbore storage/skin factors, permeability and porosity affect pressure signal at both wells especially observation well. In direction of this purpose, figures are given in this

section below. In addition to these, pressure signals belonging to observation well are shown with reference line source (Theis) solution which doesn't take into consideration wellbore storage effects at both wells. Reservoir properties are given in Table 2.2.

2.4.3.1 Case 3.1 : In this case, to see how the wellbore storage/skin terms affect pressure changes and pressure-derivative data at the active and the observation well, several computations were done in forward mode. In this case, parameters belonging to active and observation wells such as wellbore storage and skin effects were used as $C_a = C_o = 0.5\,RB/psi$, *and* $s_a = s_o = 5$ where C_a and C_o denote wellbore storages at active and observation wells, respectively. s_a and s_o denotes skin effects at active and observation wells, respectively. Furthermore, the active well produces at constant surface rate q_{sa}=1000 RB/day and the observation well shut-in at all times (q_{so}=0 RB/day) during interference test.

In Figure 2.24, pressure change and pressure-derivative at active well are shown with line source solution. As seen in the figure, line source solution (E1 reference solution) demonstrates a very serious deviation from pressure changes and pressure-derivative curves at early times (until approximately 10 and/or 100 hours). Cause of this behaviour results from wellbore storage at the active well. Since line source solution doesn't take into account wellbore storage effects though it takes into account skin terms at both wells, all pressure data don't match with reference solutions at all times. However, pressure changes and pressure derivative curves with wellbore storage effects begin matching line source solution (E1 reference solution) after about 100 hours, because wellbore storage effects appear only at early times.

In Figure 2.25, pressure changes and pressure-derivative at the observation well are shown with reference solutions. Comparison of pressure changes and pressure-derivative to reference solutions is shown on this figure as been in Figure 2.24. Interference test data don't match reference solutions at early times until approximately 10~100 hours, because wellbore storage effects are available at the active and observation wells. Wellbore storage effects are available at both wells, reference solutions separate from interference test data at early times. Namely in this period, the active well produces from wellbore not only reservoir. Since wellbore storage effects don't appear over pressure data at late times, pressure changes and

pressure-derivative data match reference solution at the observation well, as been at active well in Figure 2.24. When the time goes ahead, wellbore storage effects start disappearing at both wells.

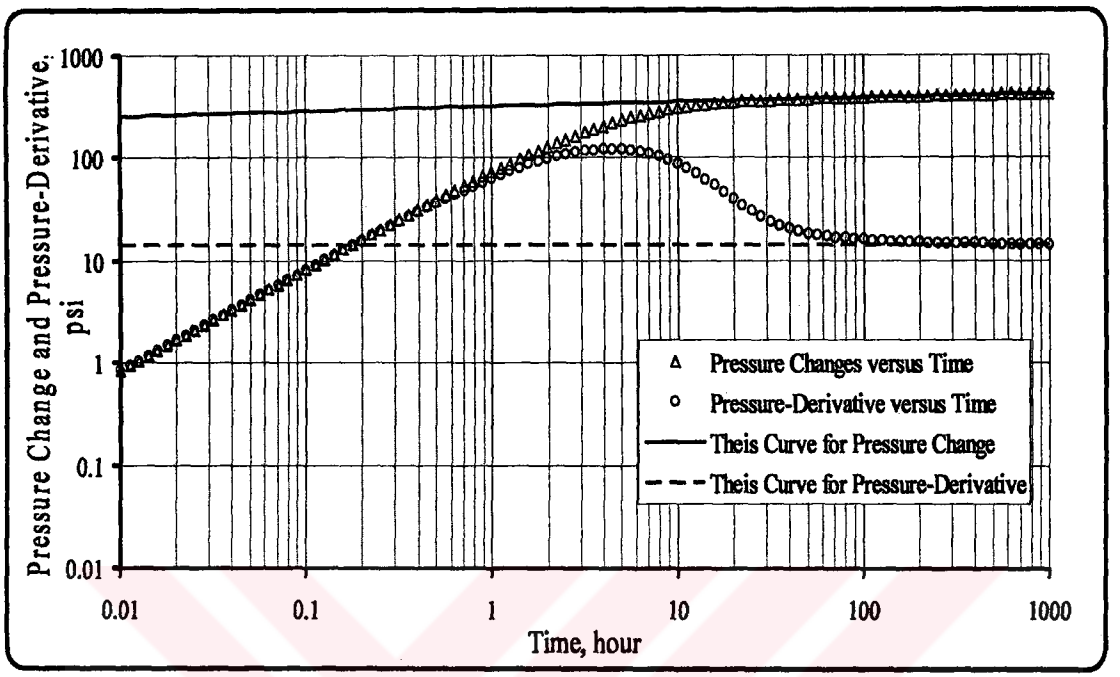

Figure 2.24 Pressure change and pressure-derivative versus time at the active well together with line source solution (E1).

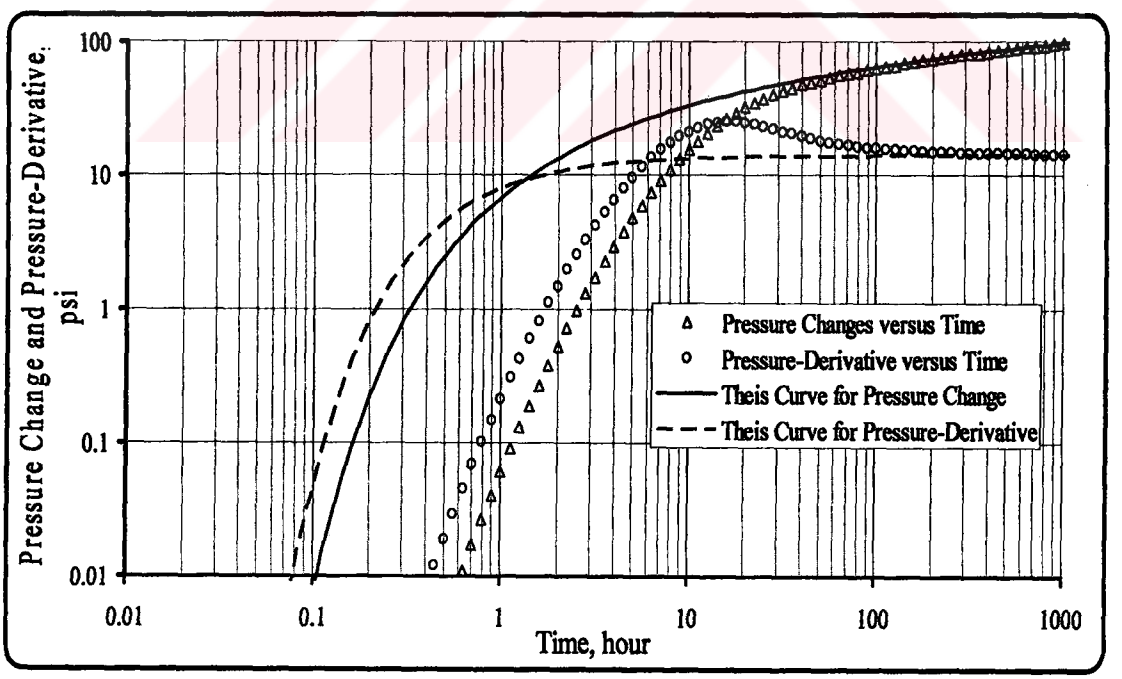

Figure 2.25 Pressure change and pressure-derivative versus time at the observation well together with line source solution (E1).

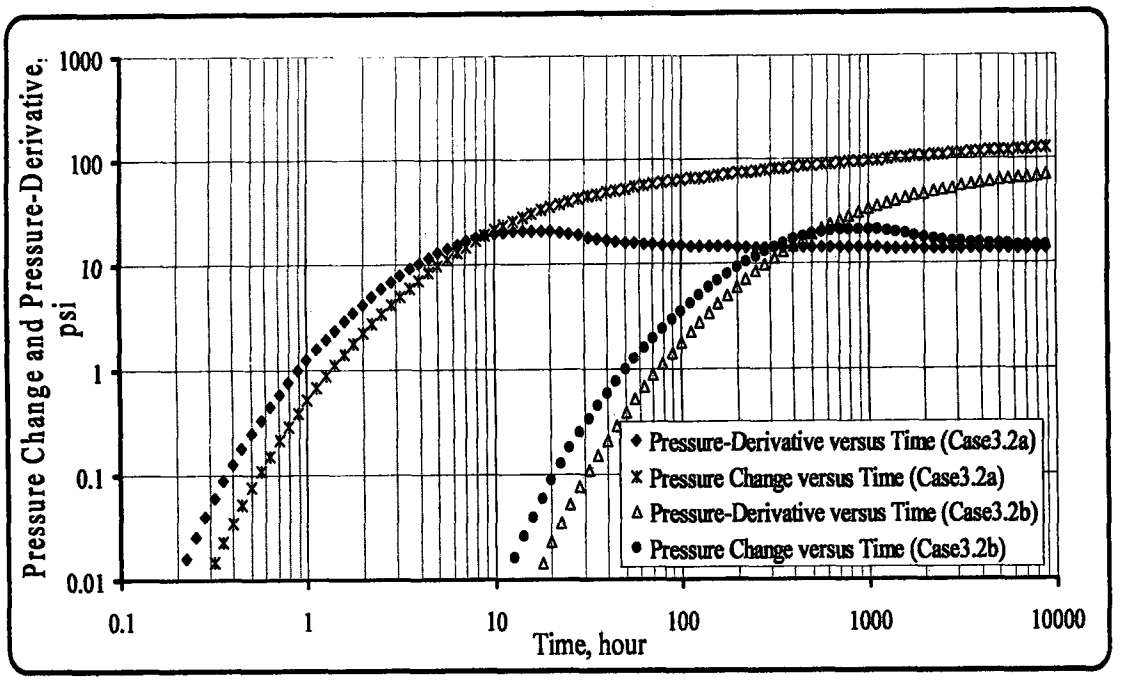

Figure 2.28 Demonstration of both curve sets in Cases 3.2a and 3.2b on the same graph.

When we look at Figure 2.28, interference test data belonging to both Subsections 2.a and 2.b begin matching each other after approximately 10000 hours. Reason of this behavior can be explained like that distance between both wells and wellbore storage/skin effects disappear at very late times, because we takes into consideration an infinite acting reservoir.

2.4.3.3 Case 3.3 : In this case, one-layered reservoir system is considered as been in Case 3.2. Basic parameters such as viscosity, porosity, total compressibility, layer thickness, radii of both wells and distance between active and observation wells are the same as values in Table 2.2. This case is divided to two different subsections where permeabilities belonging to the reservoir have different numerical values. Wellbore storages and skin effects aren't present at both wells. Furthermore, the active well produces at constant surface rate q_{sa}=1000 RB/day and the observation well shut-in at all times (q_{so}=0 RB/day) during interference test, as been in Case 3.2. Subsections are given below :

Subsection 3.a : $k = 1000\,md$

Subsection 3.b : $k = 0.1\ md$

Pressure change and pressure-derivative data belonging to these Subsections 3.a and 3.b are shown given below figures by comparing with line source solutions.

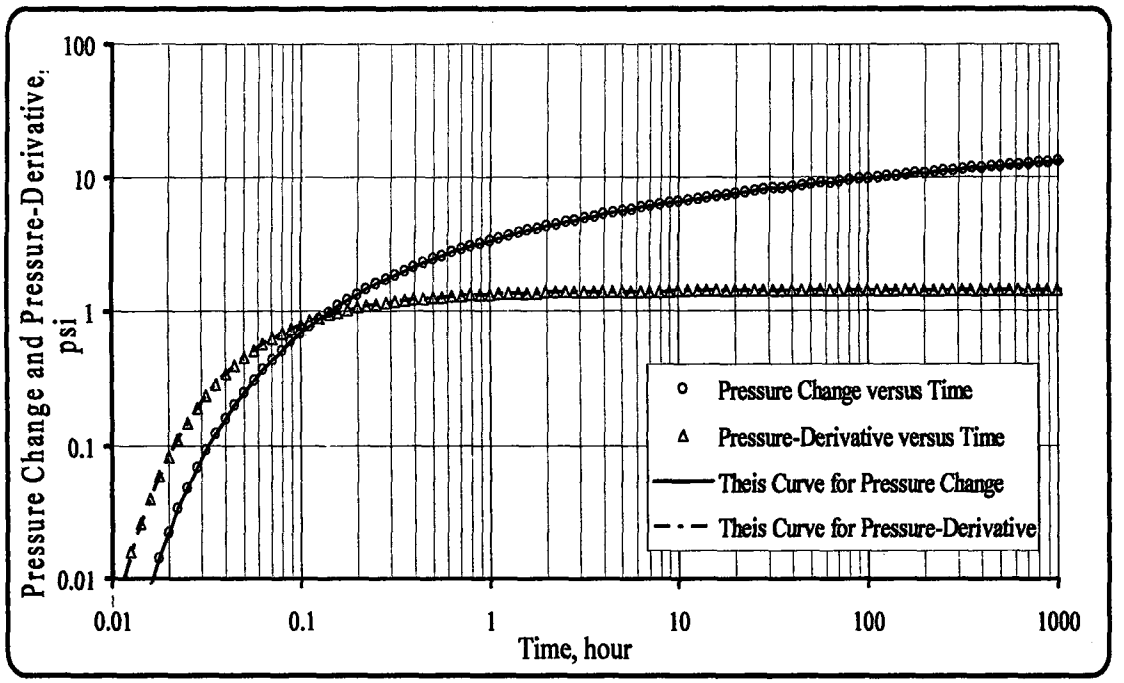

Figure 2.29 Pressure change and pressure-derivative versus time at the observation well together with line source solution for Case 3.3. ($k = 1000$ *md*)

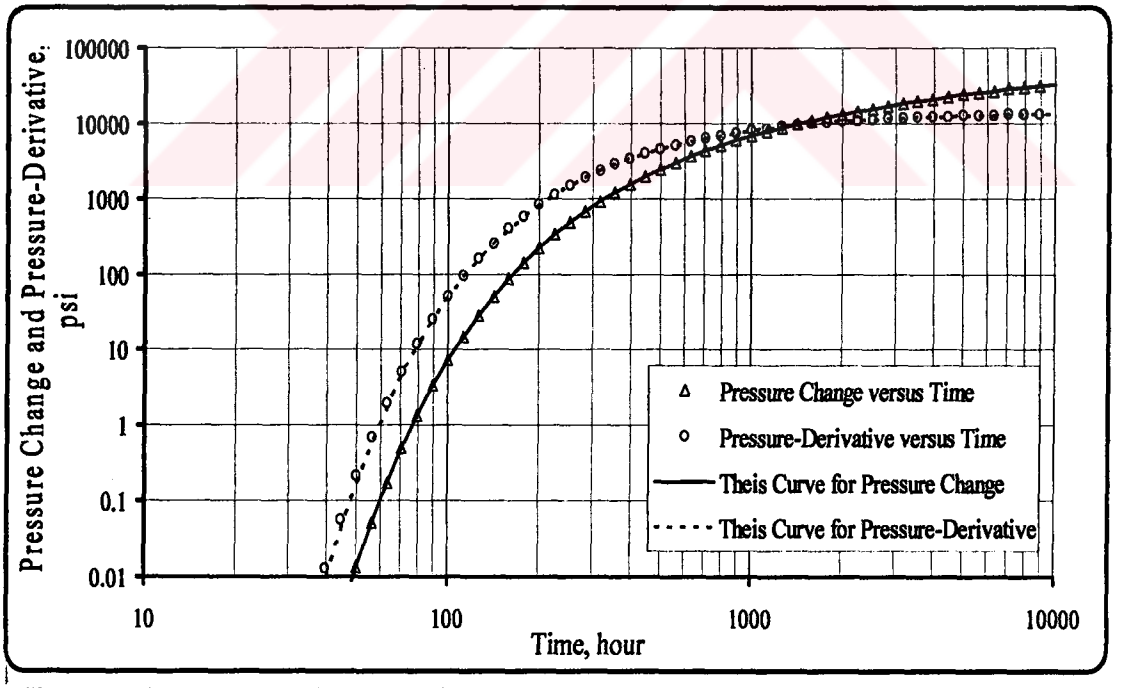

Figure 2.30 Pressure change and pressure-derivative versus time at the observation well together with line source solution for Case 3.3. ($k = 0.1$ *md*)

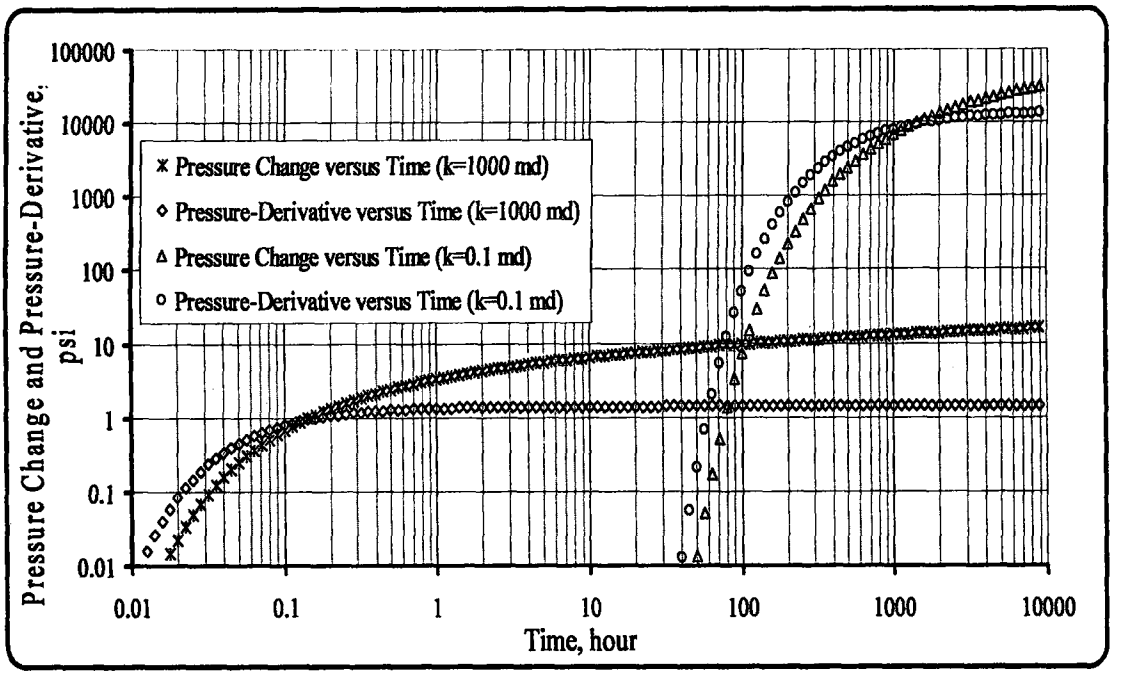

Figure 2.31 Interference well test data belonging to both subsections versus time at the observation well with line source solution for Case 3.3.

As can be seen from the results given in Figures 2.31, as permeability increases, the effect of production at the active well on the observation well pressure change is felt in a short time and that magnitude of pressure drop at the observation well decreases. In Subsection 3.a, since permeability parameter has 1000 md numerical value, bottom hole flow pressure needs to be decreased as much as ~1 psi to produce with surface flow rate (q_{sa} = 1000 RB/day) from the active well. Namely in order to reach the radial flow in reservoir, it is enough that bottom hole flow pressure drop is set to about 1 psi. Figure 2.30 displays interference well test data belonging to an impermeable/little permeable reservoir. In Subcase 3.b (shown by Figure 2.30), in order to reach the radial flow in reservoir, bottom hole flow pressure drop at observation well needs to be increased considerably until approximately 10000 psi. Figure 2.31 is a combined form of Figures 2.29 and 2.30. It's show that permeability is a very sensitive parameter, because interference well test data changes considerably by altering only permeability.

2.4.3.4 Case 3.4 : In this case, all parameters are the same as been in Case 3.3 except for permeability and porosity. Effect of porosity over interference well test data is investigated differently from Case 3.2. This case is again divided to two subcases taking into account different porosity values. Reservoir is considered as single layered system with 100 md of permeability. In this case, it is accepted that there

aren't wellbore storage and skin effects at both wells like Case 3.3. On the other hand, other parameters are the same as been in Table 2.2. The active well is produced at a constant rate with 1000 RB/day and the observation well is shut-in at all times.

Subsection 4.a : $\phi = 0.15$ (porosity)

Subsection 4.b : $\phi = 0.015$ (")

Pressure change and pressure-derivative data at observation well belonging to these two subsections are shown by figures given below. As can be seen from Figures 2.32 and 2.33, interference well test data matches line source solution perfectly, because wellbore storages and skin effects aren't available at both wells. Figure 2.34 displays two interference well test pressure data for two different values of porosity at the observation well. Pressure drop at the observation well corresponding to $\phi = 0.15$ is less than pressure drop in a reservoir having $\phi = 0.015$. In subsection 4.a, radial flow can be appeared after 4 hours. However, in subsection 4.b, radial flow begins to be appeared after 0.4 hours, because porosities in both subsection are different from each other. Moreover, it can be seen that two interference well test data belonging to subsections 4.a and 4.b match each other at late times, as seen in Figure 2.34.

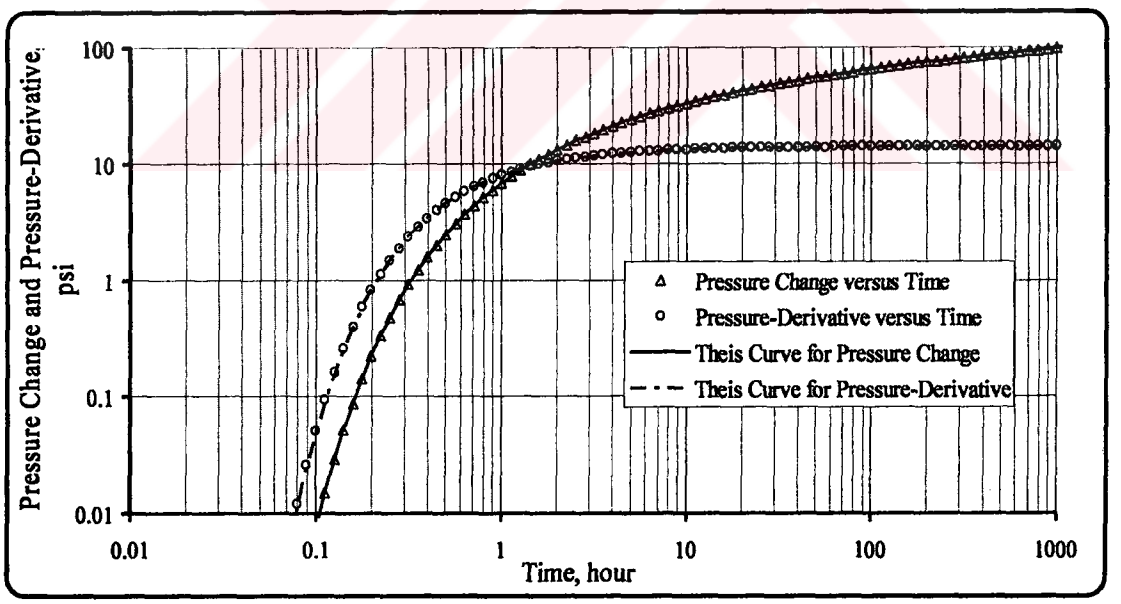

Figure 2.32 Interference well test data versus time at the observation well together with line source solution for Case 3.4. ($\phi = 0.15$)

The results also indicate that increasing porosity delays the effect of production at the active well and the observation well pressure. This is due to the fact that increasing

porosity, other parameters being the same, decreases diffusivity constant which is a measure of the speed of pressure propagation in the reservoir.

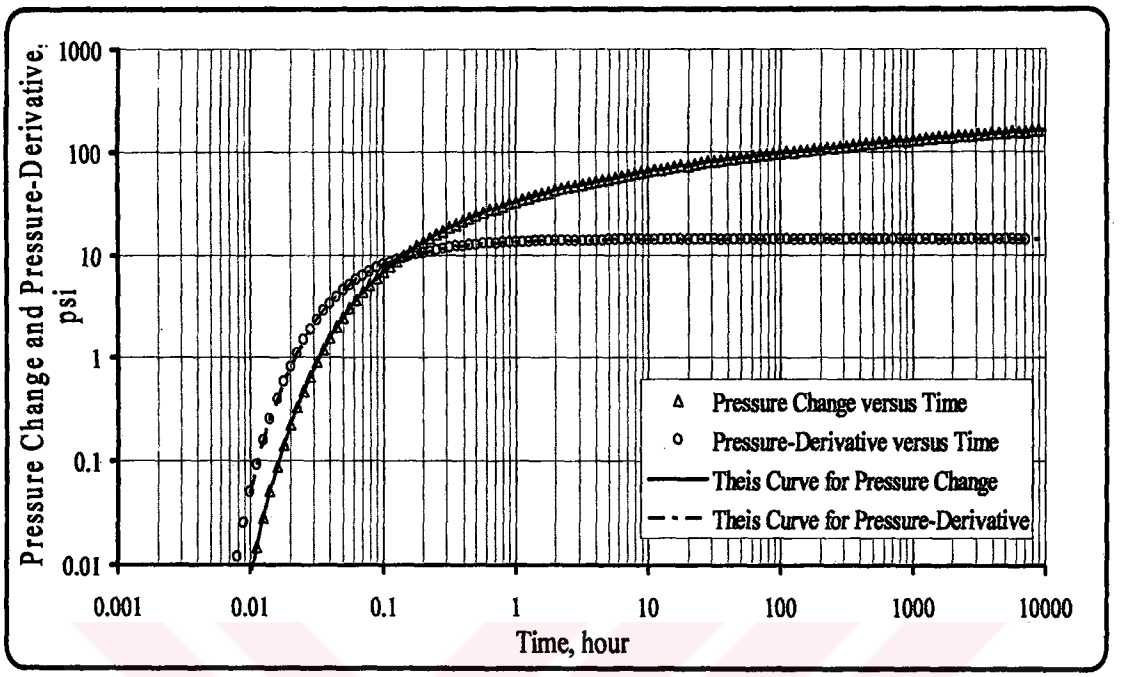

Figure 2.33 Interference well test data versus time at the observation well together with line source solution for Case 3.4. ($\phi = 0.015$)

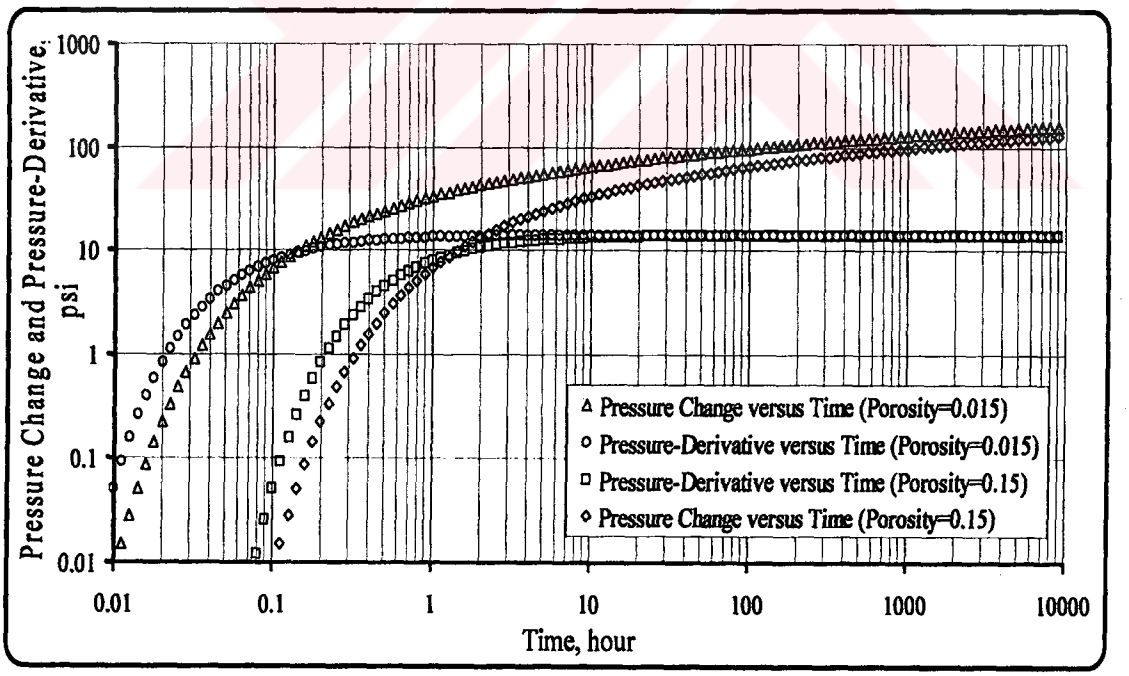

Figure 2.34 Comparison of interference well test data belonging to both subsections on the same graph for Case 3.4.

2.4.3.5 Case 3.5 : In this case, analysis of interference well test data with variable flow rate is investigated. A single layered reservoir is considered in this case and

basic parameters are the same as been in Table 2.2. Wellbore storages and skin effects are neglected at both wells for this case. Production with variable flow rate is done from active well and production scenario is given below :

q_{sa} = 100 RB/day, between t = 0 and t =10 hours
q_{sa} = 500 RB/day, between t = 10 and t =100 hours
q_{sa} = 0.0 RB/day, between t = 100 and t =500 hours
q_{sa} = 500 RB/day, between t = 500 and t =1000 hours

Figures belonging to pressure drops and sandface flow rates at both wells are given below.

Figure 2.35 displays pressure drop and sandface flow rate changes at the active and observation wells under production scenario with variable surface flow rate. Since the active well produces at a constant rate with 100 RB/day between 0 and 10 hours, pressure drop occured at the active well is four times greater than pressure drop occured at the observation well due to distance of active well from observation well. Pressure drops at the active well and observation well increase very quickly between 10 and 100 hours, because surface flow rate at the active well is risen to 500 RB/day from 100 RB/day.

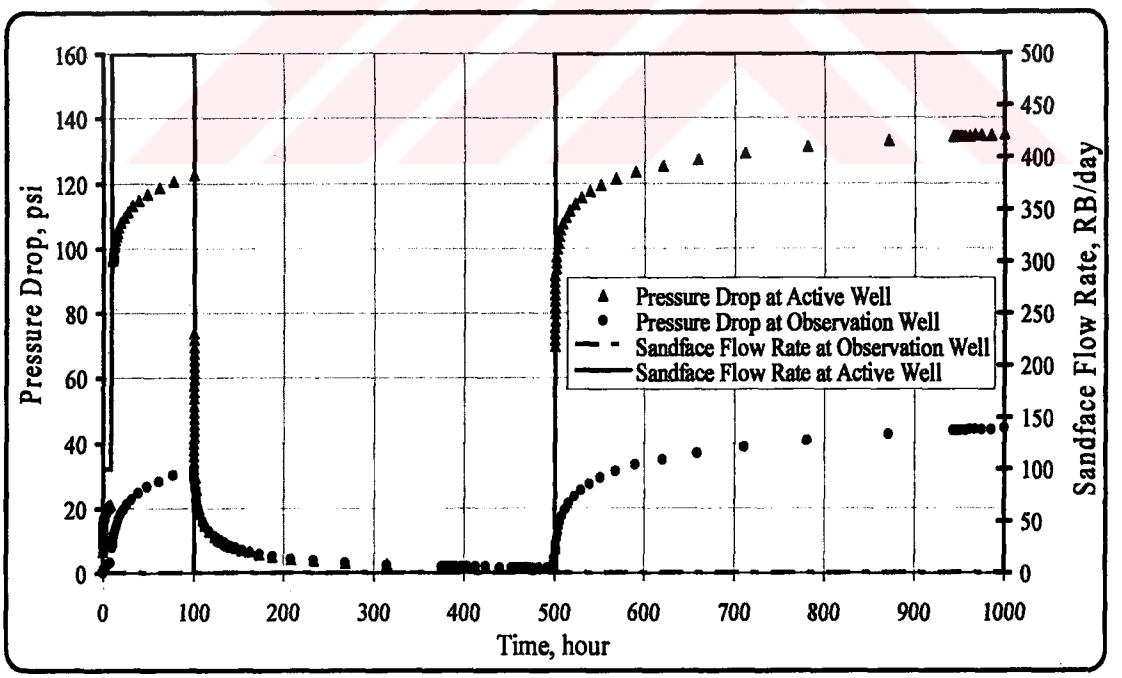

Figure 2.35 Pressure drop and sandface flow rate changes at both wells for Case 3.5.

Since the active well is shut-in between 100 and 500 hours, pressure drops at both wells decreased quickly, but after 500th hours, pressure drops at the active and

observation well begin increasing dramatically, because the active well produces at 500 RB/day from reservoir then. Sandface flow rates equal to surface total flow rate at both wells, because there aren't wellbore storages and skin effects at the active and the observation wells.

2.4.3.6 Case 3.6 : In this case, analysis of interference well test data with variable flow rate is investigated like Case 3.5. A single-layered reservoir is considered in this case and basic parameters are the same as been in Table 2.2. Wellbore storage and skin effect are neglected at only observation well for this case. There is wellbore storage and skin factor at the active well. Numerical values of these parameters belonging to the active well are $C_a = 0.1\,RB/psi$ and $s_a = 10$. As been in Case 3.5, production with variable flow rate is done from active well and production scenario is given below :

q_{sa} = 100 RB/day, between t = 0 and t =10 hours
q_{sa} = 500 RB/day, between t = 10 and t =100 hours
q_{sa} = 0.0 RB/day, between t = 100 and t =500 hours
q_{sa} = 500 RB/day, between t = 500 and t =1000 hours

Figures belonging to pressure drops and sandface flow rates at both wells are given below.

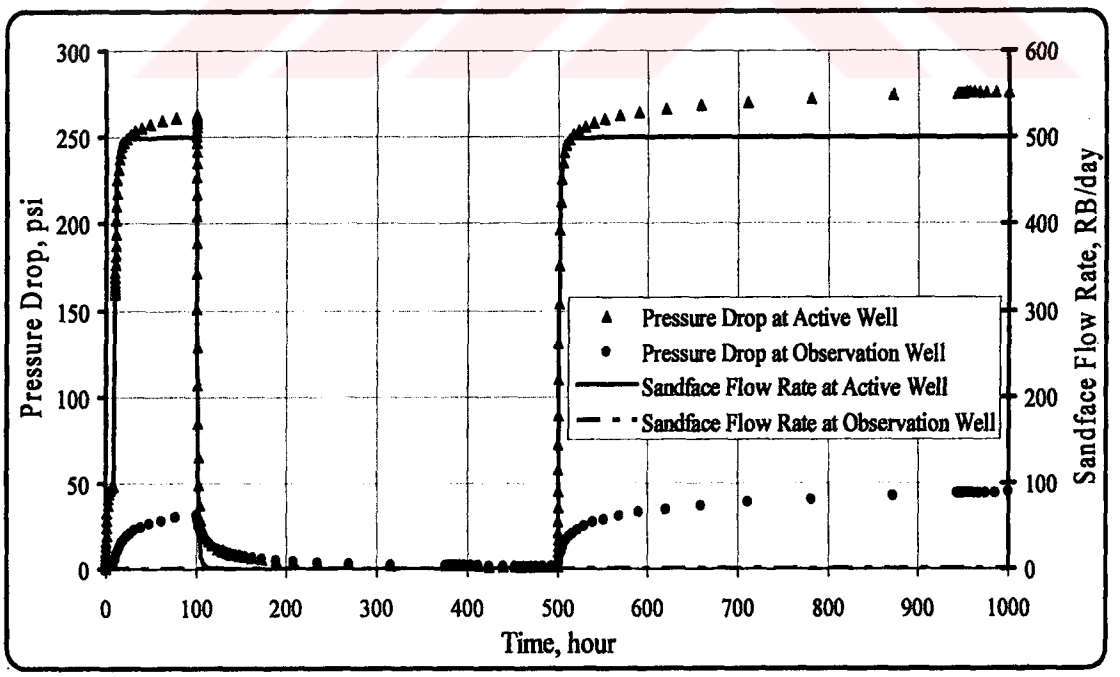

Figure 2.36 Pressure drop and sandface flow rate changes at both wells for Case 3.6.

Although Figure 2.36 gives the same tendency as been in Figure 2.35, pressure drops increased at especially production periods as much as two times of pressure drops in Case 3.5, due to existence of wellbore storage and skin effects at the active well. Conversely, pressure drops at the observation well don't change extraordinarily, because of not available wellbore storage and skin effects at the observation well. Consequently, we can say that wellbore storage and skin terms at the active well don't affect considerably pressure drops and sandface flow rate at the observation well. Sandface flow rates at the active well cannot be equal to surface flow rate at early times at the active well, owing to existence of wellbore storage/skin effects at the active well, because the active well produces at early times or open perionds from both wellbore and reservoir.

2.4.3.7 Case 3.7 : In this case, analysis of interference well test data with variable flow rate is investigated like Case 3.6. A single-layered reservoir is considered and basic parameters are the same as given in Table 2.2. There are wellbore storages and skin factors at both wells. Numerical values of these parameters belonging to the active well are $C_a = 0.1\,RB/psi$, $C_o = 0.1\,RB/psi$, $s_a = 10$ and $s_o = 10$. As been in Case 3.6, production with variable flow rate is done from active well and production scenario is given below :

q_{sa} = 100 RB/day, between t = 0 and t =10 hours
q_{sa} = 500 RB/day, between t = 10 and t =100 hours
q_{sa} = 0.0 RB/day, between t = 100 and t =500 hours
q_{sa} = 500 RB/day, between t = 500 and t =1000 hours

Figures belonging to pressure drops and sandface flow rates at both wells are given below.

In Case 3.7, existence of wellbore storage and skin effect at the observation well are considered differently from Case 3.6. However, since there is no available surface flow rate at the observation well, bottomhole pressure drop doesn't show any changes according to Case 3.6. In the same manner, when we look at pressure drops at the active well, pressure drop changes different from previous case cannot be observed at the active well. We can explain its reason by that wellbore storage and skin effects at the observation well doesn't affect pressure change at active well. Only changed parameters in this case differently from Case 3.6, are the sandface flow rates at both wells.

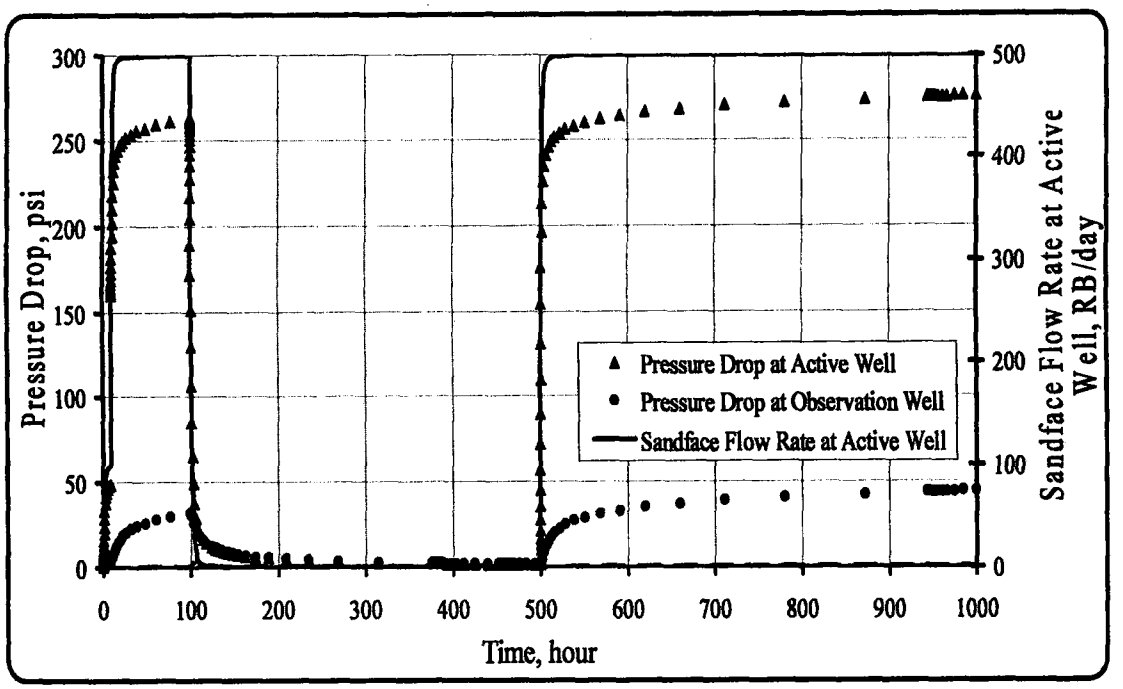

Figure 2.37 Pressure drops at both wells and sandface flow rate changes at the active well for Case 3.7.

In Figure 2.37, sandface flow rates cannot be equal to surface flow rate at early times at the active well, due to existence of wellbore storage at the active well. In Figure 2.38, sandface flow rate changes at the observation well are shown differently from Figure 2.37. At early times or open/closure period, sandface flow rates take negative values at the observation well, because the observation well injects fluid into layer by expanding volume of fluid into the wellbore at the observation well. After surface rate is increased to 500 RB/day, sandface flow rate at observation well converges to zero quickly. As soon as the active well is shut-in after 100^{th} hour, sandface flow rate at the observation well displays a sharp increase towards direction of positive. However, sandface flow rate at the observation well decreases to zero asymptotically at close period between 100^{th} and 500^{th} hours. After the active well launches to produce at 500 RB/day beginning from 500^{th} hour, sandface flow rate at the observation well shows a sharp decrease towards direction of negative and then it rises to zero asymptotically at 100 hours. Sandface flow rate changes at open/closure period at observation well result from wellbore storage and skin effects at observation well.

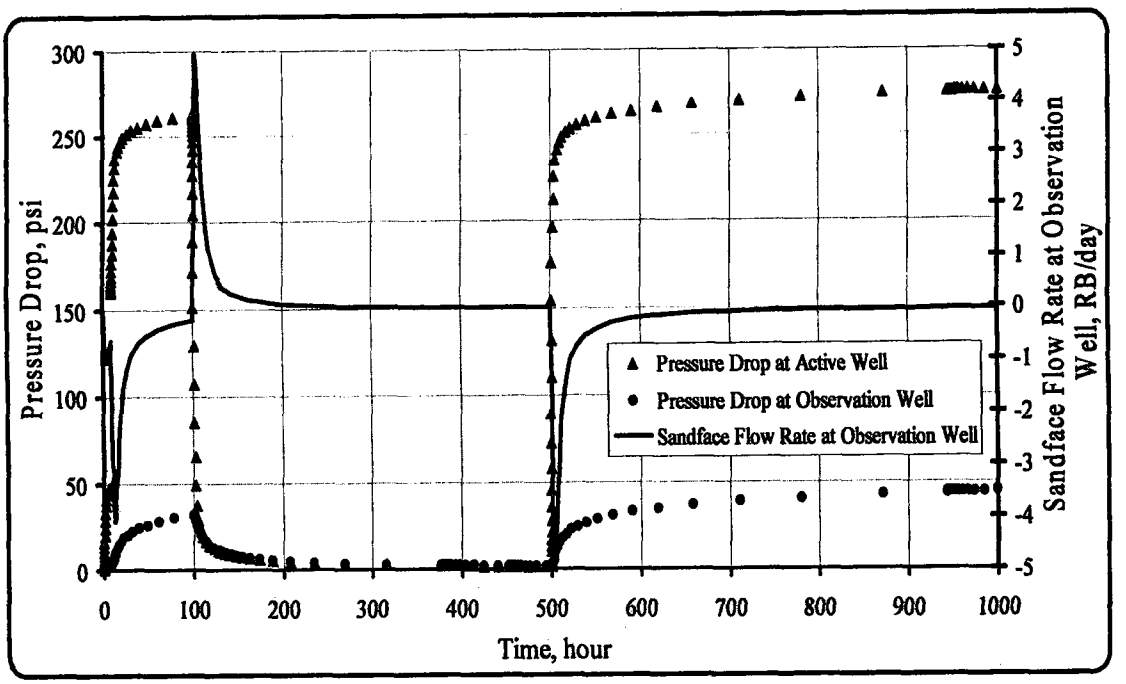

Figure 2.38 Pressure drops at both wells and sandface flow rate changes at the observation well for Case 3.7.

2.4.4 Two-Layered System : In this application, drawdown test and buildup tests are considered for both wells. This forward application is divided to two subsections. Wellbore storage effects are neglected for both subsections, but skin effects are investigated in these sub sections. Layer and wellbore properties are shown in Tables 2.7-2.8 for both subsections. The active well produces with surface rate of 1000 RB/day till 1000 hours and then the active well is shut-in 1000 hours later. The observation well is shut-in at all times. The distance between wells is $r = 350$ ft.

2.4.4.1 Case 4.1 : In this subsection, it is considered that skin terms for both wells do not exist at individual layers. Pressure change and sandface flow rate change at individual layers are investigated for both wells. Graphs about this case are given in Figures 2.39-2.41.

Figure 2.39 illustrates plots of pressure changes at both wells. Since the active well is open to production until end of drawdown test period and the observation well is shut-in at all times, pressure drop at active well increases considerably and decreases sharply after 1000th hour. Although the observation well is shut-in at all times, pressure drop at the observation well increases quite a lot, because production at the active well creates pressure drop at the observation well. In buildup period, pressure drop resulted from active well pressure drop decreases

gradually at the observation well, becasue pressure drop at the active well cannot affect pressure drop at the observation well too much.

Table 2.7 Layer properties for Case 4.1

Parameters	Layer 1	Layer 2
k, md	100	50
ϕ	0.15	0.30
c_t, psia^{-1}	$1x10^{-5}$	$25x10^{-5}$
μ, cp	1.0	1.0
h, ft	50	100
Skin factors at the active well, S_{aj}	0.0	0.0
Skin factors at the observation well, S_{oj}	0.0	0.0

Table 2.8 Well Data for Case 4.1.

	Active Well	Observation Well
r_w, ft	0.35	0.35
Flow rate, q_s, RB/day	1000	0.0
Wellbore storage, C, RB/psi	0.0	0.0

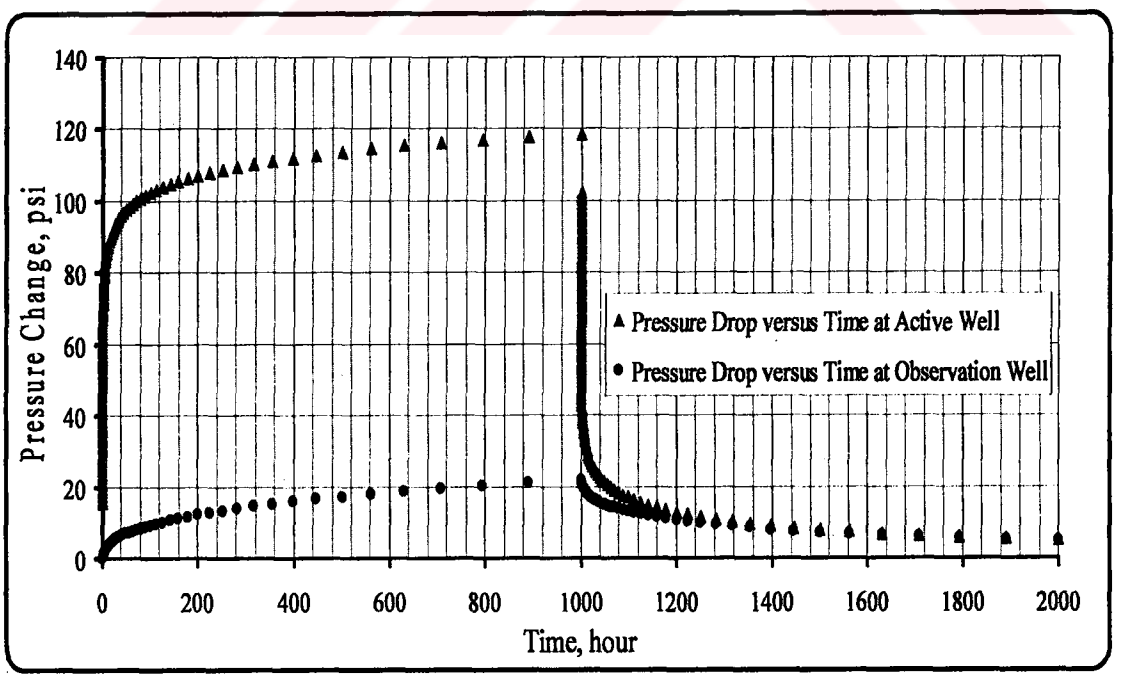

Figure 2.39 Pressure drop change during draw-down and build-up test for both wells (Case 4.1).

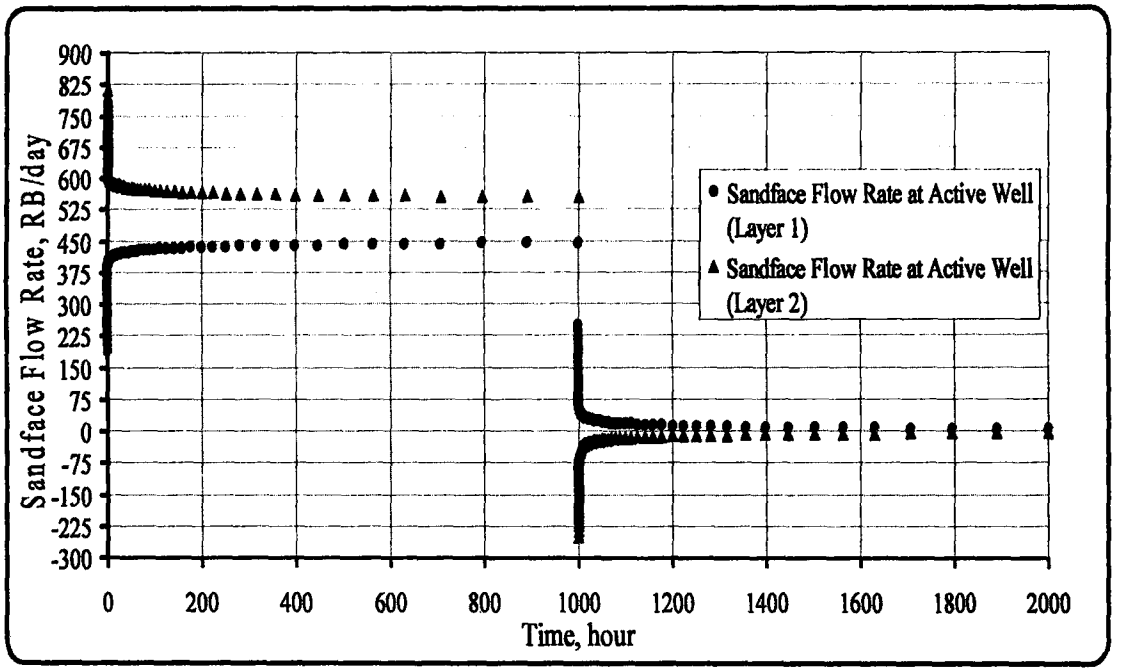

Figure 2.40 Sandface flow rate change at each layer for the active well (Case 4.1).

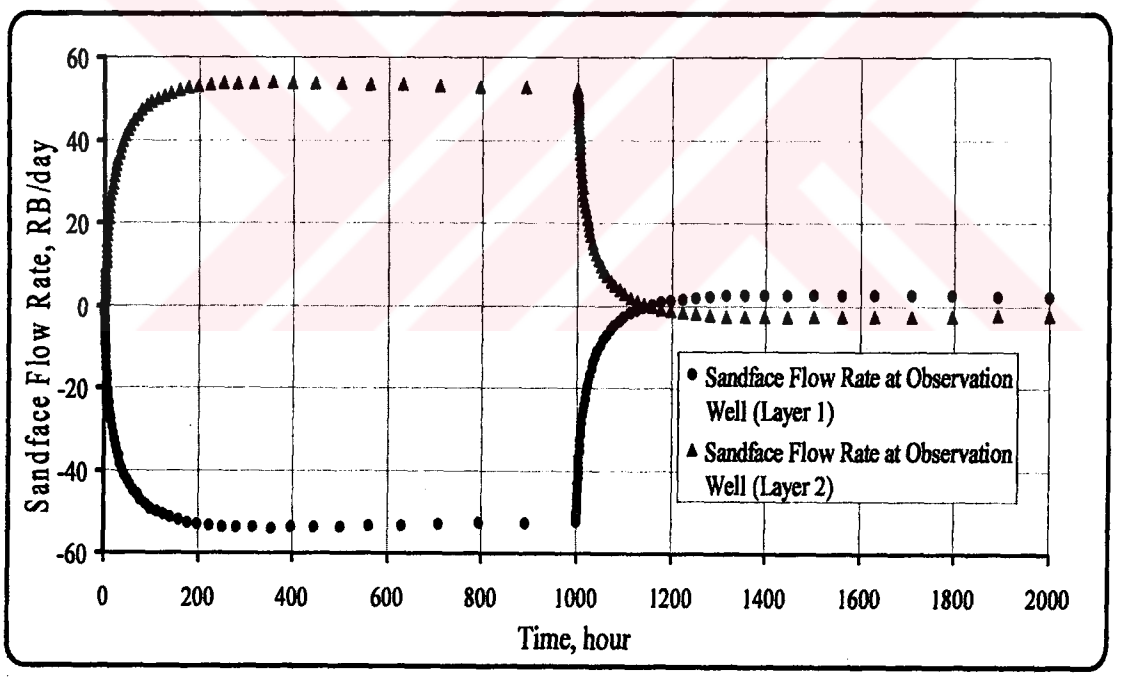

Figure 2.41 Sandface flow rate change at each layer for the observation well (Case 4.1).

Figure 2.40 shows plots of sandface flow rates for both layers at the active well. In cases of $\eta_r > 1$ and $f_r = 1$, $\frac{q_{a1}}{q_{a1} + q_{a2}} < 0.5$, it is mean that production is peformed from 2nd layer much more than done from 1st layer. This case shows that layer with low diffusivity produces much more than layer with high diffusivity, so

this case is a special and interesting result. However, in buildup period, production relationship between layers reverses and 1st layer with high diffusivity injects fluid into 2nd layer with low diffusivity until balance between layers reaches to stability.

Figure 2.41 shows plots of sandface flow rates for both layers at the observation well. In drawdown period, 2nd layer with low diffusivity injects fluid into 1st layer with high diffusivity, because pressure drop of 1st layer at active well reduces pressure drop of 1st layer at the observation well quicklier than that pressure drop of 2nd layer at active well reduces pressure drop of 2nd layer at the observation well. When the time is passed, injection decreases gradually from 2nd layer to 1st layer, because pressure drop of 2nd layer at the active well begins reducing the pressure drop of 2nd layer at the observation well. In buildup period, cross-flow between layers begins decreasing sharply and after 1200 hours cross-flow reverses among layers, because pressure drop of 1st layer decreases at observation well faster than pressure drop of 2st layer at observation well. When the time is passed, 1st layer with high diffusivity injects fluid into 2nd layer with low diffusivity.

2.4.4.2 Case 4.2 : In this subsection, it is considered that skin terms for both wells exist at individual layers. Numerical values of skin terms are shown in Table 2.9. Well data are the same as been in Table 2.8. Pressure change and sandface flow rate change at individual layers are investigated for both wells. Graphs about this case are given in Figures 2.42-2.44.

Table 2.9 Layer properties for Case 4.2.

Parameters	Layer 1	Layer 2
k, md	100	50
ϕ	0.15	0.30
c_t, psia^{-1}	1×10^{-5}	25×10^{-5}
μ, cp	1.0	1.0
h, ft	50	100
Skin factors at the active well, S_{aj}	5.0	20.0
Skin factors at the observation well, S_{oj}	2.0	10.0

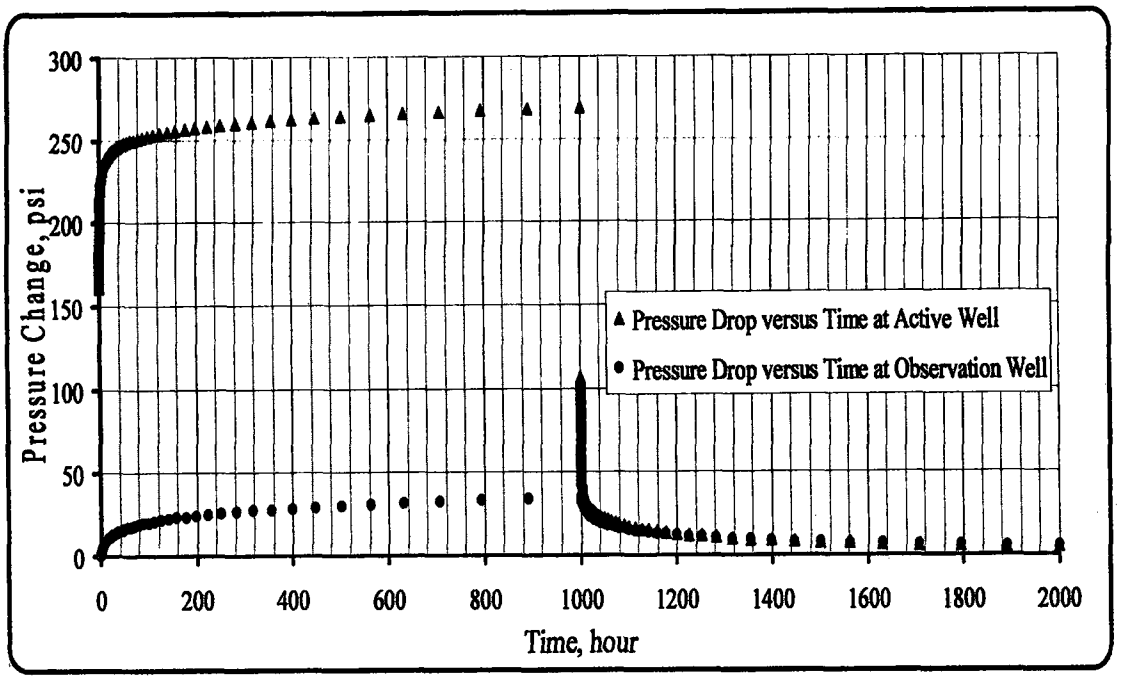

Figure 2.42 Pressure drop change during drawdown and buildup test for both wells (Case 4.2).

Figure 2.42 illustrates plots of pressure changes at both wells for Case 4.2. Since skin factors exist at both individual layers for both wells, pressure drop increases considerably in order to obtain same surface production rate from the active well until end of drawdown test period. In buildup period, pressure drop resulted from active well pressure drop decreases gradually at the observation well, becasue pressure drop at the active well cannot affect pressure drop at the observation well too much.

Figure 2.43 shows plots of sandface flow rates of individual layers at the active well. Since skin term of 2nd layer is much bigger than skin term of 1st layer at the active well, pressure drop of 1st layer is bigger than pressure of 2nd layer at the active well in the drawdown period. Accordingly, production is performed from 1st layer much more than 2nd layer. In buildup period, 2nd layer with low diffusivity injects fluid into 1st layer for a short time and then cross-flow among the layers decreases sharply until balance between layers reaches to stability.

Figure 2.44 illustrates plots of sandface flow rates for both layers at the observation well. In drawdown period, 2nd layer with low diffusivity injects fluid into 1st layer with high diffusivity, because pressure drop of 1st layer at the active well reduces pressure drop of 1st layer at the observation well quicklier than that pressure

drop of 2nd layer at active well reduces pressure drop of 2nd layer at the observation well.

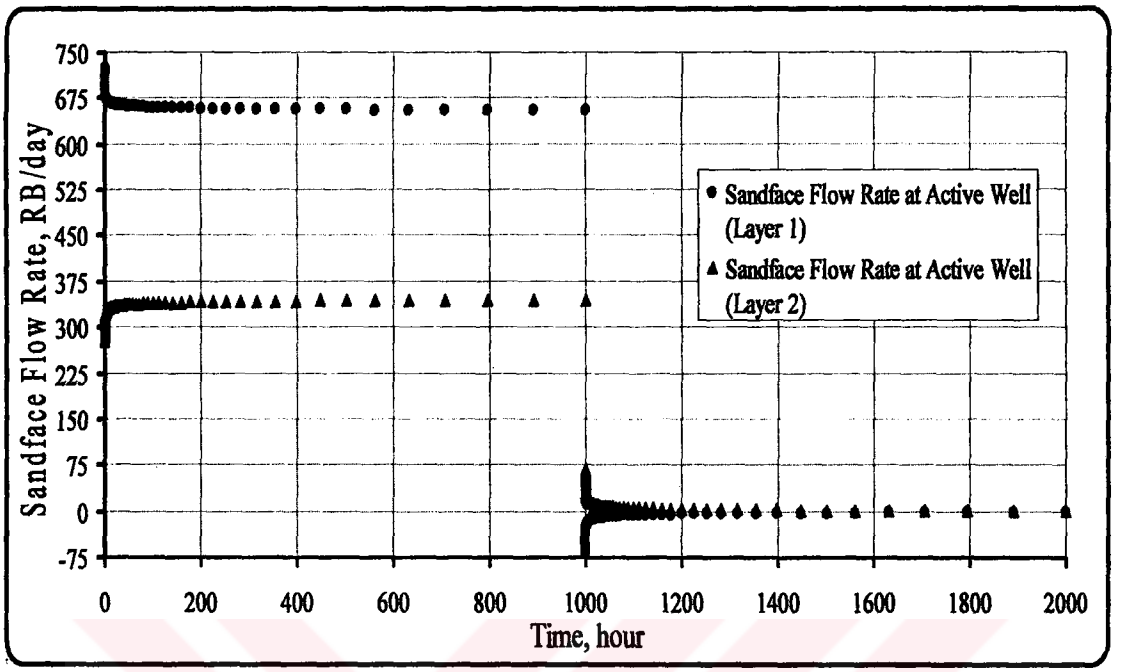

Figure 2.43 Sandface flow rate change at each layer for the active well (Case 4.2).

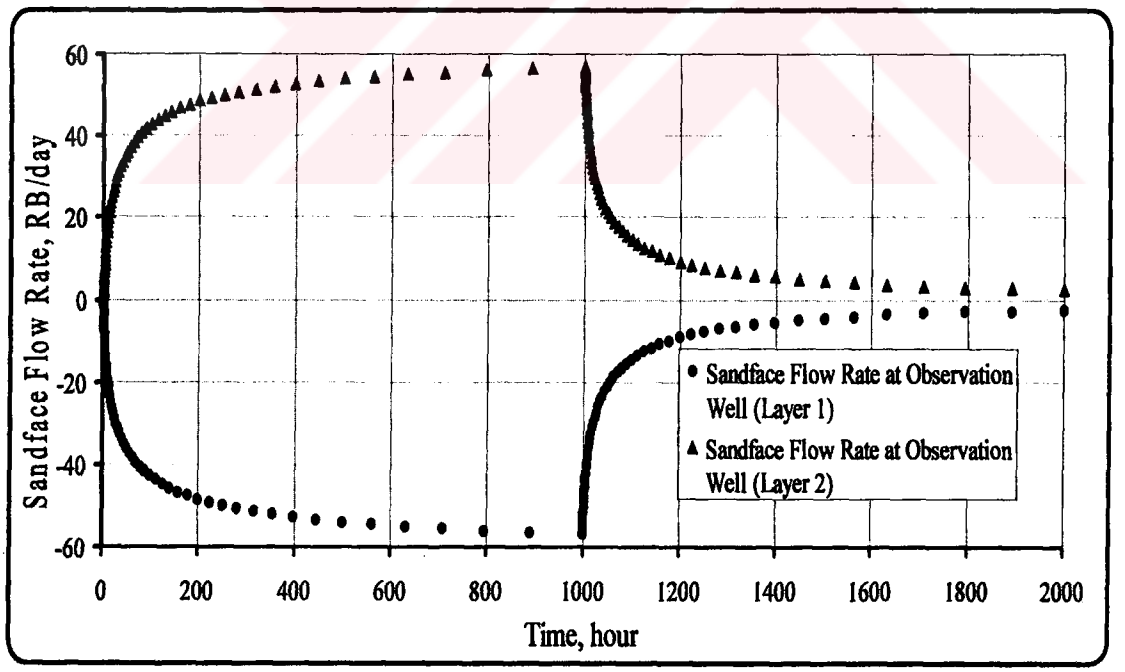

Figure 2.44 Sandface flow rate change at each layer for the observation well (Case 4.2).

When the time is passed, injection increases gradually from 2nd layer to 1st layer, because pressure drop of 2nd layer at the active well cannot reduce the pressure drop

of 2nd layer at the observation well due to high skin factor. In buildup period, cross-flow between layers begins decreasing considerably, because pressure drop of 1st layer begins decreasing at observation well together with pressure drop of 2st layer at observation well. When the time is passed, cross-flow between both layers decreases and then disappears at late times, because of reaching to stability.

2.4.5 Three-Layered System : In this application, three-layered and very heterogeneous reservoir is considered. Wellbore storage and skin effects are investigated in this application. Reservoir and wellbore properties are shown in Tables 2.10-2.11. The active well produces with surface rate of 1000 RB/day and the observation well is shut-in at all times. The distance between wells is $r = 350$ ft.

Table 2.10 Reservoir properties for three-layered system.

Parameters	Layer 1	Layer 2	Layer 3
k, md	15	30	100
ϕ	0.1	0.2	0.3
c_t, psia^{-1}	$1x10^{-5}$	$5x10^{-5}$	$1x10^{-4}$
μ, cp	1.0	1.0	1.0
h, ft	20	10	30
Skin factors at the active well, S_{aj}	5.0	0.5	1.0
Skin factors at the observation well, S_{oj}	3.0	2.0	0.5

Table 2.11 Well Data for three-layered system.

	Active Well	Observation Well
r_w, ft	0.35	0.35
Flow rate, q_s, RB/day	1000	0.0
Wellbore storage, C, RB/psi	0.1	0.1

Figure 2.45 shows log-log plots of pressure change and pressure-derivative for both wells on the same graph. As can be seen from Figure 2.45, radial flow begins appearing after 10 hours at the active well, but after 300 hours at the observation well. Wellbore storage effects are seen at early times for both wells, because of existence of wellbore storage at both wells.

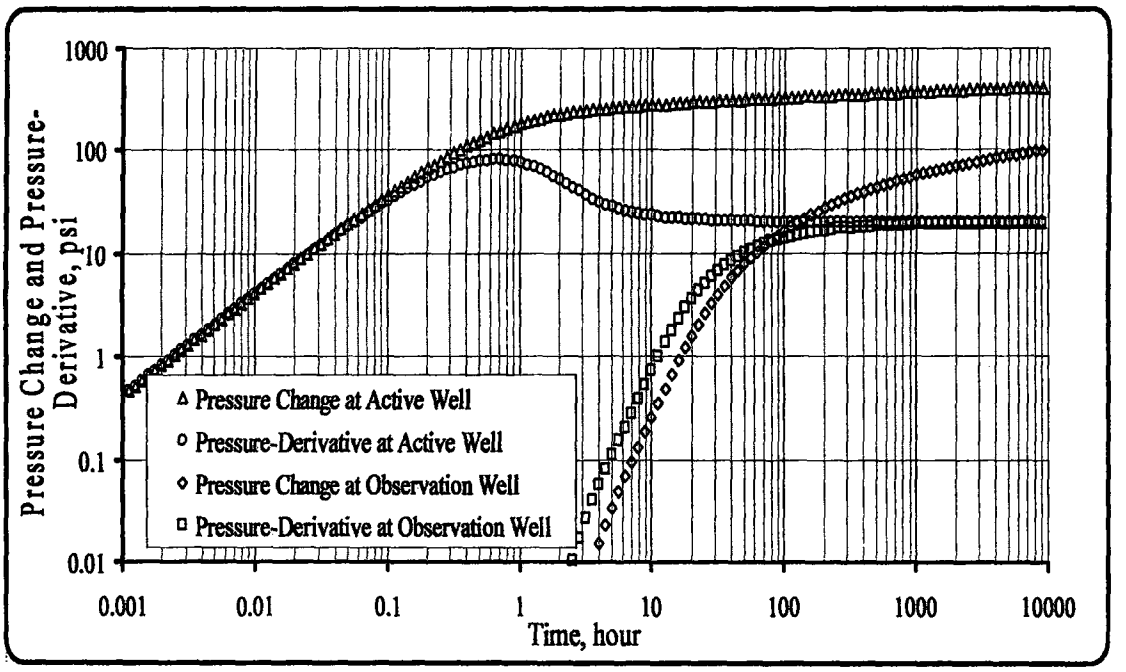

Figure 2.45 Pressure change and pressure-derivative versus time for both wells.

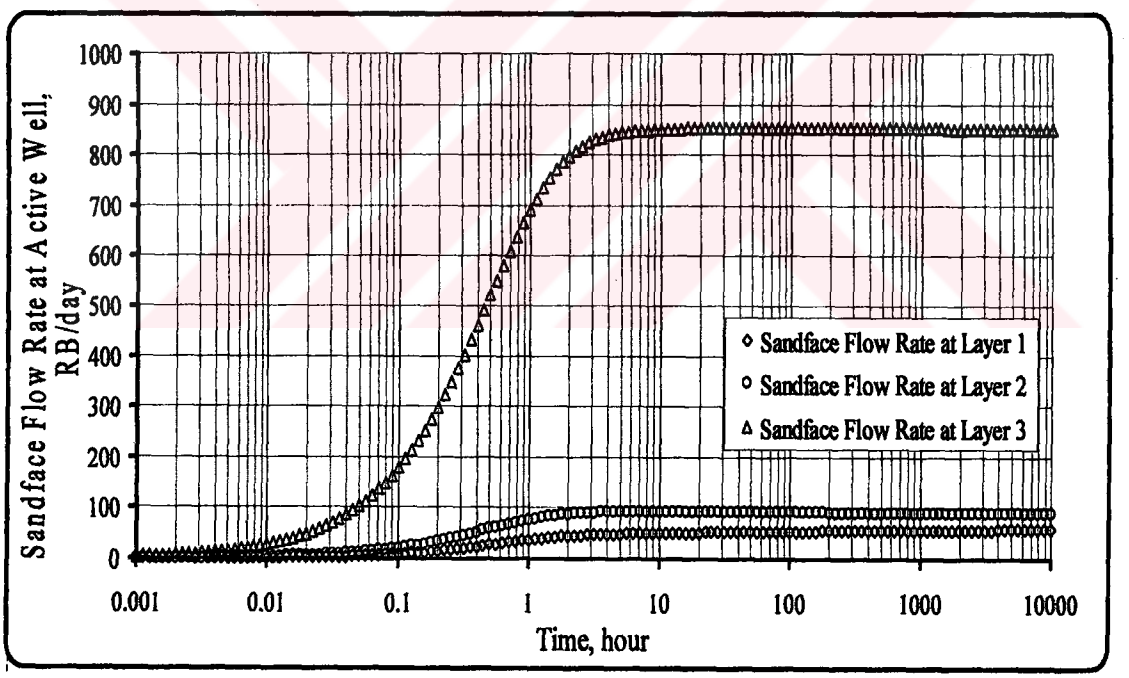

Figure 2.46 Sandface flow rate at layers versus time for the active well.

Figure 2.46 illustrates sandface flow rate changes at all layers for the active well. As can be seen from Figure 2.46, most of production at the active well is performed from 3rd layer though 3rd layer has a low diffusivity coefficient. Conversely, less of production at the active well is carried out from 1st layer, though

1st layer has a high diffusivity coefficient. Reason for this situation is due to skin terms at individual layers.

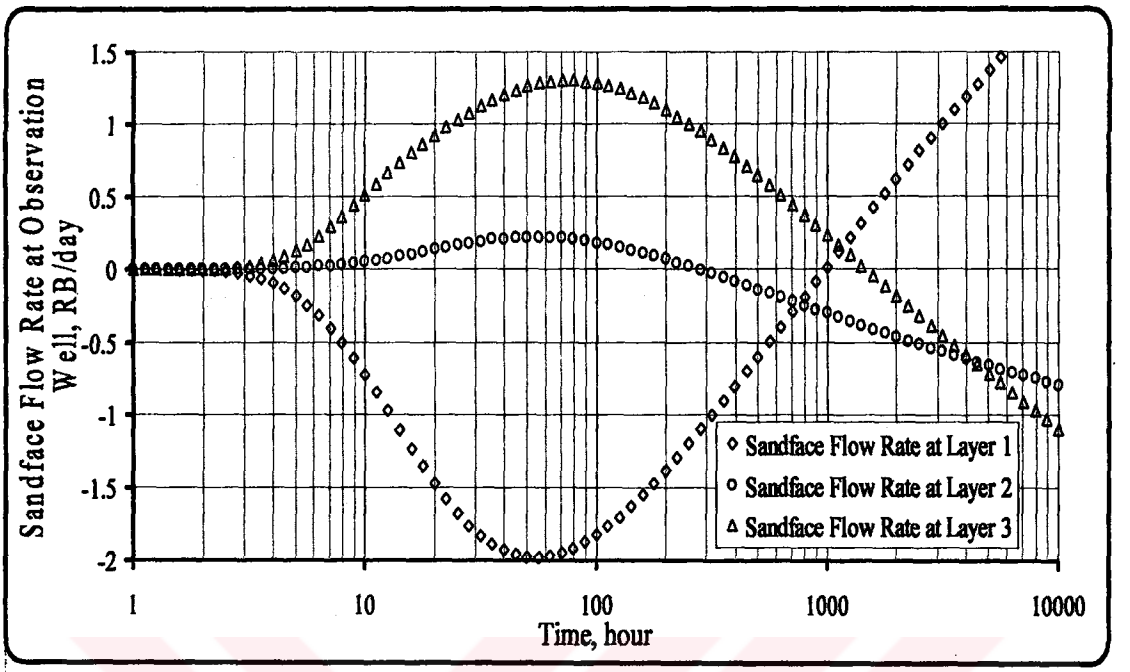

Figure 2.47 Sandface flow rate at layers versus time for the observation well.

Figure 2.47 illustrates sandface flow rate changes at all layers for the observation well. As can be seen from Figure 2.47, sandface flow rates belonging to all layers change versus time incredibly. Since 1st layer has the highest diffusivity coefficient, pressure propagation occurs there faster than the others. Moreover, 3st layer has the second highest diffusivity coefficient, pressure propagation occurs there faster than 2nd layer. Reason for this situation is due to different skin terms at individual layers for both wells.

CHAPTER III

NONLINEAR OPTIMIZATION TECHNIQUES FOR PARAMETER ESTIMATION

Three different optimization algorithms were used in this study and one of them is Levenberg-Marquardt method which is a gradient-based algorithm. Since the Levenberg-Marquardt algorithm uses derivative information of functions to be optimized, it enables to user very fast solution. Therefore it is used widely to optimize functions and to estimate parameter in different disciplines. Another optimization technique we used in this study is simulated annealing method. It is a non-gradient and iterative algorithm, because it doesn't use derivative information contrary to the Levenberg-Marquardt. Since it's claimed that it converges to global minimum independently from initial guesses, it's named as a global optimization technique. Third optimization technique used in this study is polytope algorithm. Although it doesn't use derivative information of functions to be optimized, it's a very fast iterative technique even if it isn't very fast as much as Levenberg-Marquardt. Detailed information about these optimization techniques is given in this chapter like below.

3.1 Levenberg-Marquardt Algorithm

The Levenberg-Marquardt algorithm was proposed independently by Levenberg [18] and Marquardt [19]. Fletcher [20] has proposed an algorithm that adjusts the value of λ_k in (Eq.3.1) according to the relationship between the actual and predicted change in the sum of squares. Alternatively, Δ' may be adjusted and the implicitly defined value of λ_k can be computed using a variant of Hebden's [21] method that is specially tailored to least-squares problems (see :Hebden [21] and Notes for Section 4.4 in Practical Optimization [15]). A popular alternative to the Gauss-Newton method is the Levenberg-Marquardt method.

The Levenberg-Marquardt modification of the Gauss-Newton algorithm for the minimization of non-quadratic objective functions was found to be an efficient

and robust method for most parameter estimation problems. After local linearization of the objective function with respect to the parameters to be estimated, the Levenberg-Marquardt algorithm performs initially small, but robust steps along the steepest descent direction, and switches to more efficient quadratic Gauss-Newton steps as the minimum is approached. The derivatives are calculated numerically using the perturbation method in this study.

The Levenberg-Marquardt method uses a search direction that is a solution of the linear set of equations

$$\left[J(x_k)^T J(x) + \lambda_k I\right] d_k = -J(x_k) F(x_k) \tag{3.1}$$

where the scalar λ_k is a non-negative scalar and controls both the magnitude and direction of d_k. When λ_k is zero, the direction d_k is identical to that of the Gauss-Newton method. As λ_k tends to infinity, d_k tends towards a vector of zeros and a steepest descent direction. This implies that for some sufficiently large λ_k, the term $F(x_k + d_k) < F(x_k)$ holds true. The term λ_k can therefore be controlled to ensure descent even when second order terms, which restrict the efficiency of the Gauss-Newton method, are encountered. The Levenberg-Marquardt method therefore uses a search direction that is a cross between the Gauss-Newton direction and the steepest descent. A unit step is always taken along d_k, i.e., x_{k+1} is given by $x_k + d_k$. It can be shown that, for some scalar Δ' related to λ_k, the vector d_k is the solution of the constrained subproblem

$$\left.\begin{array}{l} \underset{d \in \mathrm{R}^n}{\text{minimize}} \ \frac{1}{2}\|J_k d + f_k\|_2^2 \\ \text{subject to} \ \|d\|_2 \le \Delta'. \end{array}\right\} \tag{3.2}$$

Hence, the Levenberg-Marquardt algorithm is of the trust-region type (discussed in the Notes at the end of Section 4.4 in Practical Optimization [15]), and a "good" value of λ_k (or Δ') must be chosen in order to ensure descent. If λ_k is zero, d_k is the Gauss-Newton direction; as $\lambda_k \to \infty$, $\|d_k\| \to 0$ and d_k becomes parallel to the

steepest-descent direction. This implies that $F(x_k + d_k) < F_k$ for sufficiently large λ_k.

Let $d_{LM}(\lambda_k)$ denote the solution of (3.1) for a specified value of x_k, where λ_k is positive. If J_k is rank-deficient, in general

$$\frac{\|d_N - d_{LM}(\lambda_k)\|}{\|d_N\|} = O(1), \tag{3.3}$$

regardless of the size of $\|Q(x)\|$ or λ_k.

We use in this study publicly available code LMDER1 from Argonne [22] for the Levenberg-Marquardt method. Error tolerance for termination is used value of $1x10^{-6}$ for Levenberg-Marquardt.

3.2 Simulated Annealing

Simulated annealing's roots are in thermodynamics, where one studies a system's thermal energy. A description of the cooling of molten metal motivates this algorithm. After slow cooling (annealing), the metal arrives at a low energy state. Inherent random fluctuations in energy allows the annealing system to escape local energy minima to achieve the global minimum. But if cooled very quickly (or "quenched"), it might not escape local energy minima and when fully cooled it may contain more energy than annealed metal. Simulated annealing attempts to minimize some analogue of energy in a manner similar to annealing to find the global minimum. Details can be found in Press et al [11].

According to Goffe et al [23], early simulated annealing algorithms considered combinatorial systems, where the system's state depends on the configuration of variables. Perhaps the best known is the traveling salesman problem, in which one tries to find the minimum trip distance connecting a number of cities. Combinatorial simulated annealing has been used successfully in computer and circuit design (Kirkpatrick et al [24] and Wong et al [25]), pollution control (Derwent [26]), a special case of 0-1 programming (Drexl [27]), neural networks (Wasserman et al [28]), reconstruction of polycrystalline structures (Telly et al [29]) and image processing (Carnevali et al [30]). Ouenes et al [31] have studied over accelerating the convergence of the algorithm by adjusting the reduction factor automatically.

This study uses Corana et al's [32] extensive source code named SIMANN of simulated algorithm modified by Goffe [23]. Corana et al [32] introduces extensions to the simulated algorithm and its Fortran90 version prepared by A. Miller [33]. One modification checks that the global optimum is indeed achieved, while another allows the researcher to restrict optimization to a subset of the parameter space (this can be very useful for understanding the function). The third extension allows the researcher to determine a critical initial parameter for the algorithm, while the final one directs the selection of parameters that control the robustness of the algorithm. This allows the researcher to minimize the execution time of the algorithm. The Corana et al [32]. implementation of simulated annealing for continuous variable problems appears to offer the best combination of ease of use and robustness, so it is used in this study.

The problem of determining the position in n-space of the minimum of a given function of n variables has been tackled using nonlinear programming methods for many years, in practice since digital computers have been available.

If the cost function is unimodal in the domain of interest, one can choose among many good alternatives. Some of the available minimization algorithms (direct methods) involve only function evaluations, such as Nelder and Mead. Others also use the evaluation of the derivatives of the cost function such as Levenberg-Marquardt and are considered to be more efficient than direct methods; but they are also more complicated and inclined to terminate far from the minimum if the cost function is very ill-conditioned.

Under mild conditions on the test functions, these stochastic methods guarantee asymptotic convergence to the global optimum as the number of sample points increases. All of these techniques are efficient in the case of functions with a few local minima; but, in practice, many optimization problems deal with a large number of variables (up to tens or hundreds) and/or a very large number of local minima that is often an increasing function of the number of variables. In this situation, traditional methods offer low efficiency and limited reliability.

Recently, a global optimization algorithm called Simulated Annealing (SA) has been proposed in the area of combinatorial optimization, that is, when the cost function is defined in a discrete domain. This method is reported to perform well in the presence of a very high number of variables (even tens of thousands). It is based on random evaluations of the cost function, in such a way that transitions out of a

local minimum are possible. It does not guarantee, of course, to find the global minimum, but if the function has many good near optimal solutions, it should find one. In particular, this method is able to discriminate between "gross behavior" of the function and finer "wrinkles". First, it reaches an area in the function domain where a global minimum should be present, following the gross behavior irrespectively of small local minima found on the way. It then develops finer details, finding a good, near-optimal local minimum, if not the global minimum itself.

3.2.1 Approach of Simulated Annealing

Let x be vector in R^n and $(x_1, x_2, ..., x_n)$ its components. Let $f(x)$ be the function to minimize and let $a_1 < x_1 < b_1, ..., a_n < x_n < b_n$ be its n variables, each ranging in a finite, continuous interval. f does not need to be continuous but it must be bounded.

Simulated Annealing algorithm is schematically shown in Figure 3.1. It proceeds iteratively : Starting from a given point x_0, it generates a succession of points : $x_0, x_1, ..., x_i, ...$ tending to the global minimum of the cost function. New candidate points are generated around the current point x_i applying random moves along each coordinate direction, in turn. The new coordinate values are uniformly distributed in intervals centered around the corresponding coordinate of x_i. Half the size of these intervals along each coordinate is recorded in the step vector v. If the point falls outside the definition domain of f, a new point is randomly generated until a point belonging to the definition domain is found. A candidate point x' is accepted or rejected according the Metropolis [34] criterion :

If $\Delta f \leq 0$, then accept the new point : $x_{i+1} = x'$

else accept the new point with probability:

$$p(\Delta f) = \exp(-\Delta f / T) \tag{3.4}$$

where $\Delta f = f(x') - f(x_i)$ and T is a parameter called temperature.

At a fixed value of T the succession of points $x_0, x_1, ..., x_i, ...$ is not downhill, except when $T = 0$. For values of T large compared to the mean value of

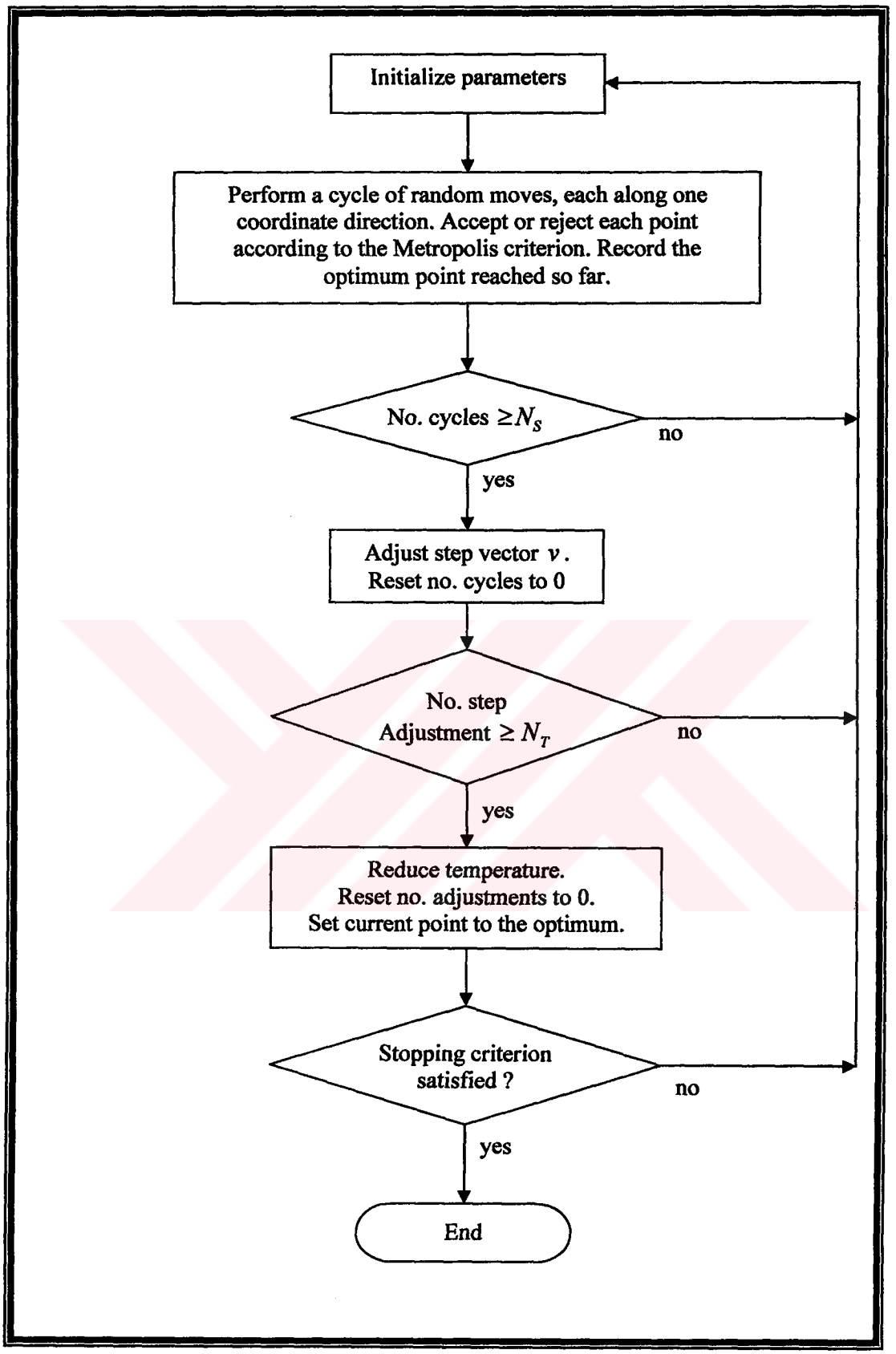

Figure 3.1 Flow chart of simulated annealing algorithm.

$|f(x_h) - f(x_k)|$ (x_h and x_k are points randomly chosen inside the definition domain of f) almost all new points are accepted and succession is a random sampling of f.

The SA algorithm starts at some "high" temperature T_0 given by the user. A sequence of points is then generated until a sort of "equilibrium" is approached; that is a sequence of points x_i whose average value of f reaches a stable value as i increases. During this phase the step vector v_m is periodically adjusted to better follow the function behavior. The best point reached is recorded as x_{opt}.

After thermal equilibration, the temperature T is reduced and a new sequence of moves is made starting from x_{opt}, until thermal equilibrium is reached again, and so on. The process is stopped at a temperature low enough that no more useful improvement can be expected, according to a stopping criterion that we will describe later. The SA optimization algorithm can be considered analogous to the physical process by which a material changes state while minimizing its energy. A slow, careful cooling brings the material to a highly ordered, crystalline state of lowest energy. A rapid cooling instead yields defects and glass-like intrusions inside the material.

From an optimization point of view, an iterative search accepting only new points with lowest function values is like rapidly quenching a physical system at zero temperature. It is very likely to get stuck in a metastable, local minimum. On the contrary, SA permits uphill moves under the control of a temperature parameter. At higher temperature only the gross behavior of the cost function is relevant to the search. As temperature decreases, finer details can be developed to get a good final point. While the optimality of the final point cannot be guaranteed, the method is able to proceed toward better minima even the presence of many local minima.

A detailed description of the algorithm follows :

Step 0 (Initialization)

Choose

A starting point x_0.

A starting step vector v_0.

A starting temperature T_0.

A terminating criterion ϵ and a number of successive temperature reductions to test for termination N_ϵ.

A test for step variation N_S and a varying criterion c.

A test for temperature reduction N_T and a reduction coefficient r_T.

Set i, j, m, k to 0. i is the index denoting successive points, j denotes successive cycles along every direction, m describes successive step adjustments, and k covers successive temperature reductions.

Set h to 1. h is the index denoting the direction along which the trial point is generated, starting from the last accepted point.

Compute $f_0 = f(x_0)$.

Set $x_{opt} = x_0$, $f_{opt} = f_0$.

Set $n_u = 0$, $u = 1,2,...,n$.

Set $f_u^* = f_0$, $u = 1,2,...,-N_\epsilon + 1$.

Step 1

Starting from the point x_i, generate a random point x' along the direction h:

$$x' = x_i + r\, v_{m_h} e_h \tag{3.5}$$

where r is a random number generated in the range $[-1,1]$ by a pseudorandom number generator; e_h is the vector of the hth coordinate direction; and v_{m_h} is the component of the step vector v_m along the same direction.

Step 2

If the h^{th} coordinate of x' lies outside the definition domain of f, that is, if $x'_h < a_h$ *or* $x'_h > b_h$, then return to step 1.

Step 3

Compute $f' = f(x')$.

If $f' \le f_i$, then accept the new point:

set $x_{i+1} = x'$,

set $f_{i+1} = f'$,

add 1 to n_h ;

if $f' < f_{opt}$, then set

$$x_{opt} = x',$$
$$f_{opt} = f'.$$

endif;

else $(f' > f_i)$ accept or reject the point with acceptance probability p (Metropolis move) :

$$p = \exp\left(\frac{f_i - f'}{T_k}\right) \tag{3.6}$$

In practice, a pseudorandom number p' is generated in the range $[0,1]$ and is compared with p . If $p' < p$, the point is accepted, otherwise it is rejected.

In the case of acceptance:

set $x_{i+1} = x'$,

set $f_{i+1} = f'$,

add 1 to i,

add 1 to n_h.

Step 4

Add 1 to h.

if $h \le n$, then goto step 1;

else set h to 1 and add 1 to j.

Step 5

If $j < N_S$, then goto step 1;

else update the step vector v_m :

for each direction u the new step vector component v'_u is

$$v'_u = v_{m_u}\left(1 + c_u \frac{n_u/N_S - 0.6}{0.4}\right) \qquad \text{if} \quad n_u > 0.6 N_S,$$

$$v'_u = \frac{v_{m_u}}{1 + c_u \dfrac{0.4 - n_u/N_S}{0.4}} \qquad \text{if} \quad n_u < 0.4 N_S, \tag{3.7}$$

$$v'_u = v_{m_u} \qquad \textit{otherwise.}$$

Set $v_{m+1} = v'$,

set j to 0,

set n_u to 0, $u = 1,2,...,n$,

add 1 to m.

The aim of these variations in step length is to maintain the average percentage of accepted moves at about one-half of the total number of moves. The rather complicated formula used is discussed at the end of this part. The c_u parameter controls the step variation along each u^{th} direction.

Step 6

If $m < N_T$, then go to step 1;

else, it is time to reduce the temperature T_k:

set $T_{k+1} = r_T . T_k$,

set $f_k^* = f_i$,

add 1 to k,

set m to 0.

It is worth noting that a temperature reduction occurs every $N_S . N_T$ cycles of moves along every direction and after N_T step adjustments.

Step 7 (Terminating Criterion)

If:

$$\left| f_k^* - f_{k-u}^* \right| \leq \epsilon, \qquad u = 1,2,...,N_\epsilon \tag{3.8}$$

$$f_k^* - f_{opt} \leq \epsilon$$

then stop the search;

else:

add 1 to i,

set $x_i = x_{opt}$,

set $f_i = f_{opt}$.

Go to step 1.

Reasonable values, found after some test optimizations done by Corana et al [32], of the parameters that control the simulated annealing are

$$N_S = 20.$$
$$N_T = \max(100, 5 * n).$$
$$c_i = 2, \quad i = 1,2,....,n.$$
$$N_\epsilon = 4.$$
$$r_T = 0.85$$

In this study, as control parameters which simulated annealing's performance depends on, these numerical values are used like N_s=20, N_T=5, $c_i = 2$, $N_\epsilon = 4$, $\varepsilon = 10^{-6}$ and $r_T = 0.95$.

3.3 Polytope Algorithm

This method was primarily introduced by Spendley et al [35], as an ingenious idea for tracking optimum operating conditions by evaluating the output from a system at a set of points forming a simplex in the factor-space, and continually forming new simplices by reflecting one point in the hyperplane of the remaining points. This idea is clearly applicable to the problem of minimizing a mathematical function of several variables, as was recognized by J.A. Nelder and R. Mead [14]. This method was described by Nelder and Mead for the minimization of a function of n variables, which depends on the comparison of function values at the $(n+1)$ vertices of a general simplex, followed by the replacement of the vertex with the highest value by another point. The simplex adapts itself to the local landscape, and contracts on to the final minimum. The method is shown to be effective and computationally compact.

Gill et al [15] considered briefly the ***polytope*** method, which is usually termed the "simplex" method in order to give the flavour of a typical direct search method,. However, they preferred not to use the latter name, in order to avoid confusion with the better-known simplex method for linear programming.

Polytope is an optimization technique in which one finds the best response in a multidimensional space, where the variables may be interrelated. The polytope is computationally slow but is quick and easy to implement. The essence of the method is to observe the response of a system, change variables intelligently, not the new response, change variables, etc. One is searching for a minimum or a maximum in a response surface. The response surface is in n-dimensional space where the axes correspond to the variables of the problem. A polytope is a geometric figure with

$n+1$ vertices in an n-dimensional space. To illustrate this concept, consider a two parameter space.

The polytope method requires only function evaluations, not derivatives. It is not very efficient in terms of the number of function evaluations that it requires. However the polytope method may frequently be the best method to use if the figure of merit is "get something quickly" for a problem whose computational burden is small.

At each stage of the algorithm, $n+1$ points $x_1, x_2, ..., x_{n+1}$ are retained, together with the function values at these points, which are ordered so that $F_{n+1} \geq F_n \geq ... \geq F_2 \geq F_1$. The method derives its name because these points can be considered to be the vertices of a polytope in n-space. At each iteration, a new polytope will be generated by producing a new point to replace the "*worst*" point x_{n+1} (i.e., the point with the highest function value).

Let c denote the centroid of the best n vertices $x_1, x_2, ..., x_n$, given by

$$c = \frac{1}{n}\sum_{j=1}^{n} x_j \tag{3.9}$$

At the beginning of each iteration , a trial point is generated by a single *reflection* step in which Gill et al constructed the point $x_r = c + \alpha(c - x_{n+1})$, where α $(\alpha > 0)$ is the *reflection coefficient.* The function is evaluated at x_r, yielding F_r.

There are three cases to consider.

1. If $F_1 \leq F_r \leq F_n$ (i.e., x_r is not either a new best point or a new worst point), x_r replaces x_{n+1} and the next iteration is begun.
2. If $F_r < F_1$, so that x_r is the new best point, Gill et al [15] assume that the direction of reflection is a "good" direction, and attempt to expand the polytope in this direction by defining an expanded point x_e such that $x_e = c + \beta(x_r - c)$, where $\beta(\beta > 1)$ is the *expansion coefficient.* If $F_e < F_r$, the expansion is successful, and x_e replaces x_{n+1}. Otherwise, the expansion has failed, and x_{n+1} is replaced by x_r.

3. If $F_r > F_n$, the polytope is assumed to be too large, and should be contracted. A *contraction step* is carried out by defining

$$x_c = \begin{cases} c + \gamma(x_{n+1} - c), & \text{if } F_r \geq F_{n+1}; \\ c + \gamma(x_r - c), & \text{if } F_r < F_{n+1}, \end{cases} \tag{3.10}$$

where $\gamma (0 < \gamma < 1)$ is the *contraction coefficient*. If $F_c < \min\{F_r, F_{n+1}\}$, the contraction step has succeeded, and x_c replaces x_{n+1}. Otherwise, a further contraction is carried out. Figure 3.2 illustrates the position of the reflected and expansion steps for a polytope in two dimensions.

Occasionally, the most recent polytope is discarded and replaced by a regular polytope. This procedure is known as ***restarting***. Restarting can be used to prevent the polytope from becoming unbalanced after several successive expansions are made. In this case the best two points are retained and their vector-difference determines the length of the side of the new regular polytope. A restart may also be made to check the validity of a solution. In this case, the regular polytope may be given the centre x_1 and side $\|x_1 - x_{n+1}\|_2$. If the algorithm re-converges to the same point, or $2n$ iterations are made without finding a lower point, x_1 is regarded as an adequate solution [15].

Modifications can be made to the polytope method that significantly improve its performance. For example, during the contraction step described above, a new point is found on a line joining what could be two poor points (the worst point and the reflected point). In this case it is better to compute a point biased toward the best point of the polytope. A modified contraction step that achieves this bias is given in the following variation of Step 3 of the original algorithm.

3'. If $F_r > F_n$, a contraction step is carried out by defining

$$x_c = \begin{cases} x_1 + \gamma(x_{n+1} - x_1), & \text{if } F_r \geq F_{n+1}; \\ x_1 + \gamma(x_r - x_1), & \text{if } F_r < F_{n+1}. \end{cases} \tag{3.11}$$

Another modification involves *shrinking* the polytope if the contraction step is unsuccessful, or if the best point remains unchanged for many iterations. The

polytope is shrunk by moving the vertices half-way toward the current best point in the order $x_2, x_3, \ldots$. Note that the best point may change during the shrinking process.

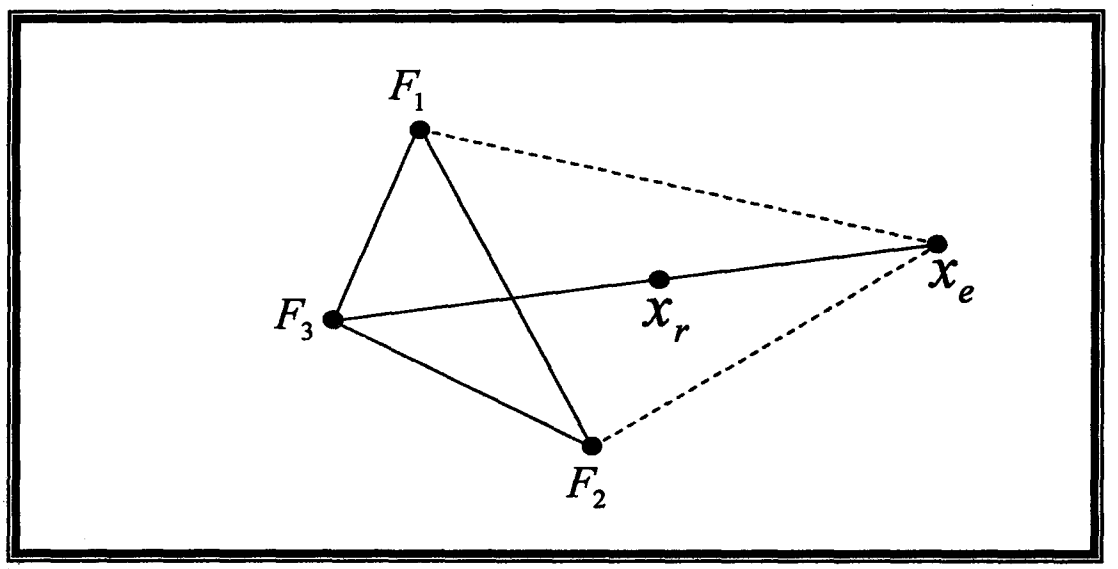

Figure 3.2 The position of the reflected point x_r and expanded point x_e for a polytope in two dimensions. The vertex of the polytope corresponding to the highest function value is marked on the figure as F_3.

The method has a geometrical naturalness about it which makes it delightful to describe or work through. A simplex or polytope is the geometrical figure consisting, in n dimensions, of $n+1$ points (or vertices) and all their interconnecting line segments, polygonal faces, etc. In two dimensions, a polytope is a triangle. In three dimensions it is a tetrahedron, not necessarily the regular tetrahedron. In general William H. Press et al are only interested in polytopes that are non-degenerate, i.e. which enclose a finite inner n-dimensional volume. If any point of a non-degenerated polytope is taken as the origin, then the n other points define vector directions that span the n-dimensional vector space.

In one-dimensional minimization, it was possible to bracket a minimum, so that the success of a subsequent isolation was guaranteed. There is no analogous procedure in multidimensional space. For multidimensional minimization, the best we can do is to give this algorithm a starting guess, that is, an n-vector of independent variables as the first point to try. The algorithm is then supposed to make its own way downhill through the unimaginable complexity of an n-dimensional topography, until it encounters an (at least local) minimum [11].

This algorithm may be more appropriate and efficient when the gradient of F is hard to calculate, or when the function value contains noise. For an n-dimensional problem, this method maintains a simplex of $n+1$ points (a triangle in two dimensions, or a pyramid in three dimensions). This method is slow and can be applied only to problems in which n is small. It is, however, extremely popular, since it requires the user to supply only function values, not derivatives. In this study, MINIM.F90 programmed by B. E. Shaw [36] and further amended by Alan Miller [37] has been used as a source code of Polytope algorithm. We also use slightly different values of control parameters which polytope algorithm's performance depends on them. These are stopping criterion (eps $=10^{-6}$), criterion for expanding the simplex to overcome rounding errors (simp= 10^{-20}) and initial step sizes (step(number of unknown parameters)=0.4).

3.4 Confidence Intervals :

Confidence intervals predicts the uncertainty for a parameter in the estimated parameters. Large confidence intervals for a parameter indicate that the uncertainty is bigger in the estimated parameters. Similarly, small confidence intervals for a model parameter indicate that the parameter is determined more confidently.

We use the standard definition of confidence interval [38,39]. For example, when we perform regression on pressure data, we compute the $\gamma \times 100\%$ confidence intervals from

$$\begin{aligned} \beta_i^{\infty} - t(1-\gamma/2, N_d - N_p) s \sqrt{\left[\left(H(\vec{\beta}^{\infty})\right)^{-1}\right]_{ii}} \le \tilde{\beta}_i \\ \le \beta_i^{\infty} + t(1-\gamma/2, N_d - N_p) s \sqrt{\left[\left(H(\vec{\beta}^{\infty})\right)^{-1}\right]_{ii}} \end{aligned} \tag{3.12}$$

where β^{∞} denotes the estimate obtained by minimizing $J(\vec{\beta})$ (Eq.4.1), β_i^{∞} denotes the estimate of ith model parameter at the minimum, $H(\vec{\beta}^{\infty})$ denotes the sensitivity coefficient matrix (containing derivatives of pressure data with respect to model parameters) evaluated at the estimate β^{∞}, $\tilde{\beta}_i$ represents the true, but unknown value of the model parameter, β_i, and $t(1-\gamma/2, N_d - N_p)$ is the value that cuts off $(1-\gamma)/2 \times 100\%$ in the upper tail of t-distribution with $N_d - N_p$ degrees of freedom. In Eq. (3.12), s is computed from

$$s = \sqrt{\frac{J(\bar{\beta}^{\infty})}{N_d - N_p}} \tag{3.13}$$

where N_d denotes number of observed pressure and sandface flow rate data, N_p denotes number of unknown parameters.

We also use RMS (Root Mean Square Error) computations to calculate standard deviation over pressure or sandface flow rate data. This expression helps us to decide whether optimization algorithms carry out parameter estimation successfully or not. For example; for only pressure data, RMS can be shown by

$$RMS = \sqrt{\frac{1}{N}\sum_{i=1}^{N}(\Delta p_{obs} - \Delta p_{model})^2} \tag{3.14}$$

where N denotes number of data points.

In our applications, we minimize the appropriate objective function with the Levenberg-Marquardt and polytope methods with a restricted step procedure as described by Fletcher [40], and constrain the unknown parameters in regression by using the so-called imaging method of Carvalho et al [41]. Computer program designed and written in this thesis study is attached with recordable CD inside back page of this thesis. Also input page of this program which includes forward and inverse computations is given in Appendix D.

CHAPTER IV

APPLICATIONS OF NONLINEAR PARAMETER ESTIMATION TO INTERFERENCE WELL TESTS

In this section, we focus on parameter estimation from interference tests in a multilayer commingled system. The results given in this chapter pertain to ideal data where the exact model is assumed to be known and are obtained by the automatic type curve matching program developed in this work. We generate several synthetic test cases pertaining to single, two and three-layer systems using the forward model developed in this work, and then corrupt pressure and/or rate data using random normal errors with zero mean and specified standard deviation to simulate "real" test cases. Then, by matching observed pressure and/or rate data corresponding to these test cases with three different optimization algorithms, we investigate parameter estimation problem for interference tests in multilayer commingled systems. As mentioned previously, we consider Levenberg-Marquardt, polytope and simulated annealing methods for nonlinear parameter estimation.

In this study, the objective function which we try to minimize can be given in the following general form :

$$J(\vec{\beta}) = \sum_{i=1}^{N_w=2} \sum_{j}^{N_d} \left[\frac{\Delta p_m(\vec{\beta}) - \Delta p_{obs}}{\sigma_{p_i}} \right]^2 + \sum_{i=1}^{N_w=2} \sum_{l=1}^{N_l} \sum_{j=1}^{N_d} \left[\frac{q_m(\vec{\beta}) - q_{obs}}{\sigma_{q_{i,l}}} \right]^2 \qquad (4.1)$$

In this equation , $\vec{\beta}$ denotes unknown parameter vector. σ_{p_i} and $\sigma_{q_{i,l}}$ denote standard deviations on pressure change and sandface flow rate.. Moreover, $\Delta p_m(\vec{\beta})$ and $q_m(\vec{\beta})$ refer to pressure changes and sandface flow rates at both active and observation wells computed by the model. In the same manner, Δp_{obs} and q_{obs} refer to pressure changes and sandface flow rates measured at both wells. N_w denotes the number of wells which is equal to 2 (the active and observation wells) in our study. N_d denotes the number of data points on pressure and sandface flow rate data. N_l

denotes the number of layers in reservoir. It is worth noting from Eq. (4.1) that Eq. (4.1) allows us to use different standard deviations for pressure change data sets measured at the active and/or observation wells as well as different standard deviations for sandface flow rate data measured from individual layers at both wells. As can be seen in equation (4.1), the objective function has been structured in a least-squares form. In least-squares method, measurement errors are assumed to be a Gaussian random variable with zero mean and specified standard deviation. Indeed, in the literature, it is usually assumed that measurement errors are Gaussian.

4.1 Parameter Estimation in A Single-Layered Reservoir :

First, we look at parameter estimation for an interference test in a single-layered reservoir system. In this application, the unknown parameters are permeability, porosity, wellbore storage and skin factors at both the active and observation wells. So, the total number of unknown parameters is 6. Here, we will consider the use of different data sets to investigate which unknown parameters can be reliably estimated from which data sets for this single-layer example. In order to carry out this target, pressure data at only active well, pressure data at both wells and pressure data and sandface flow rate data at both wells are considered as alternative data sets in parameter estimation. Therefore, it'll be possible to see which parameters can be reliably estimated by using which observed data sets at the well. Tables 4.1 and 4.2 presents the input model parameters used to generate the interference test case to be considered in this application.

Table 4.1 Layer properties for regression 1 case.

	Layer
k, md (permeability)	100
ϕ (porosity)	0.15
c_t, psia^{-1} (Total compressibility)	1×10^{-5}
μ, cp (Fluid viscosity)	1.0
h, ft (Thickness of layer)	50
r, ft (The distance between wells)	200
S_a, Skin factor at the active well	5
S_o, Skin factor at the observation well	5

Table 4.2 Well data for regression 1 case.

	Active Well	Observation Well
r_w and r_o ft	0.33	0.33
C, RB/psi (Wellbore storage)	0.5	0.5
Flow rate, *q*, RB/Day	1000	0

Because our aim is that a realistic regression analysis can be performed to estimate the parameters of interest, active well pressure data were corrupted by adding them normal errors with zero mean and 2 psi standard deviation, while observation well pressure data were corrupted by adding them normal errors with zero mean and 0.5 psi standard deviation. No random errors were added to sandface flow rates at both the active and observation wells.

4.1.1 Matching Only Pressure Data at Active Well: In this sub section, we assume that we have pressure data measured only at the active well. Thus, we only match active well pressure data to estimate all 6 unknown parameters. For performing matching in all cases given in this section, we consider the Levenberg-Marquardt method. In Table 4.3, the results of regression are presented together with the initial guesses and confidence limits for the parameters. As can be seen from the table, only permeability and wellbore storage coefficient at the active well could be obtained reliably and confidently by matching only pressure data at the active well. Other parameters couldn't be estimated from the active well pressure data, because observation well pressure data are needed.

Table 4.3 Results of Regression 1.1 to estimate all parameters.

PARAMETERS	INITIAL GUESSES	TRUE VALUES	OPTIMIZED VALUES	CONFIDENCE LIMIT
k, md	200	100	**98.939403**	± 4.575
ϕ	0.3	0.15	0.001404	± 1.722E-3
C_a, RB/psi	0.001	0.5	**0.498976**	± 9.3594E-3
C_o, RB/psi	0.001	0.5	0.003276	± 0.1798
S_a	2.0	5.0	2.517103	± 4.36405E-4
S_o	2.0	5.0	42.830449	± 0.13444

Now, we investigate whether optimized values in Table 4.3 provide acceptable matches of pressure data at both wells.. Therefore, curve matching to pressure data at both wells is done separately by calculating interference well test data with

optimized values obtained from inverse problem. Curve matching processes over the active and observation pressure data are shown in Figures 4.1 and 4.2.

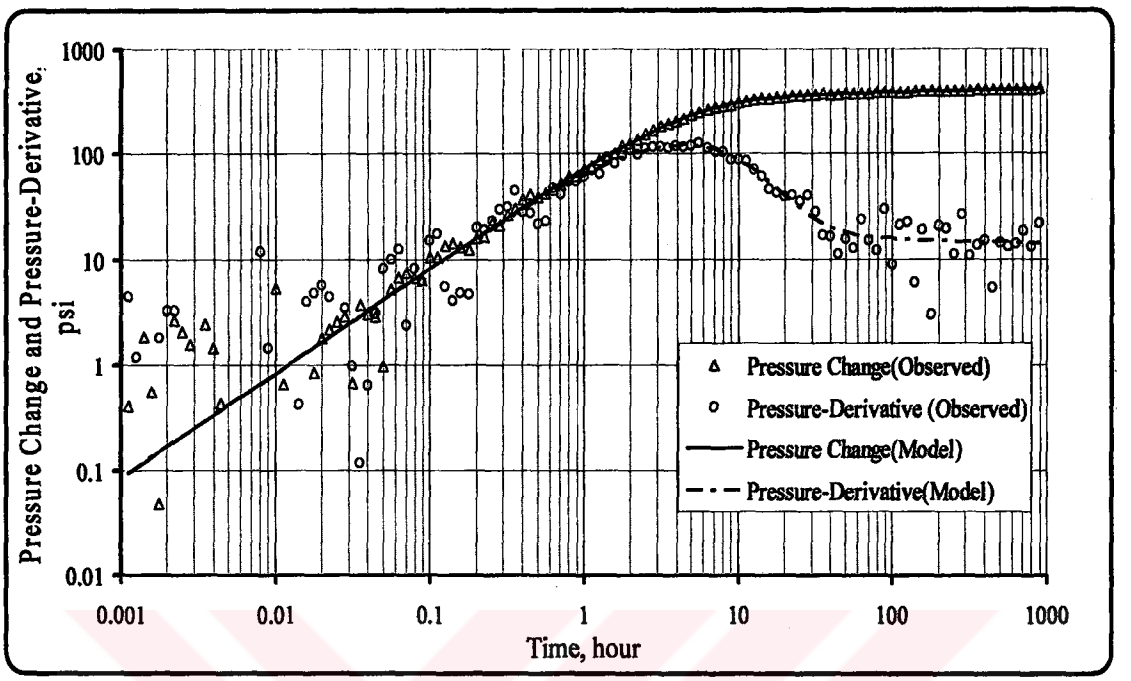

Figure 4.1 Comparison of curve matches of true data with optimized data for pressure drop at active well (Regression 1.1).

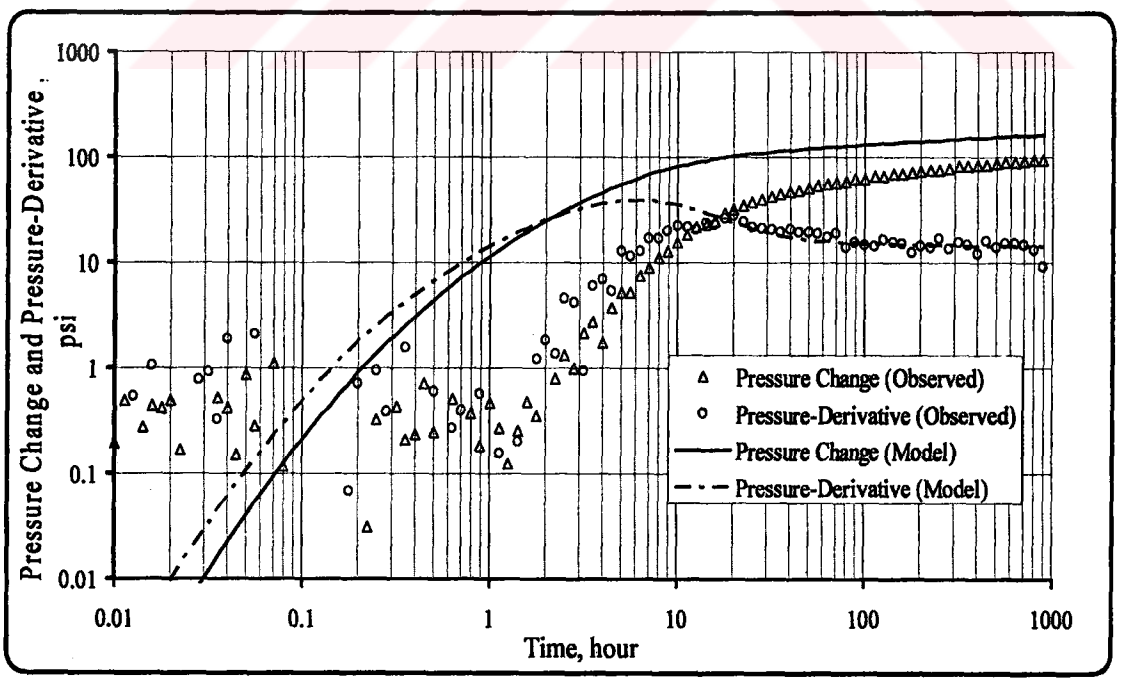

Figure 4.2 Comparison of curve matches of true data with optimized data for pressure drop at observation well (Regression 1.1).

As is seen from Figure 4.1, pressure data obtained from true initial values and pressure drop data obtained from optimized values are matched perfectly for the active well. Although matches for the active well pressure data are very good, the match of observation well pressure data with the model observation pressure data is quite poor. These results indicate that other parameters such as porosity and wellbore storage and skin at the observation well cannot be estimated by using only active well pressure data. Accordingly, pressure data at the observation well should be used to estimate other parameters in regression, in addition to pressure data at the active well.

4.1.2 Matching Pressure Data at Both Active and Observation Wells: In this subsection (Regression 1.2), we consider that we have pressure data at both the active and observation wells, but no flow rate data. We performed regression analysis to estimate the same six parameters as in section 4.1. In Table 4.4, the results of regression are presented together with initial guesses and confidence limits for parameters. The results indicate that porosity and skin at the active well in addition to permeability and wellbore storage at the active well are reliably and confidently estimated by matching pressure data at both the active and observation wells. Note that wellbore storage and skin at the observation well are still could not be determined confidently even if we considered observation well pressure data in matching.

Table 4.4 Results of Regression 1.2 to estimate all parameters.

PARAMETERS	INITIAL GUESSES	TRUE VALUES	OPTIMIZED VALUES	CONFIDENCE LIMIT
k, md	200	100	**101.317165**	± 0.26209
ϕ	0.3	0.15	**0.139996**	± 7.8827E-3
C_a, RB/psi	0.001	0.5	**0.500539**	± 2.83206E-3
C_o, RB/psi	0.001	0.5	0.873005	± 0.13522
S_a	2.0	5.0	**5.152430**	± 1.08422E-2
S_o	2.0	5.0	0.297684	± 1.50105

Next, we investigate whether the set of optimized parameters values in Table 4.4 provides good matches of pressure data and sandface flow rate data at both wells or not. Therefore, curve matching to both pressure data and sandface flow rate data is done separately by calculating interference well test data with optimized values

obtained from inverse problem. Curve matching processes over pressure data and sandface flow rate data are shown in Figures 4.3 and 4.5.

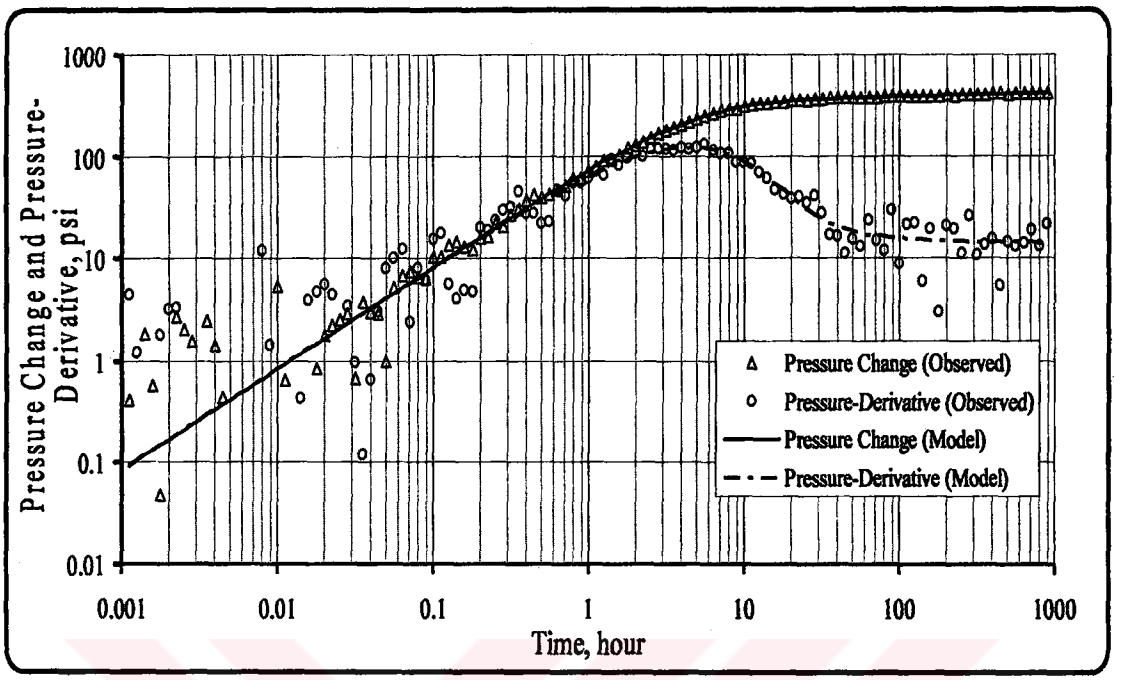

Figure 4.3 Comparison of curve matches of true data with optimized data for pressure drop at the active well (Regression 1.2).

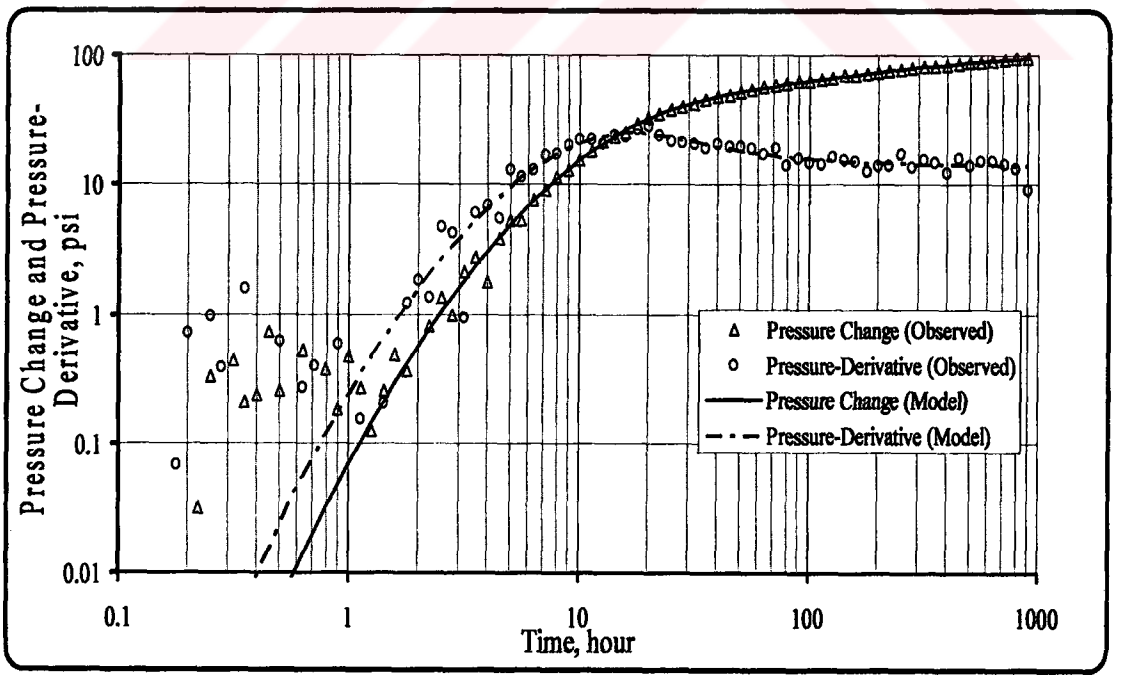

Figure 4.4 Comparison of curve matches of true data with optimized data for pressure drop at observation well (Regression 1.2).

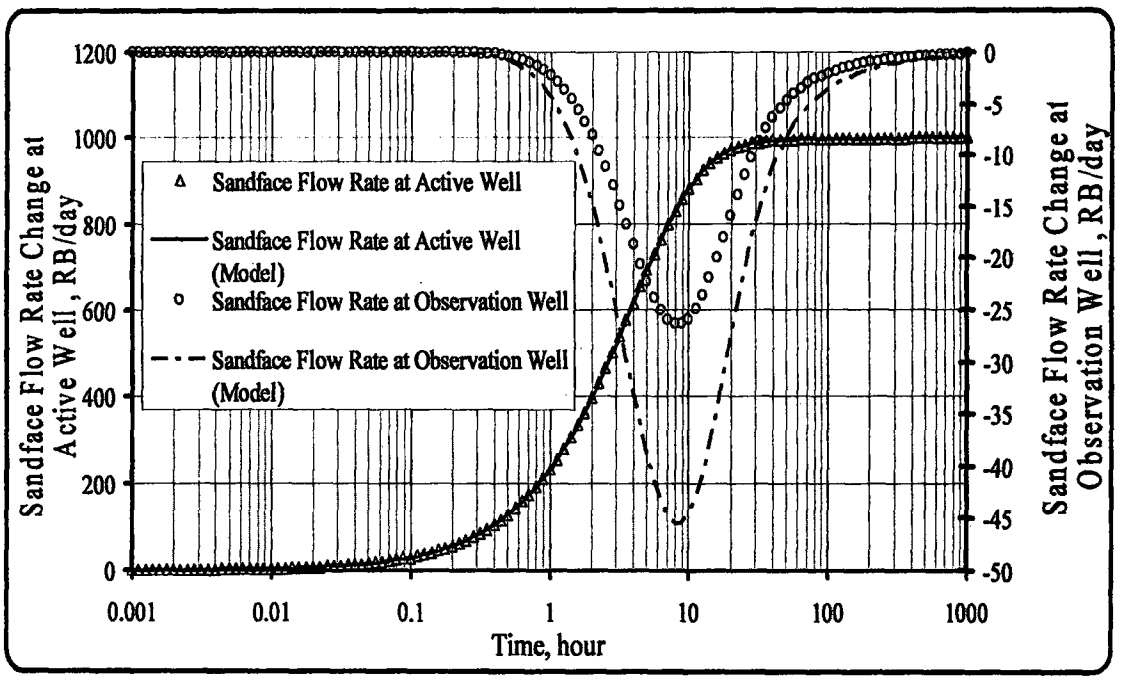

Figure 4.5 Comparison of curve matches of true data with optimized data for sandface flow rates at both active and observation wells (Regression 1.2).

As can be seen from Figures 4.3 and 4.4, the matches of active and observation well pressure data with the corresponding model curves are quite good. However, the match of sandface flow rate at the observation well with the corresponding model curve is quite poor. The reason for this poor match on sandface flow rate data is due to poor optimized estimates of wellbore storage and skin at the observation well. Although pressure data matches for the active and observation wells are very good , all parameters except wellbore storage and skin factor at observation well could be obtained exactly by matching both the active and observation pressure data. Therefore, we can state that wellbore storage and skin at the observation well cannot be estimated reliably from pressure data at both the active and observation wells. Accordingly, next we investigate whether adding sandface flow rate data measured at the observation well in addition to pressure data at the both wells can help resolving these two parameters.

4.1.3 Matching Pressure Data at Both Wells and Sandface Flow Rate Data at Only Observation Well : In this subsection (Regression 1.3), we assume that we have pressure data at both wells and the sandface flow rate data only at the observation well. We performed regression analysis to estimate the six parameters considered previously. In Table 4.5, the results of this regression application are presented together with initial guesses and confidence limits. As can be seen, all

parameters including wellbore storage and skin at the observation well can now be estimated confidently . As can be seen from Table 4.5, confidence limits for the parameters are very small indicating high confidence in the optimized values. .

As been in previous regression steps, now we want to investigate again that whether optimized values in Table 4.5 can match pressure data and sandface flow rate data at both wells or not. Therefore, curve matching to both pressure data and sandface flow rate data is done separately by calculating interference well test data with optimized values obtained from inverse problem. Curve matching processes over pressure and sandface flow rate data are shown in Figures 4.6-4.8.

Table 4.5 Results of Regression 1.3 to estimate all parameters.

PARAMETERS	INITIAL GUESSES	TRUE VALUES	OPTIMIZED VALUES	CONFIDENCE LIMIT
k, md	200	100	**100.29274**	± 0.186942
ϕ	0.3	0.15	**0.147952**	± 3.99527E-3
C_a, RB/psi	0.001	0.5	**0.499974**	± 1.964875E-3
C_o, RB/psi	0.001	0.5	**0.499755**	± 1.48895E-2
S_a	2.0	5.0	**5.035773**	± 2.23741E-2
S_o	2.0	5.0	**5.177492**	± 0.713833

As is seen in Figures 4.6-4.8, pressure and sandface flow rate data obtained from true initial values and pressure data obtained from optimized values are matched perfectly for both the active well. Since all pressure and sandface flow rate data belonging to the observation well are used to estimate parameter, all reservoir parameters are estimated successfully in this sub section. It can be seen that pressure data matches for the observation well are very good at all production times in Figure 4.7, distinctively from Figure 4.4. While sandface flow rate data at the observation well calculated from true initial values and optimized values don't match with each other as seen in Figure 4.5, it can be seen in Figure 4.8 that sandface flow rate data matches with each other perfectly because we used measured sandface flow rate data belonging to the observation well for regression analysis. Consequently, the more data described reservoir and wellbores we use in regression analysis, the more parameter belonging to reservoir and wellbores we estimate.

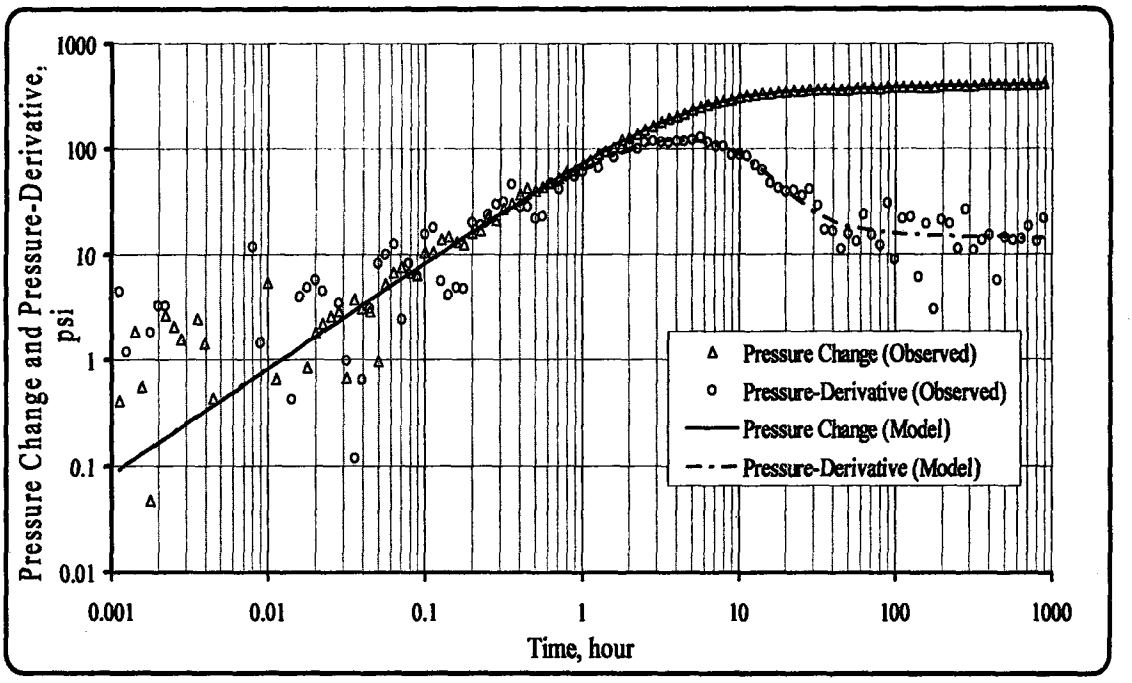

Figure 4.6 Comparison of curve matches of true data with optimized data for pressure drop at active well (Regression 1.3).

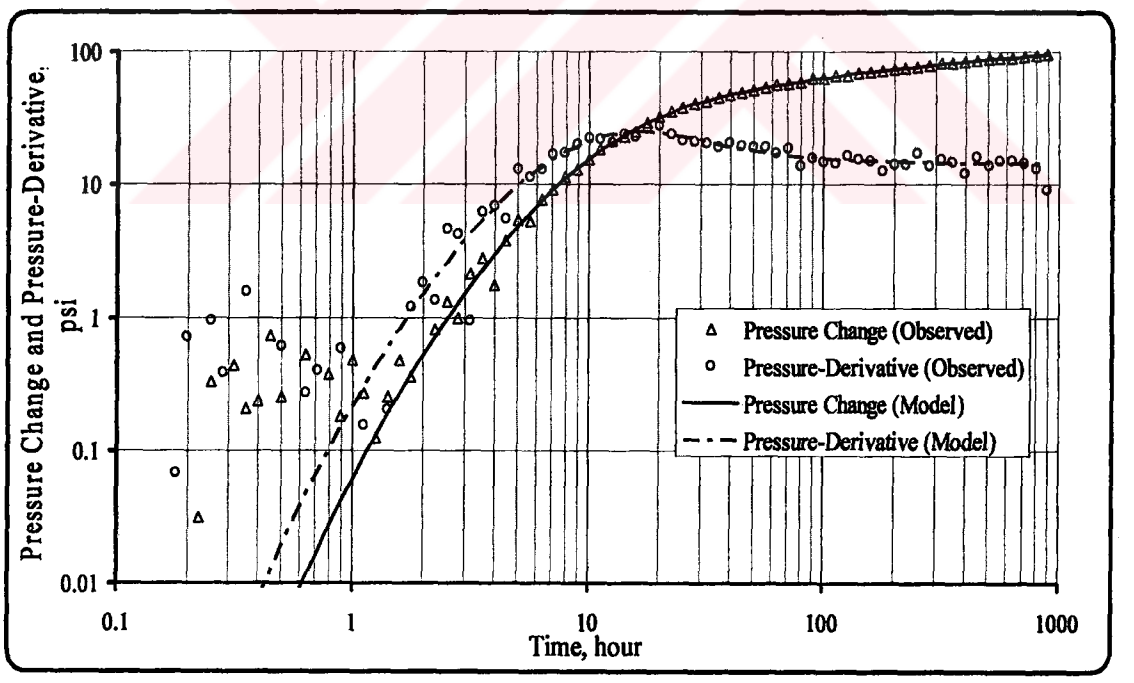

Figure 4.7 Comparison of curve matches of true data with optimized data for pressure drop at observation well (Regression 1.3).

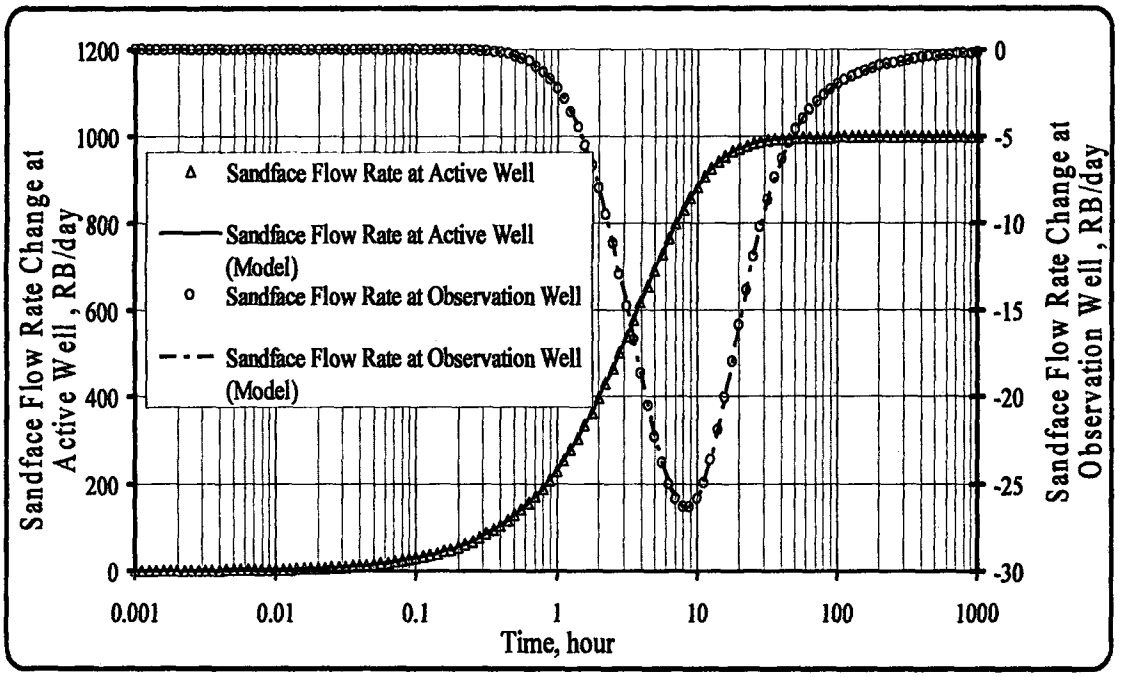

Figure 4.8 Comparison of curve matches of true data with optimized data for sandface flow rates at both active and observation well (Regression 1.3).

4.2 Demonstration of Performances of Optimization Methods :

As aforementioned, three different optimization algorithms were used to estimate parameter in this study. These algorithms are divided to two groups as gradient-based and non-gradient methods. These optimization methods were used for the above applications and comparison of performances of these algorithms is shown in Figure 4.9 in terms of reaching the global minimum of the objective function. For all methods, we considered the same set of initial guesses for parameters. As can be seen from Figure 4.9, the Levenberg-Marquardt algorithm is the fastest one with regard to reaching global minimum. Polytope algorithm is also a very fast technique in comparison to simulated annealing. Note that simulated annealing requires a long termination time and numerous number of function evaluations for this simple application. Information on runtimes of the algorithms in interest is also given in the inset of Figure 4.9. Note that simulated annealing requires almost 666 times bigger runtimes than does the Levenberg-Marquardt algorithm, while polytope requires almost ten times larger runtimes than does the Levenberg-Marquardt.

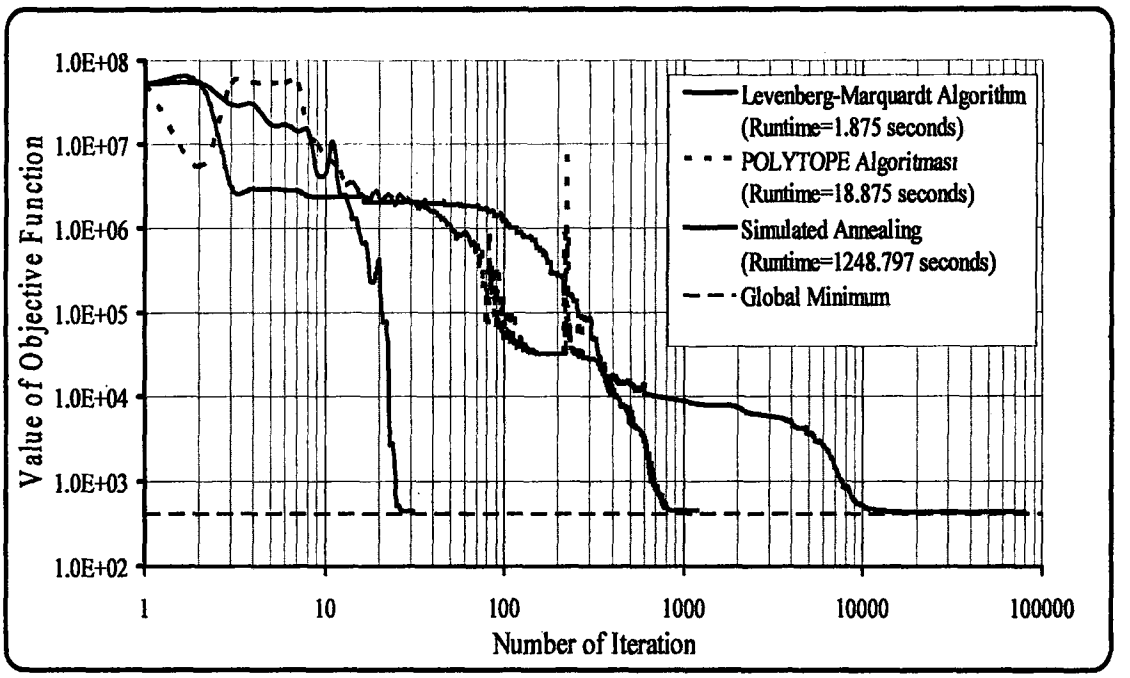

Figure 4.9 Demonstration of performances of optimization algorithms.

4.3 Parameter Estimation in A Two-Layered Reservoir :

In this section, an interference test example in a two-layered reservoir system is considered to estimate individual layer parameters. Reservoir and wellbore properties are given by Tables 4.6-4.7. The active well pressure data were corrupted by adding them normal errors with zero mean and 2 psi standard deviation, while observation well pressure data were corrupted by adding them normal errors with zero mean and 0.5 psi standard deviation. In the same manner measurement error was added to sandface flow rate at the active and observation well.

Table 4.6 Layer properties for regression 3 case.

Parameters	Layer 1	Layer 2
k, md	100	50
ϕ	0.15	0.3
c_t, psi^{-1}	$1x10^{-5}$	$25x10^{-5}$
μ, cp	1.0	1.0
h, ft	50	100
S_{ai}	5	20
S_{oi}	2	10

The distance between the active and observation wells is 350 ft.

Table 4.7 Well data for Regression 2.

	Active Well	Observation Well
r_w, *ft*	0.35	0.35
q, *RB / day*	1000	0.0
C, *RB / psi*	0.5	0.1

4.3.1 Matching Only Pressure Data at The Observation Well : In this subsection, parameter estimation has been performed by using only pressure data at the observation well. Results of parameter estimation are given below Table 4.8.

Table 4.8 Results of Regression 3.1 to estimate all parameters.

Parameters	**Initial Guesses**	**Approximately True Values**	**Optimized Values**	**Confidence Limits**
C_a, *RB / psi*	0.0001	0.5	0.13935	± 0.9461309
C_o, *RB / psi*	0.0001	0.1	0.059958	± 0.996779
k_1, *md*	50	100	**101.87**	± 4.019107
ϕ_1	0.3	0.15	**0.13333**	± 0.0165082
S_{a1}	15	5	32.579	± 0.013878
S_{o1}	12	2	29.354	± 2.81387
k_2, *md*	100	50	23.142	± 1.74289
ϕ_2	0.15	0.3	0.4999	± 0.649078
S_{a2}	2	20	30.634	± 0.1313006
S_{o2}	1	10	21.131	± 1.711581

As can be seen in Table 4.8, parameter estimation by using only pressure data at the observation well cannot be carried out successfully. Since model data obtained by using only observation well pressure response do not match with sandface flow rate data of individual layers at the observation well (Fig. 4.11), it is not possible to resolve all basic layer and wellbore parameters, even if the match for the observation well pressure data is quite good (Fig. 4.10).

with zero mean and 2 psi standard deviation has been added to only the observation well pressure to obtain realistic observed pressure data. In this application, no measurement errors were added to sandface flow rate data at the observation well. Results of parameter estimation are given below Table 4.9.

Table 4.9 Results of Regression 3.2 to estimate all parameters.

Parameters	Initial Guesses	Approximately True Values	Optimized Values	Confidence Limits
C_a, RB/psi	0.0001	0.5	**0.5631039**	± 0.0104779
C_o, RB/psi	0.0001	0.1	**0.100243**	± 0.00781712
k_1, md	50	100	**95.106444**	± 0.852026
ϕ_1	0.3	0.15	**0.13184**	± 0.00081131
S_{a1}	9	5	**4.513811**	± 0.0018495
S_{o1}	5	2	**2.28191**	± 0.049009
k_2, md	100	50	**50.88142**	± 0.0652508
ϕ_2	0.2	0.3	**0.3484408**	± 0.0098549
S_{a2}	10	20	**18.3582**	± 0.008893
S_{o2}	6	10	**10.5518**	± 0.05294

As can be seen in Table 4.9, all unknown parameters are estimated reliably by using only pressure and sandface flow rate data at the observation well. . Because we add flow rate data of individual layers into parameter estimation, , it becomes possible to estimate all individual layer and wellbore parameters, even if the matches belonging to the active well pressure and sandface flow rate data are not very good (Figs. 4.14 and 4.15) . If we added the active well pressure and sandface flow rate data into regression analysis, we would surely obtain adapted match between model and true sandface flow rate data at the active well.

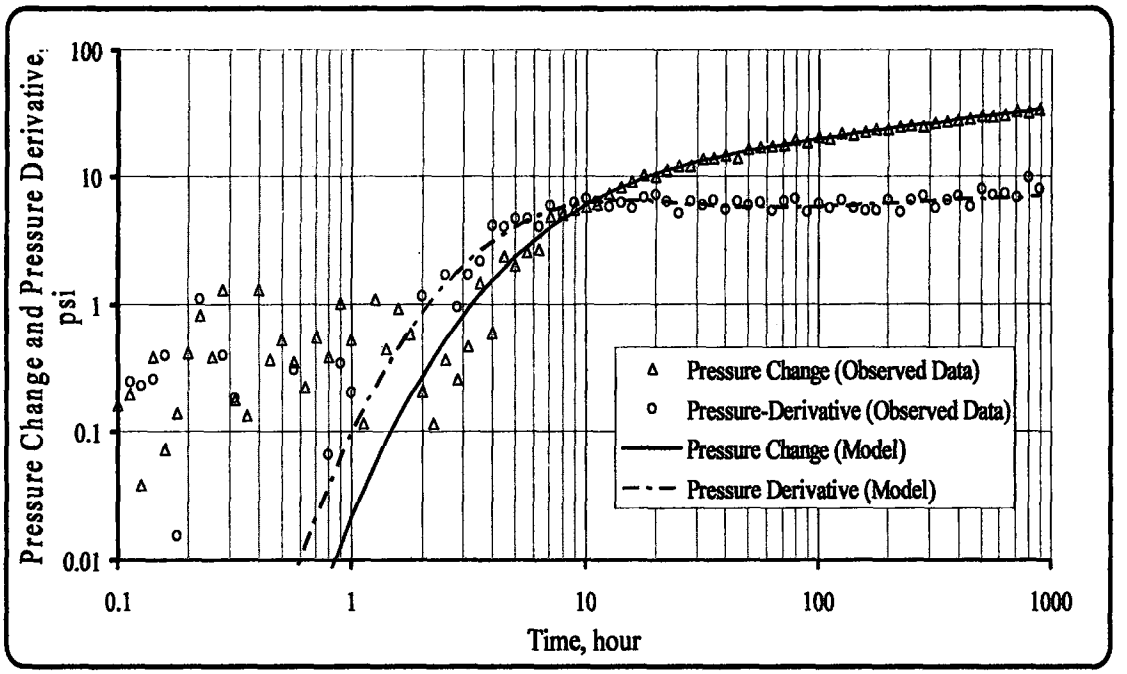

Figure 4.12 Comparison of curve matches of observed data with optimized data for pressure drop at observation well (Regression 3.2).

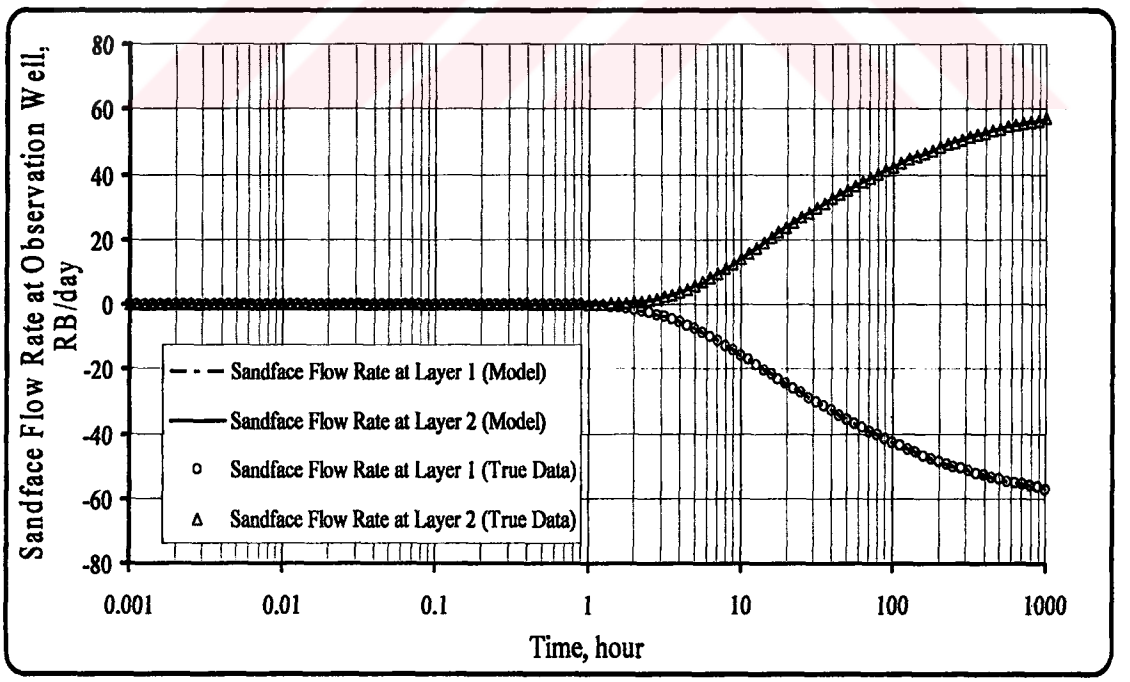

Figure 4.13 Comparison of curve matches of true data with optimized data for sandface flow rates at the observation well (Regression 3.2).

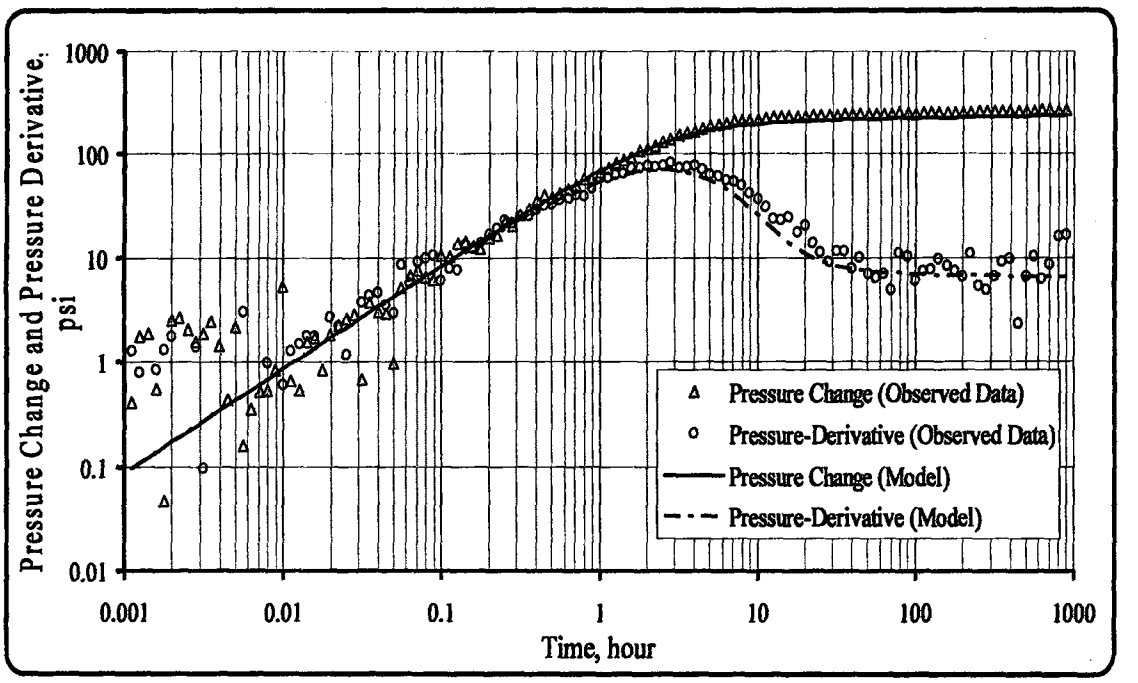

Figure 4.14 Comparison of curve matches of observed data with optimized data for pressure drop at the active well (Regression 3.2).

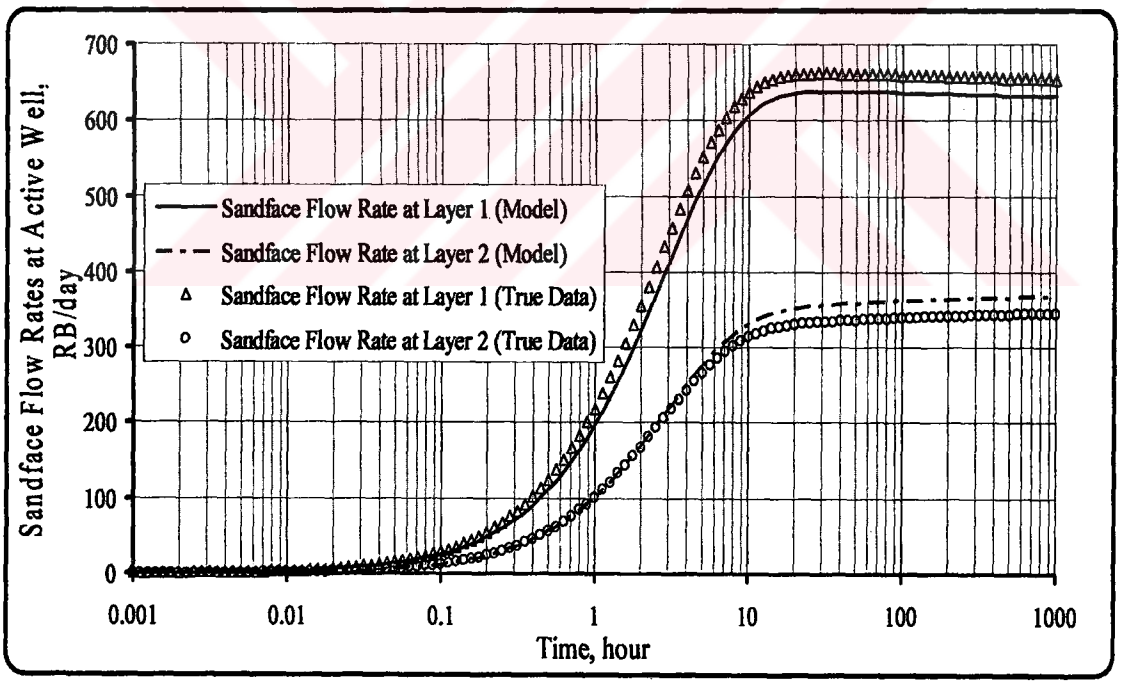

Figure 4.15 Comparison of curve matches of true data with optimized data for sandface flow rates at the active well (Regression 3.2).

4.3.3 Matching Both Pressure and Corrupted Sandface Flow Rate Data at The Observation Well : In this sub section, regression analysis has been applied to pressure response and sandface flow rate of individual layers at the observation well, as been sub section 4.2.3. However, measurement errors with zero mean and

specified standard deviations have been added to both the observation well pressure data and sandface flow rate data to obtain realistic observed pressure data. Measurement error with zero mean and 1 RB standard deviation has been added to the sandface flow rate data as a 1% weighted error at the observation well, while measurement error with zero mean and 2 psi standard deviation has been added to pressure data. Results of parameter estimation are given below Table 4.10.

As can be seen from Table 4.10, all parameters except skin factors for the first layer at both wells could be estimated correctly. The reason that the skin factors for the first layer cannot be obtained is due to lack of information about pressure and sandface flow rate data at the active well and measurement error on sandface flow rate data. If we had measured sandface flow rate data in 1st layer atthe active well, we would estimate all parameters correctly. Figures 4.16-4.19 show the matches of different data sets with the corresponding model data using the optimized values given in Table 4.10.

Table 4.10 Results of Regression 3.3 to estimate all parameters.

Parameters	Initial Guesses	Approximately True Values	Optimized Values	Confidence Limits
C_a, *RB / psi*	0.0001	0.5	**0.578386**	± 0.0158869
C_o, *RB / psi*	0.0001	0.1	**0.10047**	± 0.00880297
k_1, *md*	50	100	**90.10318**	± 0.957656
ϕ_1	0.3	0.15	**0.11374**	± 0.00136527
S_{a1}	15	5	3.40232	± 0.00217434
S_{o1}	12	2	6.19291	± 0.036707
k_2, *md*	100	50	**47.047**	± 0.062739
ϕ_2	0.15	0.3	**0.267769**	± 0.011001
S_{a2}	2	20	**21.8542**	± 0.012575
S_{o2}	1	10	**9.00528**	± 0.072548

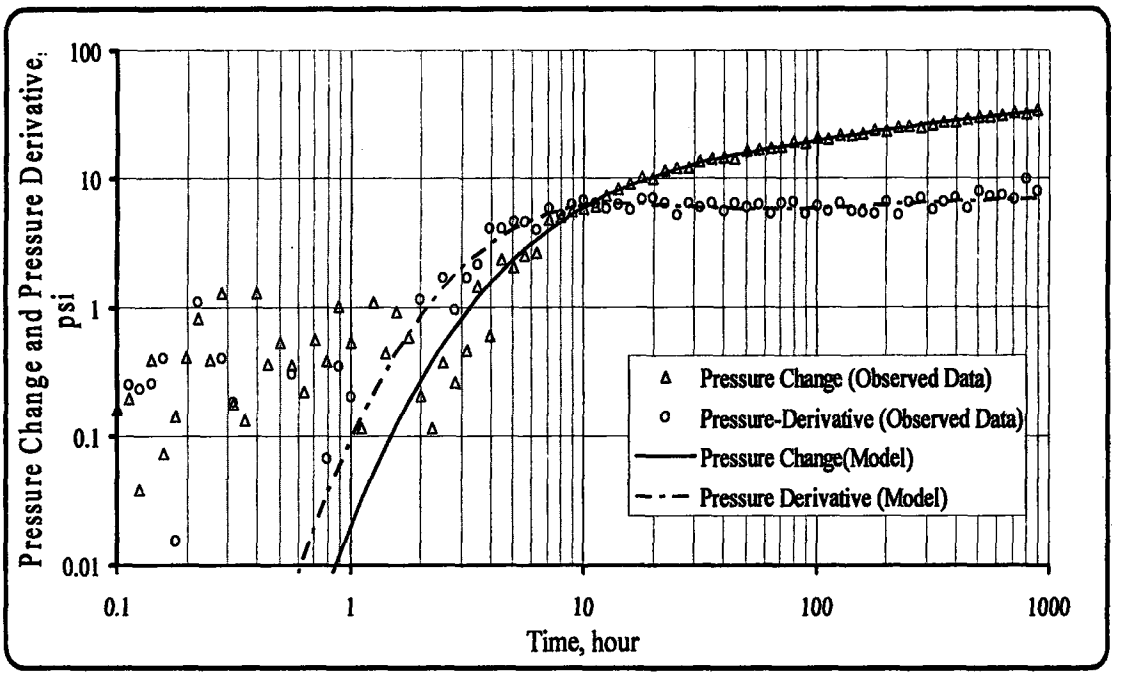

Figure 4.16 Comparison of curve matches of observed data with optimized data for pressure drop at observation well (Regression 3.3).

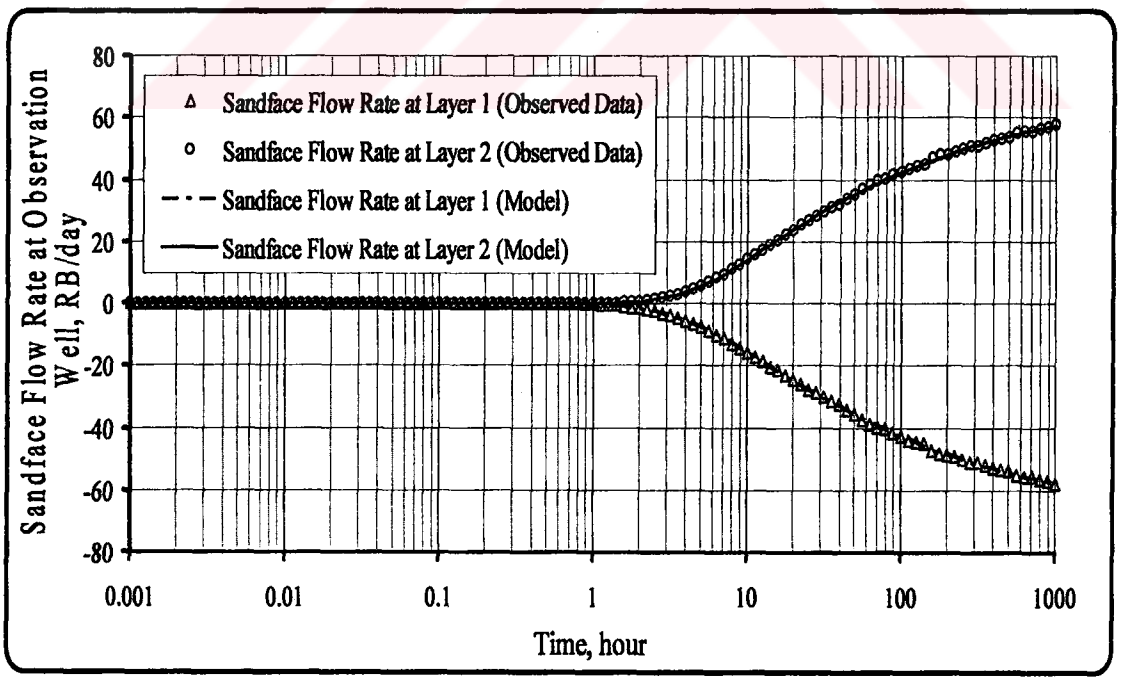

Figure 4.17 Comparison of curve matches of true data with optimized data for sandface flow rates at the observation well (Regression 3.3).

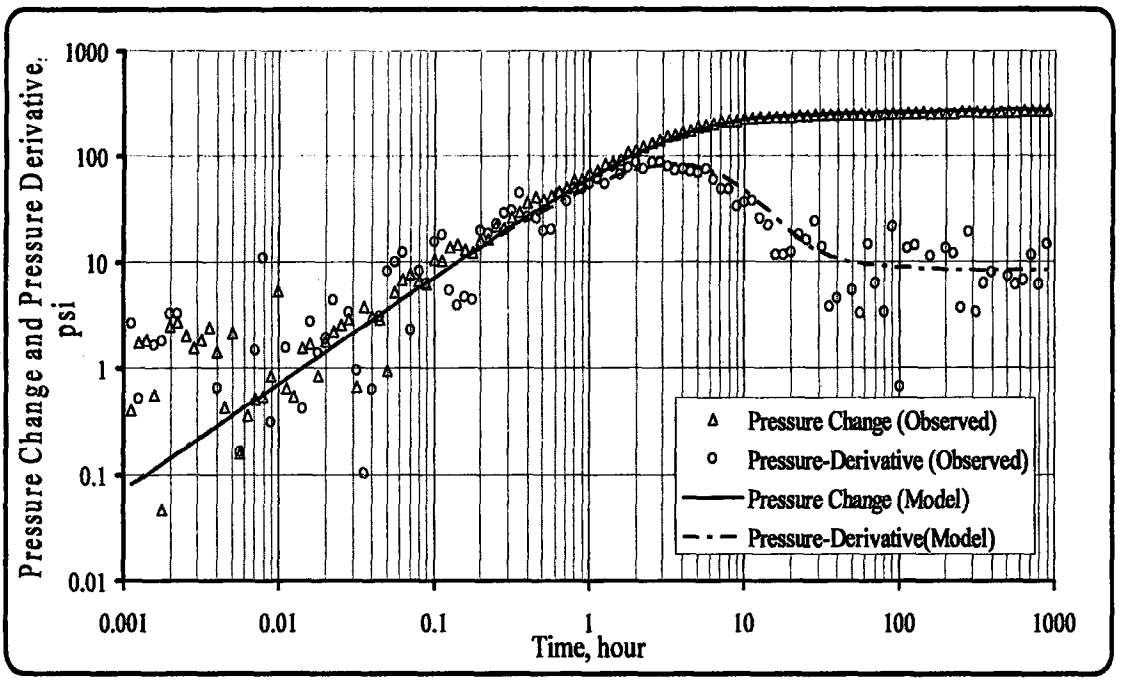

Figure 4.18 Comparison of curve matches of observed data with optimized data for pressure drop at the active well (Regression 3.3).

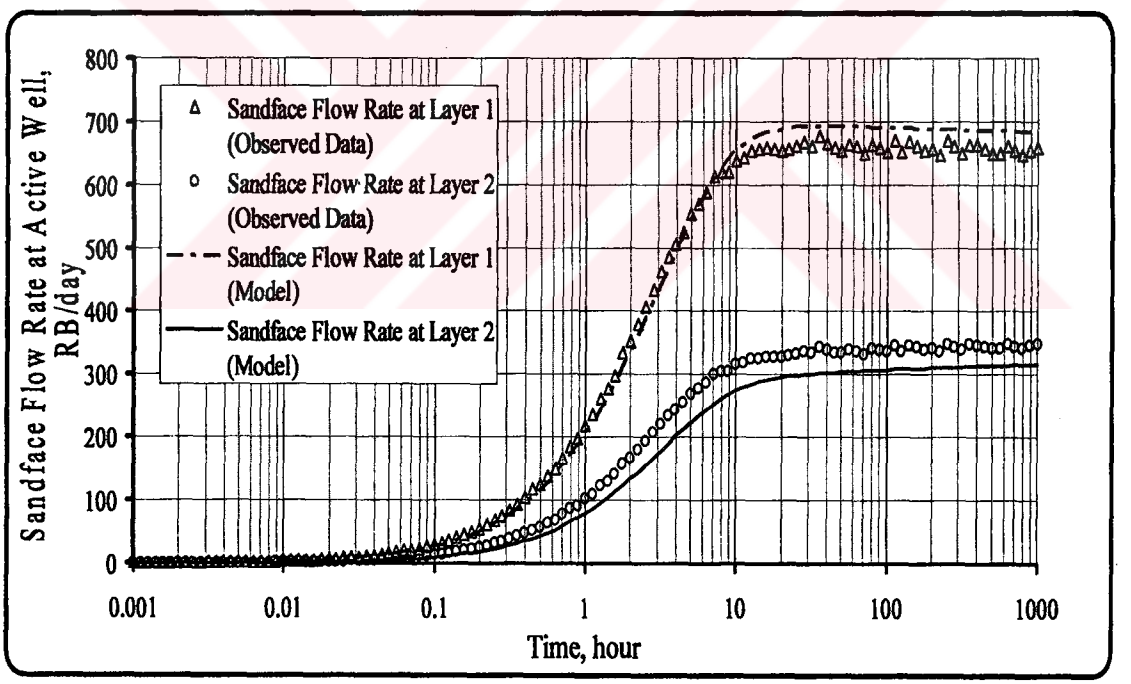

Figure 4.19 Comparison of curve matches of true data with optimized data for sandface flow rates at the active well (Regression 3.3).

4.3.4 Comparison of Performances of Optimization Techniques According to Different Initial Guess Set : In this section, regression analysis was applied to all pressure and sandface layer flow rate data at the active and observation wells to compare the performance of optimization techniques, using several different sets of

initial guesses for the parameters. We regress on ten unknown parameters as those given in Table 4.10. Randomly generated 21 trials with different sets of initial guesses were used to determine the performance of each optimization method in terms of runtime, number of iterations and the value of objective function at the minimum.

Table 4.11 Comparison of three optimization techniques.

	Success Ratio	**Average Runtime, seconds**	**Average Iteration Number**	**Average Function Minimum**
Levenberg-Marquardt	$^{18}/_{21}$	**5.21217**	**13**	**667.3082**
Polytope	$^{13}/_{21}$	**206.235**	**5574**	**726.392**
Simulated Annealing	$^{21}/_{21}$	**5180.74**	**151000**	**672.28059**

As can be seen in Table 4.11, 18 of 21 different initial guess trials for this application can be carried out successfully without getting stuck at local minima by Levenberg-Marquardt. In this problem, we can see that simulated annealing does not have any local minimum problem. This is an expected result because simulated annealing is known as a robust technique and it does not depend very much on initial guesses. However, simulated annealing method is not good as much as Levenberg-Marquardt and polytope techniques in terms of runtimes. Polytope technique is faster than simulated annealing, but it depends on initial guess set more than simulated annealing. Although Levenberg-Marquardt technique depends on initial guess set like polytope, it appears as a more efficient method with respect to runtime and function minimum value for minimization.

4.4 Hybrid Usage of L-M and SA at Three-Layered Reservoir :

In this study, a three-layered reservoir is considered and 14 unknown parameters have been tried to be estimated correctly by using Levenberg-Marquardt and simulated annealing algorithms collectively. Properties of reservoir and wellbore are given in Tables 4.12-4.13. Measurement errors with zero mean and 2 psi standard deviation have been added to pressure data at the active well. The active and observation wells sandface flow rate data consist of measurement errors with zero mean and 1 RB standard deviation as a %1 weighted error. At the same manner,

measurement errors with zero mean and 0.5 psi standard deviation have been added to pressure data at the observation.

Table 4.12 Properties of three-layered reservoir for regression 4.

Parameters	Layer 1	Layer 2	Layer 3
k, md	15	30	100
ϕ	0.1	0.2	0.3
c_t, psi^{-1}	$1x10^{-5}$	$5x10^{-5}$	$1x10^{-4}$
μ, cp	1.0	1.0	1.0
h, ft	20	10	30
S_{ai}	5	0.5	1
S_{oi}	3	2	0.5

Table 4.13 Wellbore properties for regression 4.

	Active Well	Observation Well
r_w, ft	0.35	0.35
q, RB/day	1000	0.0
C, RB/psi	0.5	0.1

In this application, SA algorithm has been firstly used to reduce value of objective function and create smart initial guesses to L-M algorithm, starting with bad initial guesses. As we recall from Figure 4.9, optimization technique which reduces value rapidly of function to be minimized in a several iteration is simulated annealing method, but it converges to global minimum of objective function gradually. To exceed problem of getting stuck at local minima of Levenberg-Marquardt, we consider using the simulated annealing in a first Monte Carlo step to create smarter initial guesses for Levenberg-Marquardt algorithm. One Monte Carlo step consists of 1400 iterations and it takes approximately 96 seconds for 14 unknown non-linear regression problem. Having run simulated annealing for one Monte Carlo step, optimal parameters obtained by using simulated annealing in one Monte Carlo step have been used as an initial guess set for Levenberg-Marquardt algorithm. Namely, inverse problem is tried to be solved by hybrid usage of Levenberg-Marquardt and simulated annealing algorithms. After smarter initial guess

set is created by using simulated annealing for one Monte Carlo step, Levenberg-Marquardt algorithm can solve this inverse problem in a few iterations which takes about 15 seconds. Thus, we can overcome the problem of Levenberg-Marquardt algorithm getting stuck to local minima by using simulated annealing technique collectively. Table 4.14 illustrates the results obtained for this hybrid application.

Table 4.14 Results of hybrid usage of Levenberg-Marquardt and simulated annealing techniques.

Parameter	Initial Guesses	Approximately True Values	SA Results After 1 Monte Carlo Step	L-M Results via SA (Hybridization)
C_a, RB/psi	0.001	0.1	9.99529	**0.099918**
C_o, RB/psi	0.001	0.1	0.12214	**0.10012**
k_1, md	100.0	15.0	73.98521	**14.90681**
ϕ_1	0.25	0.1	0.073758	**0.09969**
S_{a1}	10.0	5.0	11.68891	**4.95212**
S_{o1}	8.0	3.0	11.37028	**3.00487**
k_2, md	200.0	30.0	189.919	**29.7507**
ϕ_2	0.1	0.2	0.35294	**0.19883**
S_{a2}	3.0	0.5	2.98105	**0.46394**
S_{o2}	5.0	2.0	22.86128	**1.55182***
k_3, md	50.0	100.0	59.73917	**98.80885**
ϕ_3	0.08	0.3	0.078326	**0.29882**
S_{a3}	3.0	1.0	1.80807	**0.93513**
S_{o3}	5.0	0.5	4.575	**0.13844***
Function Minimum :	**6,197,355,413.14**	**1097.87152**	**6,235,382.2**	**1108.175**

As can be shown in Table 4.14, using simulated annealing in first Monte Carlo step result in reducing objective function value from $6x10^9$ to $6x10^6$. Moreover, Levenberg-Marquardt method can complete parameter estimation successfully by using initial guess set obtained from simulated annealing technique. To decide whether optimization algorithms can reach to global minimum or not, we should look at RMS which indicates measurement error over pressure and sandface flow rate data (see Chapter III for the definition of RMS). These RMS values are given in Table 4.15.

Table 4.15 RMS values of observed and model data.

	Approximately True Values		Hybridized Optimization Results	
	Active Well RMS	Observation Well RMS	Active Well RMS	Observation Well RMS
Pressure Data	4.16533	0.17333	4.128418	0.161401
Sandface Rate Data at Layer 1	0.32204	0.00738	0.32481	0.00712
Sandface Rate Data at Layer 2	0.61113	0.00097	0.61266	0.0009604
Sandface Rate Data at Layer 3	5.62048	0.00564	5.62681	0.0054

Since RMS values of observed and model data are almost equal to each other, we can say that parameter estimation process or match of observed and model data is performed successfully.

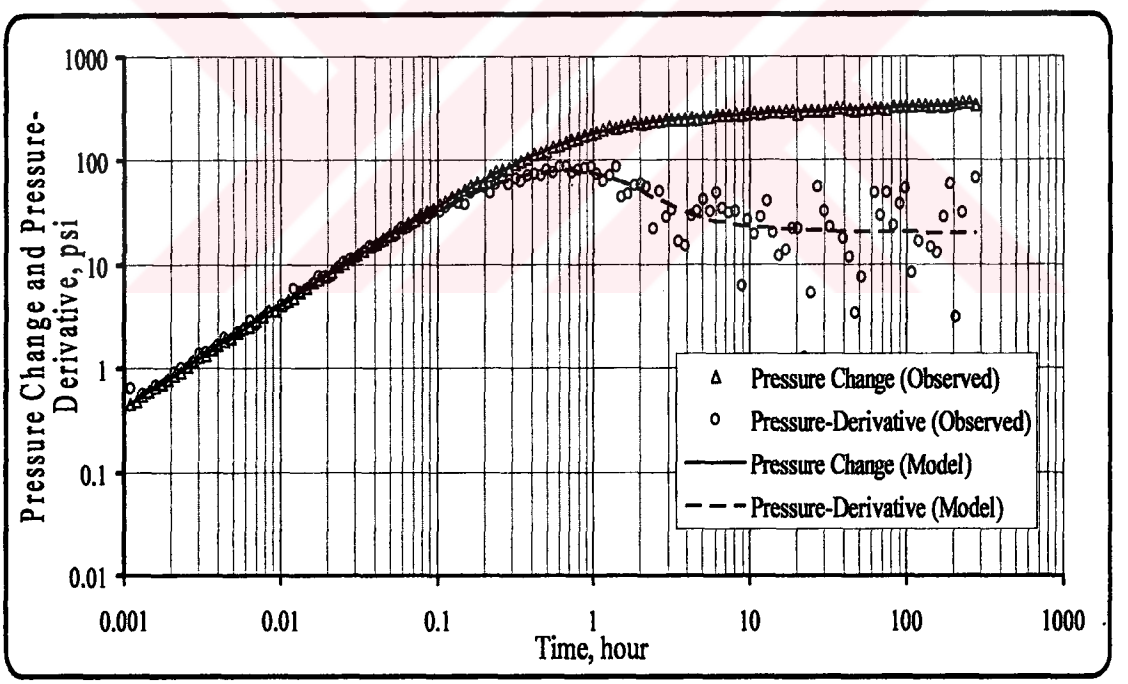

Figure 4.20 Comparison of curve matches of observed data with optimized data for pressure drop at the active well (Regression 4).

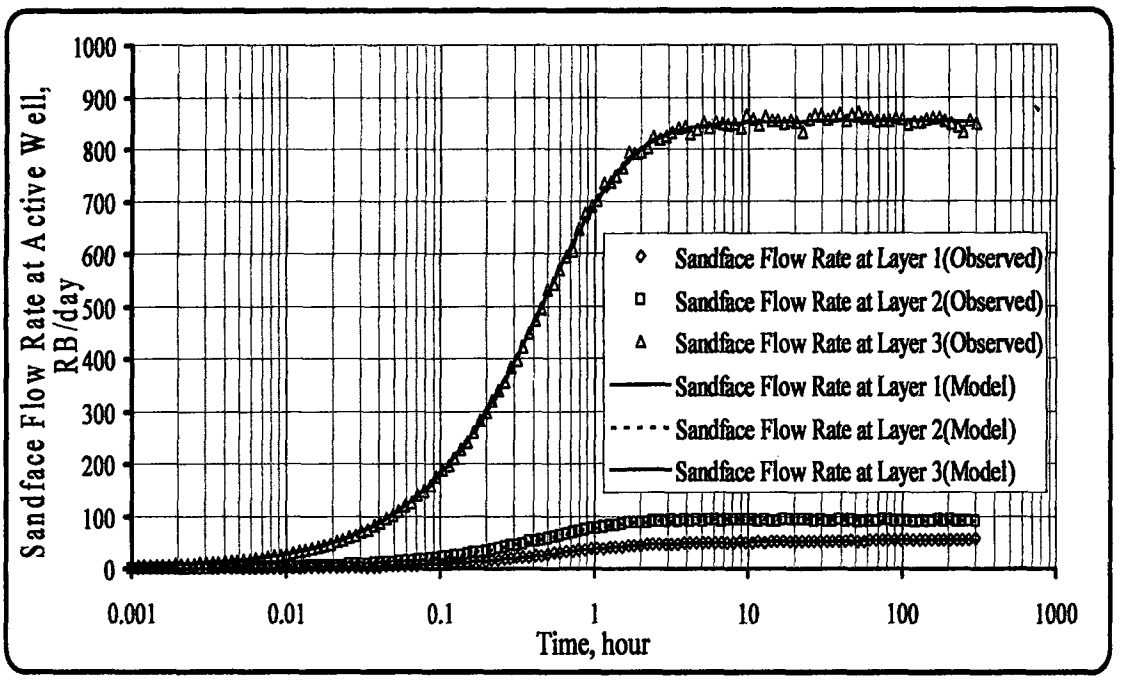

Figure 4.21 Comparison of curve matches of observed data with optimized data for sandface flow rates at the active well (Regression 4).

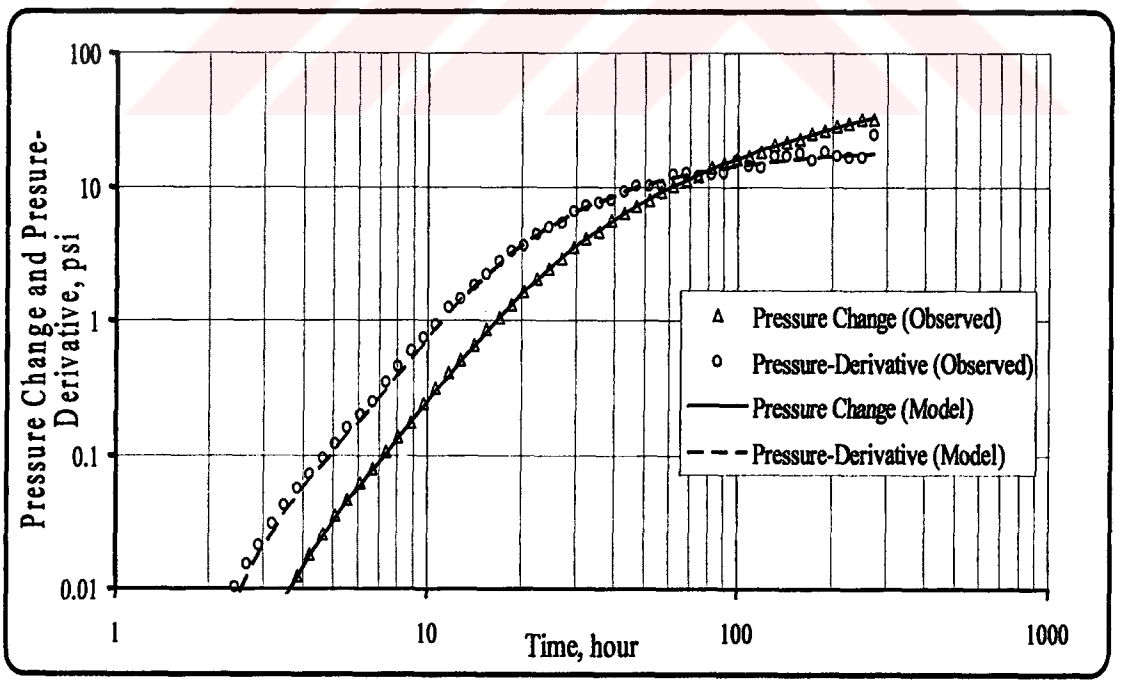

Figure 4.22 Comparison of curve matches of observed data with optimized data for pressure drop at observation well (Regression 4).

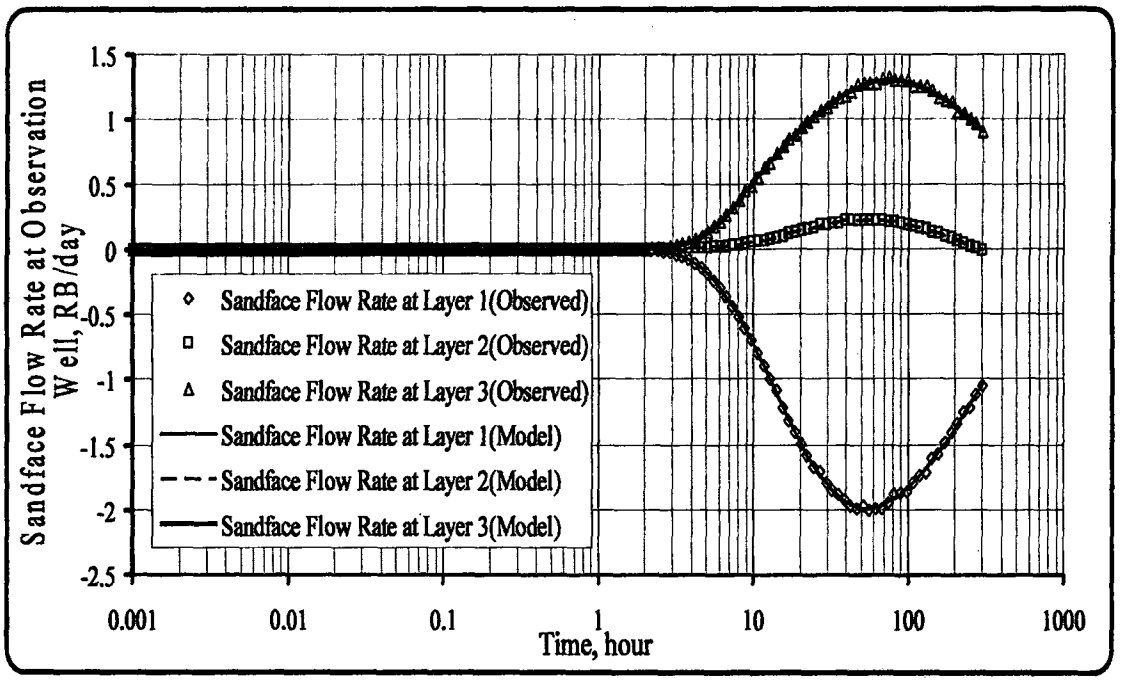

Figure 4.23 Comparison of curve matches of observed data with optimized data for sandface flow rates at the observation well (Regression 4).

As can be seen in Tables 4.19-4.21, matches of observed data and model data are very good. However, skin factors for the 2nd and 3rd layers at observation well cannot be estimated correctly, in spite of good match of all observed and model data. The reason for this can be explained from Figure 4.22, because interference well test sustained shortly till 300 hours. Therefore radial flow period could not be seen exactly from the observation well, as can be seen in Figure 4.22. To be able to estimate whole parameter correctly, we should continue interference well test such a long time that radial flow period can be exactly felt at the observation well.

CHAPTER V

CONCLUSIONS

In this study, analysis of interference tests in commingled infinite-acting multilayer reservoir systems has been considered. One well (the active well) is produced at a specified total surface flow rate, and the second well (observation or interference well) is shut-in for all times. We have presented a semi-analytical solution procedure for computing the wellbore pressure drops and individual layer sandface flow rates. This semi-analytical procedure is general in that it can be applied for any number of layers and also can be applied if wellbore storage and skin effects exist at one or both wells.

By considering simulated data generated from the semi-analytical model developed, we examined the effects of wellbore storage and skin at one or both wells both in single layer and multilayer systems. We found that the wellbore storage and skin effects have a dominant influence on the sandface flow rates and observation well pressure change so that conventional analysis procedures (e.g., type-curve matching and semilog-straight line) render useless to determine individual layer permeability and porosity and skin factors. The specific results indicate that the difference between the pressure change at the observation well and the line source solution is influenced more by the layer flow rates at the active well than the rate of crossflow at the observation well. In some cases, the effect of crossflow on the observation well pressure drop is negligible. In general the magnitude and direction of crossflow through the observation well is governed by the difference in layer pressures that would result if the layers were isolated at the observation well. For the case where all skin factors are zero, crossflow always occurs from the low diffusivity layer to the high diffusivity layer.

In the second phase of our study, both gradient-based and non-gradient based optimization algorithms have been used and applied to our problem to perform non-linear regression analysis of interference well test data. Parameter estimation applications have been performed by using these algorithms; Levenberg-Marquardt

as a gradient-based algorithm, and polytope and simulated annealing methods as non-gradient based methods. We found that the Levenberg-Marquardt algorithm is a very efficient and fast optimization tool, because it has an advantage using derivative information of functions to be optimized. However, because it is known as a local optimizer, it can get stuck at local minima when the user doesn't give smart initial guesses close to the global minimum. The second optimization algorithm used in this study alternatively to Levenberg-Marquardt is polytope method. Since this technique doesn't use any derivative information of functions to be optimized contrary to the Levenberg-Marquardt, it's named as a random direct search method. Although we found that the polytope algorithm isn't fast as Levenberg-Marquardt, when the function to be optimized is very difficult to be calculated its derivative, the polytope algorithm proves useful for being easy to implement. The final optimization method used in this study is simulated annealing. The simulated annealing doesn't use any derivative information of functions like Polytope technique. However, we found that it is very slow when it is compared to the Polytope and Levenberg-Marquardt algorithms. Simulated annealing algorithm is simple to implement like Polytope technique, because user doesn't need to prepare a subroutine calculating derivatives or sensitivities of functions to be optimized.

All things considered, if wellbore storage and/or skin effects exist in wellbores of both wells in a single or multi-layered reservoir system, it needs sandface flow rate information beside pressure data in order to estimate values of skin factor and permeability correctly. In parameter estimation, Levenberg-Marquardt method enables to solve non-linear parameter estimation problem in a very short processor time relatively to polytope and simulated annealing methods. Nevertheless, Levenberg-Marquardt and polytope methods require to be used smart initial guesses. Nonetheless, convergences of simulated annealing and polytope methods depend on control parameters of their kernel codes relatively to Levenberg-Marquardt method. Optimal values belonging to control parameters can change from a problem to another problem. Although simulated annealing method does not depend on initial guesses very much in parameter estimation, it requires a lot of processor times.

As a suggestion to new researchers, a hybrid method between Levenberg-Marquardt and simulated annealing may be developed to succeed in estimating parameters in a very short time without getting stuck at local minima.

REFERENCES

1. **Gok, I. M, :** "Değişken Debili Testlerin Analizi ve Dekonvolüsyon", M.Sc. Thesis, Istanbul Technical University, February 2000.
2. **Lefkovits, H. C., Hazebroek, P., Allen, E. E. and Matthews, C. S. :** " A Study of the Behavior of Bounded Reservoirs Composed of Stratified Layers", Trans., AIME (1961) vol. 222, 43.
3. **Larsen, L. :** "Determination of Skin Factors and Flow Capacities of Individual Layers in Two-Layered Reservoirs", paper SPE 11138, presented at the 57th Annual Technical Conference and Exhibition, New Orleans, LA, Sept. 26-29, 1982.
4. **Larsen, L. :** "Wells Producing Commingled Zones with Unequal Initial Pressures and Reservoir Properties", paper SPE 10325 presented at the 56th Annual Technical Confrence and Exhibition, San Antonio, Texas, Oct. 5-7, 1981.
5. **Onur, M. :** "The Observation Well Response in Commingled Layered Reservoirs", Master of Science Thesis, University of Tulsa, OK, 1985
6. **Van Everdingen, A.F. :** "The Skin Effect and Its Influnce on the Productive Capacity of a Well", Trans. AIME (1953) vol. 198, 171.
7. **Hurst, W. :** "Establishment of the Skin Effect and Impediment to Flud Flow into a Wellbore", Pet. Eng. (Oct. 1953) 25, B-6
8. **Ogbe, D. O. and Brigham, W.E. :** " A Model for Interference Testing with Wellbore Storage and Skin Effects at Both Wells", paper SPE 13253 presented at the SPE 59th Annual Technical Conference and Exhibition, San Francisco, CA, Sept. 16-19, 1984.
9. **Jargon, J. R. :** " Effect of Wellbore Storage and Wellbore Damage at the Active Well an Interference Test Analysis", SPE-AIME, SPE 5795, Marathon Oil Co.
10. **Menekse, K. :** "Doğal Çatlaklı Rezervuarlara Ait Kuyu Testi Verilerinin Doğrusal Olmayan Regresyon Yöntemleri ile Analizi", Ph.D Thesis, Petroleum Engineering, Istanbul Technical University, August 1996.
11. **H. Press, A. Teukolsky, P. Flannery and T. Vetterling :** *Numerical Recipes –The Art of Scientific Computing–*, p. 289-292, 326-334
12. **M. Yoshida, T. Tanaka, R. Itoi and M. Fukuda :** "Analysis of Interference Test in Fractured Reservoir, –Application of Simulated Annealing–", Geothermal Resources Council Transactions, Vol. 24, September 24-27, 2000
13. **Goktas, B. :** "Investigation of the Applicability of Simulated Annealing Method to Automated Type Curve Matching on Horizontal Well Tests", M.Sc. Thesis, New Mexico Institute of Mining and Technology, Socorro, December 1994.

14. **Nelder, J.A and Mead, R. (1965) :** "A Simplex Method for Function Minimization", Computer Journal 7, pp. 308-313

15. **Philip E. Gill, W. Murray and Margaret H. Wright :** *Practical Optimization*, p. 94-95 and 136-137

16. **Leitão, H.C., and Schiozer, D. J. :** "A New Automated History Matching Algorithm improved by Parallel Computing", SPE 53977

17. **Onur, M.:** "Advanced Well Test Analysis Class Notes", (2002) Petroleum and Natural Gas Engineering Department, Istanbul Technical University, Turkey.

18. **Levenberg, K. :** "A Method for the Solution of Certain Nonlinear Problems in Least Squares". Quart. Appl. Math. 2, pp. 164-168. (1944)

19. **Marquardt, D. W. :** "An Algorithm for Least Squares Estimation of Nonlinear Parameters". SIAM J. 11, pp. 431-441. (1963)

20. **Fletcher, R. :** "A Modified Marquardt Subroutine for Nonlinear Least Squares", Reports R6799, Atomic Energy Research Establishment, Harwell, England. (1971)

21. **Hebden, M. D. :** "An Algorithm for Minimization Using Exact Second Derivatives", Report TP515, Atomic Energy Research Establishment, Harwell, England. (1973)

22. **Burton S. Garbow, Kenneth E. Hillstrom, Jorge J. More.:** "LMDER1 source code of Levenberg-Marquardt Algorithm". Argonne National Laboratory. Minpack Project. March 1980.

23. **Goffe, W. L. et al :** "Global Optimization of Statistical Functions With Simulated Annealing", May, 1993

24. **Kirkpatrick, S., C. D. Gelatt Jr. and M. P. Vecchi. :** "Optimization by Simulated Annealing." Science 220 (1983): 671-80.

25. **Wong, D. F., H. W. Leong and C. L. Liu. :** " Simulated Annealing for VLSI Design". Boston: Kluwer Academic Publishers, 1988.

26. **Derwent, Dick. :** "A Better Way to Control Pollution." Nature 331 (1988): 575-78.

27. **Drexl, A. :** "A Simulated Annealing Approach to the Multi-constraint Zero-One Knapsack Problem". Computing 40 (1988): 1-8.

28. **Wasserman, Philip D. and Tom Schwartz. :** "Neural Networks, Part 2: What Are They and Why Is Everybody So Interested in Them Now?" IEEE Expert Spring 1988: 10-15.

29. **Telly, H., Th. M. Liebling and A. Mocellin. :** "Reconstruction of Polycrystalline Structures: a New Application of Combinatorial Optimization" Computing 38 (1987): 1-11.

30. **Carnevali, P., L. Coletti and S. Patarnello. :** "Image Processing by Simulated Annealing" IBM Journal of Research and Development 29 (1985) 569-79.

31. **Ouenes, A., Bhagavan, S.:** "Application of Simulated Annealing and Other Global Optimization Methods to Reservoir Description: Myths and Realities", SPE 28415, pp.547-561, New Mexico Petroleum Recovery Research Center.

32. **Corana, A., M. Marchesi, C. Martini and S. Ridella.:** "Minimizing Multimodal Functions of Continuous Variables with the 'Simulated Annealing' Algorithm." ACM Transactions on Mathematical Software 13 (1987): 262-80.

33. **Miller, A :** "SIMANN.F90 simulated annealing source code, F90 version". Logistic Regression; TOMS algorithms; Special code for F and NAS compilers; Miscellaneous other code Applied Statistics Algorithms.

34. **Metropolis, N., Rosenbluth, M., Teller, A., and Teller, E. :** " Equation of State Calculations by Fast Computing Machines". J. Chem. Phys. 21 (1953), 1087-1090.

35. **Spendley, W., Hext, G. R., and Himsworth, F. R. :** "Sequential Application of Simplex Designs in Optimization and Evolutionary Operation", Thecnometrics, Vol.4, p. 441.

36. **Shaw D. E., Wedderburn R. W. M and Alan, M. :** "MINIM.f90 source code of The Nelder-Mead Simplex Algorithm for Unconstrained Minimization", Csiro, Division of Mathematics & Statistics, Rothamsted Experimental Station Harpenden, Hertfordshire, England. Further amended by Alan Miller, Csiro Division of Mathematical & Information Sciences. (Fortran 90 conversion by Alan Miller)

37. **Miller, A. :** "SIMANN.F90 simulated annealing source code, F90 version". Logistic Regression; TOMS algorithms; Special code for F and NAS compilers; Miscellaneous other code Applied Statistics Algorithms.

38. **Bard, Y. :** *Nonlinear Parameter Estimation*, Academic Press Inc., New York City (1974) 184.

39. **Dogru, A.H., Dixon, T.N., and Edgar, T.F. :** "Confidence Limits on the Parameters and Predictions of Slightly Compressible, Single Phase Reservoirs", SPEJ (February 1977) 42; Trans., AIME, 263.

40. **Fletcher, R. :** *Practical Methods of Optimization*, John Willey & Sons, New York City (1987) 101.

41. **Carvalho, R. et al.** : "Simple Procedures for Imposing Constraints for Nonlinear Least Squares Optimization", SPEJ (December 1996) 395.

42. **Aziz, K. and Settari A. :** *Petroleum Reservoir Simulation*, Appendix section. Elsevier Applied Science Publishers, London (1979).

APPENDIX A

Solution and Demonstration with Matrix of Problem Including Wellbore Storage and Skin Factor Effects

Let l denote the number of layer in multi-layered reservoir system. The elements of the A matrix, $\vec{x}$ and $\vec{b}$ column vectors shown in Table 2.1 are defined by functions as given below : The elements of the coefficients matrix are

$$d_j = -P_{FCN_j}(r_{wa}, \Delta t, S_a), \qquad j = 1,2, \ldots l \tag{A.1}$$

$$e_j = -P_{FCN_j}(r_{wo}, \Delta t, S_o), \qquad j = 1,2, \ldots l \tag{A.2}$$

$$b_j = -P_{FCN_j}(r, \Delta t), \qquad j = 1,2, \ldots l \tag{A.3}$$

$$f_1 = \frac{24\, C_a}{\Delta t} \tag{A.4}$$

$$f_2 = \frac{24\, C_o}{\Delta t} \tag{A.5}$$

c_j variable series into the right hand-side vector is defined as given below :

For $j = 1,2, \ldots l$

$$\begin{aligned} c_j = {} & q_{aj}(t_1) P_{FCN_j}(r_{wa}, t_{n+1}) - q_{aj}(t_n) P_{FCN_j}(r_{wa}, t_{n+1} - t_n) \\ & + P_{FCN_j}(r_{wa}, t_{n+1} - t_1)\left(q_{aj}(t_2) - q_{aj}(t_1)\right) \\ & + \sum_{k=1}^{n-2}\left[P_{FCN_j}(r_{wa}, t_{n+1} - t_{k+1})\left(q_{aj}(t_{k+2}) - q_{aj}(t_{k+1})\right)\right] \\ & + q_{oj}(t_1) P_{FCN_j}(r, t_{n+1}) - q_{oj}(t_n) P_{FCN_j}(r, t_{n+1} - t_n) \\ & + P_{FCN_j}(r, t_{n+1} - t_1)\left(q_{oj}(t_2) - q_{oj}(t_1)\right) \\ & + \sum_{k=1}^{n-2}\left[P_{FCN_j}(r, t_{n+1} - t_{k+1})\left(q_{oj}(t_{k+2}) - q_{oj}(t_{k+1})\right)\right] \end{aligned} \tag{A.6}$$

For $j = l+1, l+2, \ldots 2l$

$$
\begin{aligned}
c_j &= q_{aj}(t_1)P_{FCN_j}(r,t_{n+1}) - q_{aj}(t_n)P_{FCN_j}(r,t_{n+1}-t_n) \\
&\quad + P_{FCN_j}(r,t_{n+1}-t_1)\left(q_{aj}(t_2)-q_{aj}(t_1)\right) \\
&\quad + \sum_{k=1}^{n-2}\left[P_{FCN_j}(r,t_{n+1}-t_{k+1})\left(q_{aj}(t_{k+2})-q_{aj}(t_{k+1})\right)\right] \\
&\quad + q_{oj}(t_1)P_{FCN_j}(r_{wo},t_{n+1}) - q_{oj}(t_n)P_{FCN_j}(r_{wo},t_{n+1}-t_n) \\
&\quad + P_{FCN_j}(r_{wo},t_{n+1}-t_1)\left(q_{oj}(t_2)-q_{oj}(t_1)\right) \\
&\quad + \sum_{k=1}^{n-2}\left[P_{FCN_j}(r_{wo},t_{n+1}-t_{k+1})\left(q_{oj}(t_{k+2})-q_{oj}(t_{k+1})\right)\right]
\end{aligned}
\tag{A.7}
$$

$$
\begin{aligned}
g_1 &= f_1\,\Delta p_{wf}(t_n) \\
g_2 &= f_2\,\Delta p_{of}(t_n)
\end{aligned}
\tag{A.8}
$$

C_a : Wellbore storage coefficient at active well, RB/psi
C_o : Wellbore storage coefficient at observation well, RB/psi
r_{wa} : Radius of active well, ft
r_{wo} : Radius of observation well, ft
q_{aj} : Sandface flow rate of j^{th} layer at active well, RB/day
q_{oj} : Sandface flow rate of j^{th} layer at observation well, RB/day
q_{as} : Total surface flow rate at active well, RB/day
q_{os} : Total surface flow rate at observation well, RB/day
Δp_{wf} : Bottom hole pressure drop at active well, psi
Δp_{of} : Bottom hole pressure drop at observation well, psi

As can be seen from Eqs. A.1-A.7, when the number of layers is increased, both locations and the size of the coefficient matrix change. To solve the matrix problem shown in Table 2.1, one can use any matrix solver based on Gauss-elimination technique. In this work we used GBAND matrix solver given in Aziz and Settari [42] to solve the matrix problem.

Firstly, if we begin from coefficient matrix in Table 2.1, this matrix forms from nine ("9") different series varying independently from each other. To be able to see the changes of these series quite easily :

For a reservoir system where number of layers equals to one ("$l = 1$"), coefficient matrix occured in solving the problem :

$$A_1(4x4)=\begin{bmatrix} d_1 & b_1 & 1 & 0 \\ b_1 & e_1 & 0 & 1 \\ 1 & 0 & f_1 & 0 \\ 0 & 1 & 0 & f_2 \end{bmatrix} \tag{A.9}$$

We make these series into the coefficient matrix read by computer program as given below :

$$\begin{aligned} &A(1)=d_1,\ A(2)=A(5)=b_1,\ A(3)=A(8)=A(9)=A(14)=1.0 \\ &A(4)=A(7)=A(10)=A(12)=A(13)=A(15)=0 \\ &A(11)=f_1,\ A(16)=f_2 \end{aligned} \tag{A.10}$$

For a multi-layered reservoir system where the number of layers equals two ("$l=2$"), the coefficient matrix occured in solving of this problem :

$$A_2(6x6)=\left[\begin{array}{cc:cc:cc} d_1 & 0 & b_1 & 0 & 1 & 0 \\ 0 & d_2 & 0 & b_2 & 1 & 0 \\ \hdashline b_1 & 0 & e_1 & 0 & 0 & 1 \\ 0 & b_2 & 0 & e_2 & 0 & 1 \\ \hdashline 1 & 1 & 0 & 0 & f_1 & 0 \\ 0 & 0 & 1 & 1 & 0 & f_2 \end{array}\right] \tag{A.11}$$

where ;

$$\begin{aligned} &A(1)=d_1,\ A(8)=d_2 && \Rightarrow \textit{Elements of Zone } 1 \\ &A(3)=b_1,\ A(10)=b_2 && \Rightarrow \textit{Elements of Zone } 2 \\ &A(5)=A(11)=1.0 && \Rightarrow \textit{Elements of Zone } 3 \\ &A(13)=b_1,\ A(20)=b_2 && \Rightarrow \textit{Elements of Zone } 4 \\ &A(15)=e_1,\ A(22)=e_2 && \Rightarrow \textit{Elements of Zone } 5 \\ &A(18)=A(24)=1.0 && \Rightarrow \textit{Elements of Zone } 6 \\ &A(25)=A(26)=1.0 && \Rightarrow \textit{Elements of Zone } 7 \\ &A(33)=A(34)=1.0 && \Rightarrow \textit{Elements of Zone } 8 \\ &A(29)=f_1,\ A(36)=f_2 && \Rightarrow \textit{Elements of Zone } 9 \end{aligned} \tag{A.12}$$

For $l=2$, rest of all the other elements of coefficients matrix equals to zero.

For a reservoir system where the number of layers equals to three ("$l=3$"), coefficients matrix occured in solving of this problem :

$$A_3(8x8)=\left[\begin{array}{ccc:ccc:cc} d_1 & 0 & 0 & b_1 & 0 & 0 & 1 & 0 \\ 0 & d_2 & 0 & 0 & b_2 & 0 & 1 & 0 \\ 0 & 0 & d_3 & 0 & 0 & b_3 & 1 & 0 \\ \hdashline b_1 & 0 & 0 & e_1 & 0 & 0 & 0 & 1 \\ 0 & b_2 & 0 & 0 & e_2 & 0 & 0 & 1 \\ 0 & 0 & b_3 & 0 & 0 & e_3 & 0 & 1 \\ \hdashline 1 & 1 & 1 & 0 & 0 & 0 & f_1 & 0 \\ 0 & 0 & 0 & 1 & 1 & 1 & 0 & f_2 \end{array}\right] \qquad \text{(A.13)}$$

We make these values into the coefficient matrix Eq.(A.13) read by computer program, as given below :

$$\begin{aligned} &A(1)=d_1,\ A(10)=d_2,\ A(19)=d_3 && \Rightarrow \textit{Elements of Zone } 1 \\ &A(4)=b_1,\ A(13)=b_2,\ A(22)=b_3 && \Rightarrow \textit{Elements of Zone } 2 \\ &A(7)=1.0,\ A(15)=1.0,\ A(23)=1.0 && \Rightarrow \textit{Elements of Zone } 3 \\ &A(25)=b_1,\ A(34)=b_2,\ A(43)=b_3 && \Rightarrow \textit{Elements of Zone } 4 \\ &A(28)=e_1,\ A(37)=e_2,\ A(46)=e_3 && \Rightarrow \textit{Elements of Zone } 5 \\ &A(32)=1.0,\ A(40)=1.0,\ A(48)=1.0 && \Rightarrow \textit{Elements of Zone } 6 \\ &A(49)=A(50)=A(51)=1.0 && \Rightarrow \textit{Elements of Zone } 7 \\ &A(60)=A(61)=A(62)=1.0 && \Rightarrow \textit{Elements of Zone } 8 \\ &A(55)=f_1,\ A(64)=f_2 && \Rightarrow \textit{Elements of Zone } 9 \end{aligned} \qquad \text{(A.14)}$$

For a multi-layered reservoir with four layers ("$l=4$"), the coefficient matrix occured in solving the matrix :

$$A_4(10x10)=\left[\begin{array}{cccc:cccc:cc} d_1 & 0 & 0 & 0 & b_1 & 0 & 0 & 0 & 1 & 0 \\ 0 & d_2 & 0 & 0 & 0 & b_2 & 0 & 0 & 1 & 0 \\ 0 & 0 & d_3 & 0 & 0 & 0 & b_3 & 0 & 1 & 0 \\ 0 & 0 & 0 & d_4 & 0 & 0 & 0 & b_4 & 1 & 0 \\ \hdashline b_1 & 0 & 0 & 0 & e_1 & 0 & 0 & 0 & 0 & 1 \\ 0 & b_2 & 0 & 0 & 0 & e_2 & 0 & 0 & 0 & 1 \\ 0 & 0 & b_3 & 0 & 0 & 0 & e_3 & 0 & 0 & 1 \\ \hdashline 0 & 0 & 0 & b_4 & 0 & 0 & 0 & e_4 & 0 & 1 \\ 1 & 1 & 1 & 1 & 0 & 0 & 0 & 0 & f_1 & 0 \\ 0 & 0 & 0 & 0 & 1 & 1 & 1 & 1 & 0 & f_2 \end{array}\right] \qquad \text{(A.15)}$$

We make again these elements into the coefficient matrix Eq.(A.15) read by computer program, as given below :

$$
\begin{aligned}
&A(1)=d_1,\ A(12)=d_2,\ A(23)=d_3,\ A(34)=d_4 && \Rightarrow \textit{Elements of Zone } 1\\
&A(5)=b_1,\ A(16)=b_2,\ A(27)=b_3,\ A(38)=b_4 && \Rightarrow \textit{Elements of Zone } 2\\
&A(9)=1.0,\ A(19)=1.0,\ A(29)=1.0,\ A(39)=1.0 && \Rightarrow \textit{Elements of Zone } 3\\
&A(41)=b_1,\ A(52)=b_2,\ A(63)=b_3,\ A(74)=b_3 && \Rightarrow \textit{Elements of Zone } 4\\
&A(45)=e_1,\ A(56)=e_2,\ A(67)=e_3,\ A(78)=e_3 && \Rightarrow \textit{Elements of Zone } 5
\end{aligned}
\qquad \text{(A.16)}
$$

$$
\begin{aligned}
&A(50)=A(60)=A(70)=A(80)=1.0 && \Rightarrow \textit{Elements of Zone } 6\\
&A(81)=A(82)=A(83)=A(84)=1.0 && \Rightarrow \textit{Elements of Zone } 7\\
&A(95)=A(96)=A(97)=A(98)=1.0 && \Rightarrow \textit{Elements of Zone } 8\\
&A(89)=f_1,\ A(100)=f_2 && \Rightarrow \textit{Elements of Zone } 9
\end{aligned}
$$

Coefficient matrices for $(l=1,2,3,4,...)$, to show how the elements into the coefficient matrix change in terms of number of layers and to prove how correlations of the series in every zones of coefficients matrix can be set up, are formed one by one. It is important note that if we denote number of elements into coefficients matrix by N, we can use expression of $N=(2l+2)^2$ easily.

Now, by starting from Zone 1 into the coefficient matrix in Table 2.1, let's show how all the variables and constant terms can be read from the matrix by using computer program.

Firstly, as an initial step, zero number is assigned to all the terms into the coefficient matrix. If we want to show this easily as a programming routine ;

For I=1, $(2l+2)^2$

A(I)=0.0

Next

A.1 Assignment of Elements in Zones 1 and 5

If we look at Table A.1 carefully, assignment of Zone 1 is completed by assigning d_1 term to first element of coefficient matrix formed for a one layered reservoir system. However, if the number of layers increases, d_j terms occur as much as the number of layers, along with d_1 is always assigned to first element of coefficients matrix. Then d_2 term is assigned to the 8^{th} element of the coefficient matrix. In the same

manner, subscripts of elements to which d_l series need to be assigned of the coefficient matrix are shown below in Table A.1, in case of the fact that the number of layers equals to 3 and 4.

Table A.1 Assignment plan of elements in zones 1 and 5.

For l =1		**For l =2**		**For l =3**		**For l =4**	
A(i)	**d(j)**	**A(i)**	**d(j)**	**A(i)**	**d(j)**	**A(i)**	**D(j)**
i=1	*j=1*	*i=1* *i=8* ↓	*j=1* *j=2*	*i=1* *i=10* *i=19* ↓	*j=1* *j=2* *j=3*	*i=1* *i=12* *i=23* *i=34* ↓	*j=1* *j=2* *j=3* *J=4*
		DIFF_2		DIFF_3		DIFF_4	
		7		9		11	

In cases that the number of layers equals to 5, 6, 7 ,..., 10,... respectively, which order number of coefficients matrix are d_l series assigned to? To reply this question, we need to look at expressions of DIFF_2, DIFF_3, DIFF_4, etc. in Table A.1. As seen in Table A.1, while these expressions proceed like 7, 9, 11, ... in form of chain, increase quantities of differences equal to each other. Namely, constant number "2" =11-9 = 9-7=2 is the same as been in 100 layered reservoir problem too. This "2" numerical value which can be defined as an increase quantity of differences gives coefficient of function used to calculate which per step can be d_l terms assigned from coefficients matrix respectively. According to this, our step function based on number of layers will be expressed by $2l + X$. If we look at Table 2.2, number X which will give number seven ("7") for $l = 2$, and number of nine ("9") for $l = 3$, is found as a number of three ("3"). Namely, our step interval function is constructed as "$2l + 3$". If we look at the matrix shown by Eq.(A.15) carefully, since e_l and d_l series are located on the same band, e_l series are assigned by the same step quantity as done in d_l from coefficients matrix. However, after final element of d_l series is assigned, subscript j will be equal to l (number of layers). From as this level, value of subscript j will need to be set to zero in order to make e_l series read from Zone 5

in coefficients matrix. We can show assignment of element into Zones 1 and 5 in the coefficients matrix explicitly by given below algorithm :

```
Counter=0
   Counter_1=0
Do  K=1,(2l+2)^2, 2l+3
      Counter= Counter +1
         If Counter ≤ l      Then
              A(K)=d(Counter)
                    Else
       Counter_1= Counter_1+1
         If Counter_1 ≤ l    Then
              A(K)=e(Counter_1)
                    Else
                    Goto 10
                    Endif
              Endif
      Enddo
10    Continue
```

A.2 Assignment of Elements in Zones 2 and 4

When we look at the coefficient matrix Eq.(A.15), elements in Zones 2 and 4 have the same step increase function as elements in Zones 1 and 5, even if initial locations of elements are different, because elements in Zones 2 and 4 are located on diagonal bands which have the same slope, as elements in Zones 1 and 5. What we only need to do here, derives formulations which gives initial order values of series in Zones 2 and 4 in terms of number of layers.

Table A.2a Assignment plan of elements in zone 2.

For l=1		**For l=2**		**For l=3**		**For l=4**	
A(i)	**b(j)**	**A(i)**	**b(j)**	**A(i)**	**b(j)**	**A(i)**	**b(j)**
i=2	j=1	**i=3** ↓	j=1	**i=4** ↓	j=1	**i=5** ↓	j=1
		i=10 ↓	j=2	i=13 ↓	j=2	i=16 ↓	j=2
				i=22 ↓	j=3	i=27 ↓	j=3
						i=33 ↓	j=4

As seen in Table A.2a, we need to begin assigning elements by initial step "$l+1$" in Zone 2 for each layer. If we note to the differences of subscripts in direction of arrows in Table A.2a, we can see that they equal to "$2l+3$" like that in Zones 1 and 5. This expression ("$2l+3$") also denotes step length. To understand

and derive assignment procedure of elements in Zone 4, we need to look at Table A.2b given below :

Table A.2b Assignment plan of elements in zone 4.

l =1 için		l =2 için		l =3 için		l =4 için	
A(i)	b(j)	A(i)	b(j)	A(i)	b(j)	A(i)	b(j)
i=5	j=1	**i=13**	j=1	**i=25**	j=1	**i=41**	j=1
		i=20	j=2	i=34	j=2	i=52	j=2
				i=43	j=3	i=63	j=3
						i=74	j=4

If we look at carefully differences of initial element subscripts in Zone 4 and Zone 2, it has been seen to proceed as a chain in form of $5-2=3$, $13-3=10$, $25-4=21$ and $41-5=36$, etc. If we look at difference of differences, we can see that they grow up by increases like 7, 11, 15, 19, ... If we look at increase quantities of these increases, we can reach to constant value "4" which means that initial value of elements in Zones 4 and 2 can be related to number of layers ("l").

Looking at Table A.2a and A.2b, differences between initial elements of series or bands in both Zones 2 and 4, can be seen as 3, 10, 24, 36, in turn by increasing number of layers. Namely, while number of layers equals to 1 ("$l=1$"), difference of order numbers of initial elements of diagonal bands in Zones 2 and 4 of the coefficients matrix, equals to three (3, for $l=1$), ten (10, for $l=2$), twenty-four (24, for $l=3$), thirty-six (36, for $l=4$) and so on. Mathematical expression of this relationship appears to be "$2l^2+l$". While elements in Zone 2 are assigned by order number of "$l+1$", elements in Zone 4 are assigned too by order number of "$l+1+\left(2l^2+l\right)$" from the coefficients matrix.

Elements in Zones 2 and 4, are assigned briefly and clearly by using algorithm given below :

```
Counter_2=0
Do K=l+1, (2l+2)^2, 2l+3
        Counter_2=Counter_2+1
        If Counter_2 ≤ l    Then
                A(K)=b(Counter_2)
                A(K+(2l^2+l))=b(Counter_2)
```

```
            Else
                Goto 20
            Endif
        Enddo
    20 Continue
```

A.3 Assignment of Elements in Zone 3

If we again look at the coefficient matrix Eq.(A.15), all elements which we need to assign from Zone 3, equal to one ("1"). (Note ; since zeros are firstly assigned from the coefficient matrix, we don't make them read second times). If correlation logic used for assigning elements of Zones 1, 2, 3 and 4 is performed in the same manner, whatever number of layers equals to any number, elements (e.g., 1's) in Zone 3 of the coefficient matrix are read easily by using algorithm given below :

```
        Counter_3=0
        Do  K=2l+1, (2l+2)^2, 2l+2
            Counter_3= Counter_3+1
                If Counter_3 ≤ l      Then
                    A(K)=1.0
                Else
              Goto 30
            Endif
        Enddo
30      Continue
```

A.4 Assignment of Elements in Zone 6

All elements in Zone 6 of the coefficient matrix Eq.(A.15) are equal to one ("1") as been in Zone 3. If the correlation logic used for assigning elements of Zones 1, 2, 3, and 4, is performed in the same manner, whatever dimensions of the coefficient matrix are, elements (e.g., 1's) in Zone 6 of such a coefficient matrix are read or assigned easily by using algorithm given below :

```
    Counter_4=0
     Do  K=2L^2 + 4L + 2,  (2L + 2)^2, 2L + 2
       Counter_4= Counter_4+1
          If Counter_4 ≤ L      Then
             A(K)=1.0
                Else
             Goto  40
          Endif
       Enddo
40     Continue
```

A.5 Assignment of Elements in Zones 7 and 8

If we again look at the coefficient matrix Eq.(A.15), all elements in Zones 7 and 8 are equal to one ("1"). To make computer program read elements in Zones 7 and 8, by using assignment logic of elements in other zones of the coefficient matrix, algorithms given below can be used easily :

```
      Counter_5=0
      Do  K= 4l^2 + 4l + 1, (2l + 2)^2, 1
          Counter_5= Counter_5+1
              If Counter_5 ≤ l    Then
                 A(K)=1.0
                   Else
                Goto  50
              Endif
          Enddo
   50 Continue
```

Assign from Zone 7

```
      .....
      Counter_6=0
      Do  K=4l^2 + 7l + 3, (2l + 2)^2, 1
          Counter_6= Counter_6+1
              If Counter_6 ≤ l    Then
                 A(K)=1.0
                   Else
                Goto  60
              Endif
          Enddo
   60 Continue
```

Assign from Zone 8

A.6 Assignment of Elements in Zone 9

In this zone, there are two variables which we need to assign. One of these f_2 is always read from order number which equals to number of all elements into the coefficients matrix, but other of these variables, f_1 is always read from order number which equals to number less as much as $2l+3$ from number of all elements into the coefficient matrix. We can express this in the simple form as given below :

$$A\left((2l+2)^2\right)= f_2$$

$$A\left((2l+2)^2-(2l+3)\right)= f_1$$

Thus, we have achieved that elements on the diagonal and horizontal bands into the coefficients matrix are assigned in the series form.

Now, let's make right hand-side vector in Table 2.1 denoted by $\vec{b}$ read and we need to assign variables into this vector to one series as defined by D(I). This process can be done extremely easily as given below :

Do K=1, l
D(K)=$c_a(K)$! Equation (A.6)
Enddo
Do K=l+1, 2l
D(K)=$c_o(K)$! Equation (A.7)
Enddo

$$D(2l+1) = q_{as}(t) + g_1$$
$$D(2l+2) = q_{os}(t) + g_2$$

Having been read all data in matrix mentioned above in series form, GBAND matrix solver [42] algorithm was used to solve this problem in forward mode.

APPENDIX B

B.1 Comparison, Accuracy and Time Efficiency Analysis

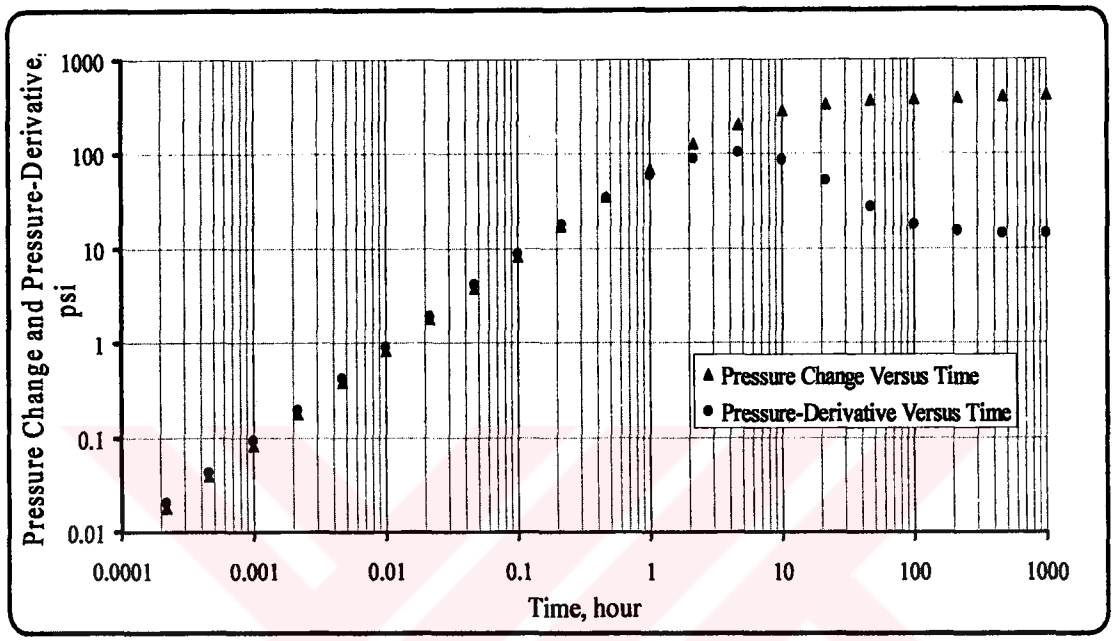

Figure B.1 Pressure change and pressure-derivative versus time at the active well which consists of 3 points on each log cycle.

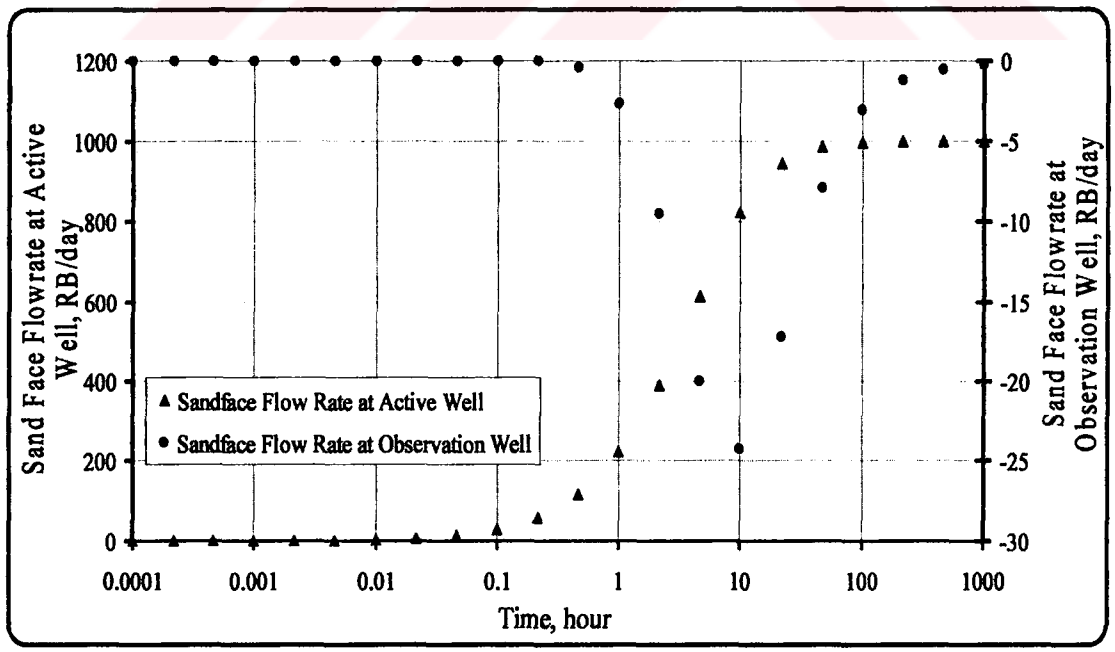

Figure B.2 Sandface flow rates versus time at both wells which consists of 3 points on each log cycle.

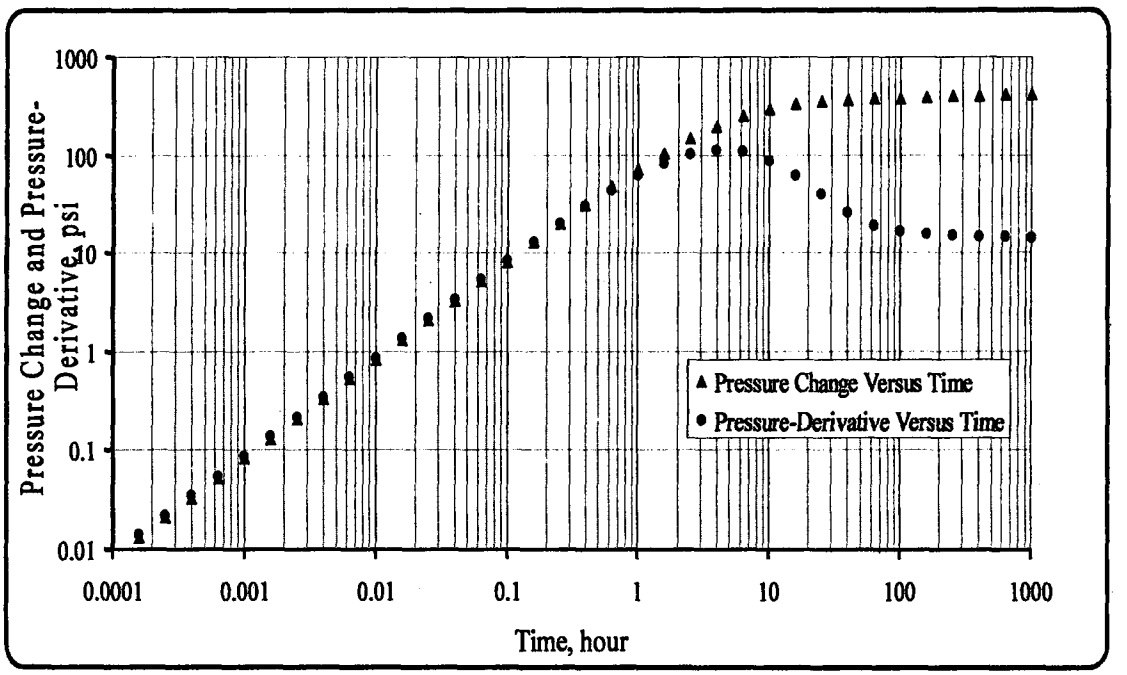

Figure B.3 Pressure change and pressure-derivative versus time at the active well which consists of 5 points on each log cycle.

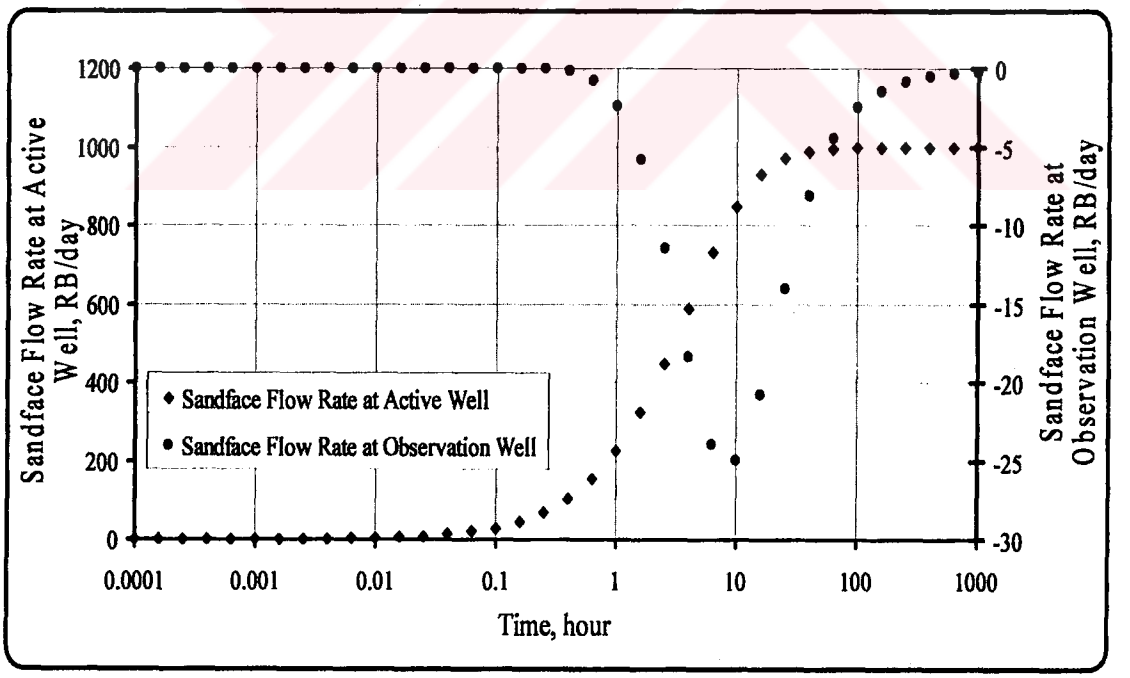

Figure B.4 Sandface flow rates versus time at both wells which consists of 5 points on each log cycle.

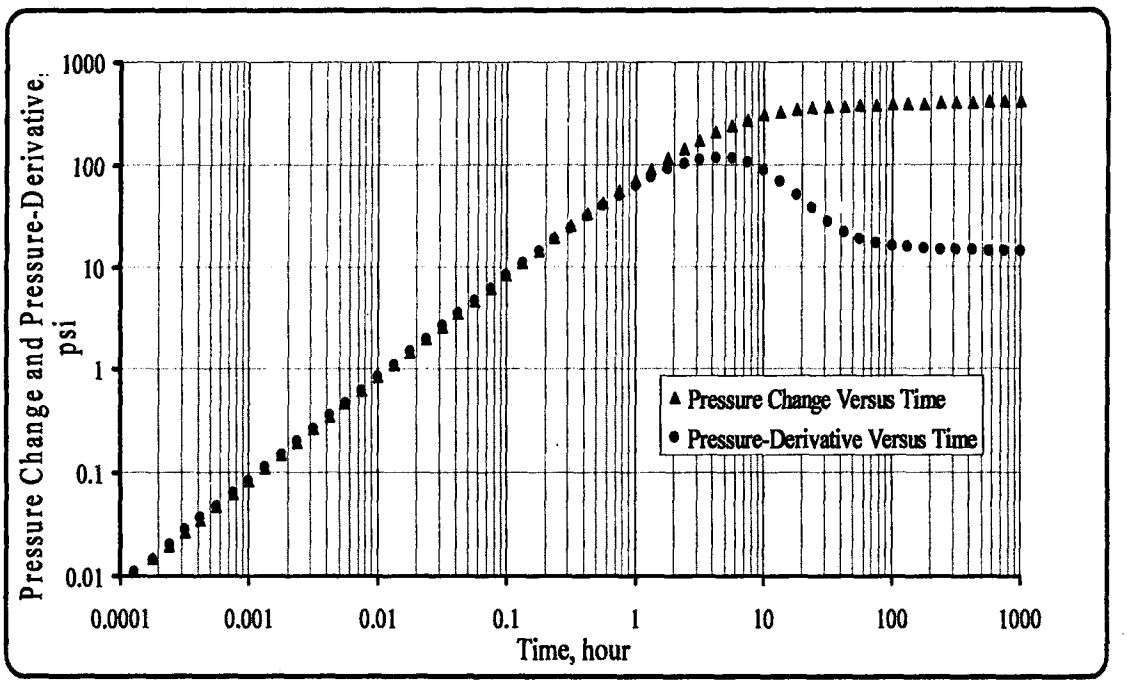

Figure B.5 Pressure changes and pressure-derivative versus time at the active well which consists of 8 points on each log cycle.

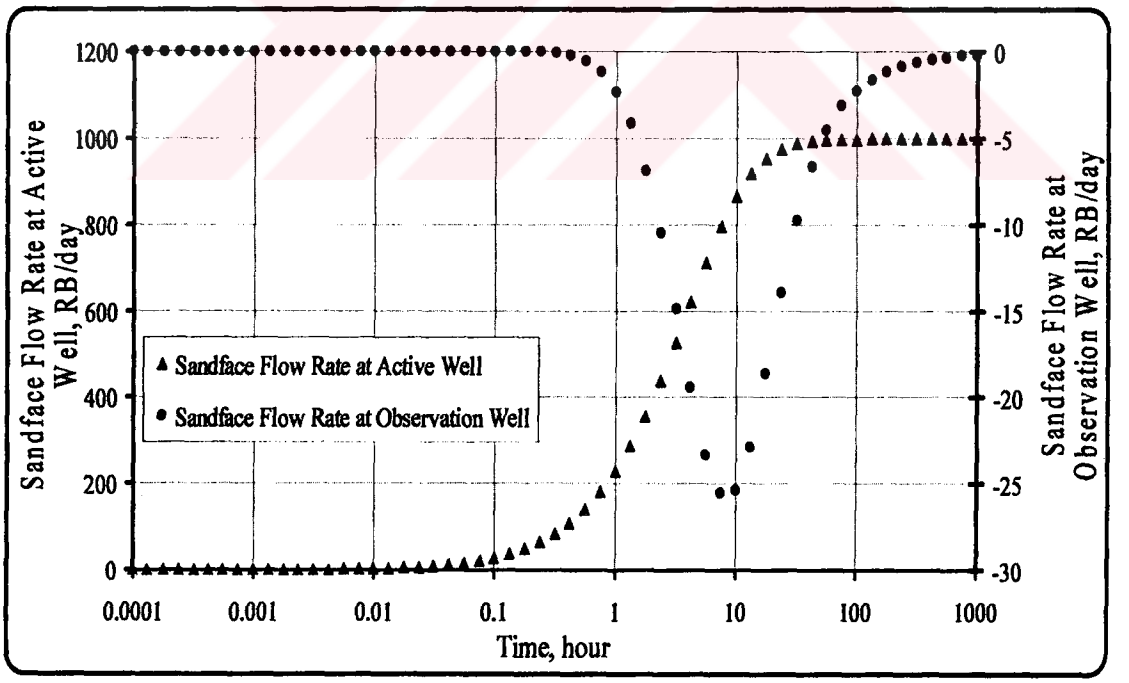

Figure B.6 Sandface flow rates versus time at both wells which consists of 8 points on each log cycle.

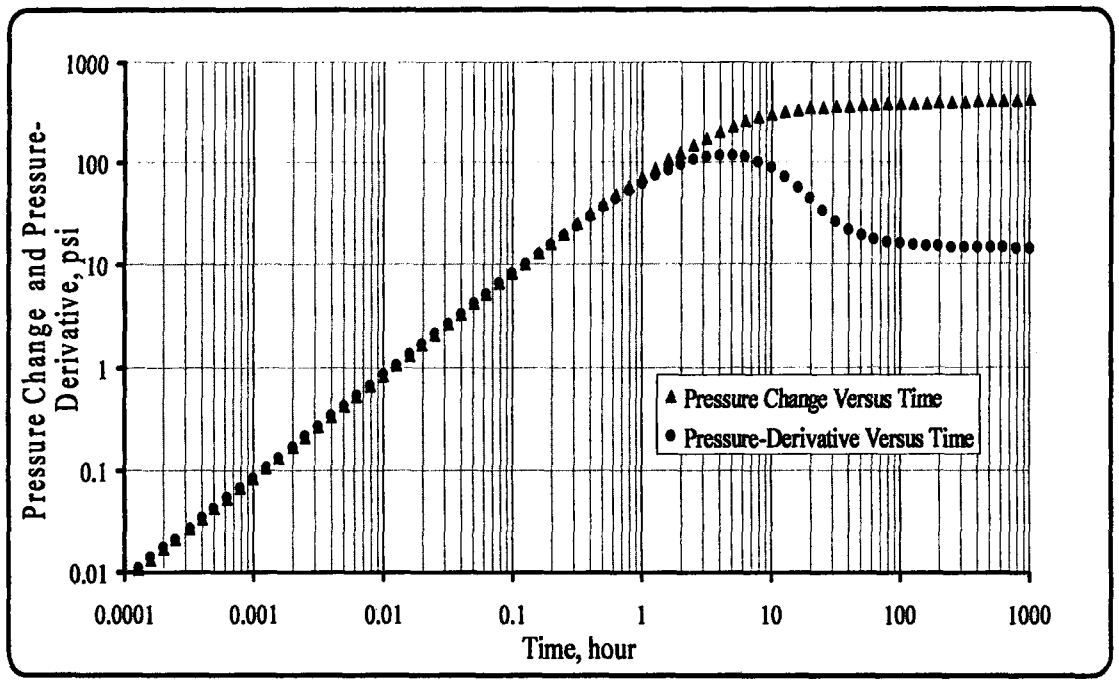

Figure B.7 Pressure change and pressure-derivative versus time at the active well which consists of 10 points on each log cycle.

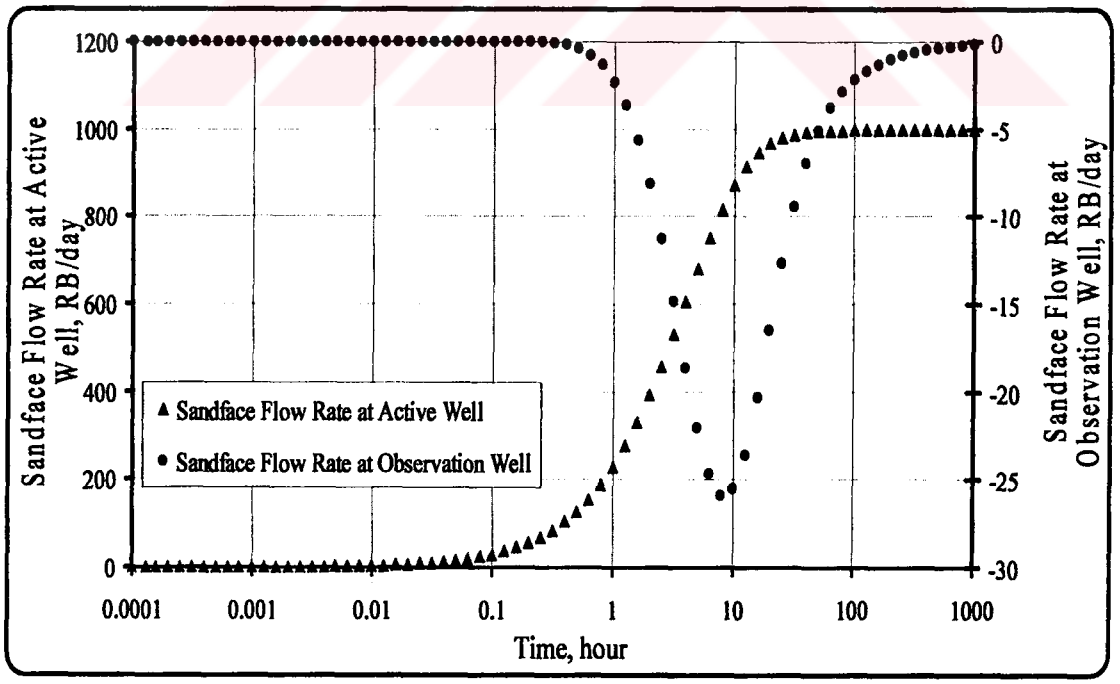

Figure B.8 Sandface flow rates versus time at both wells which consists of 10 points on each log cycle.

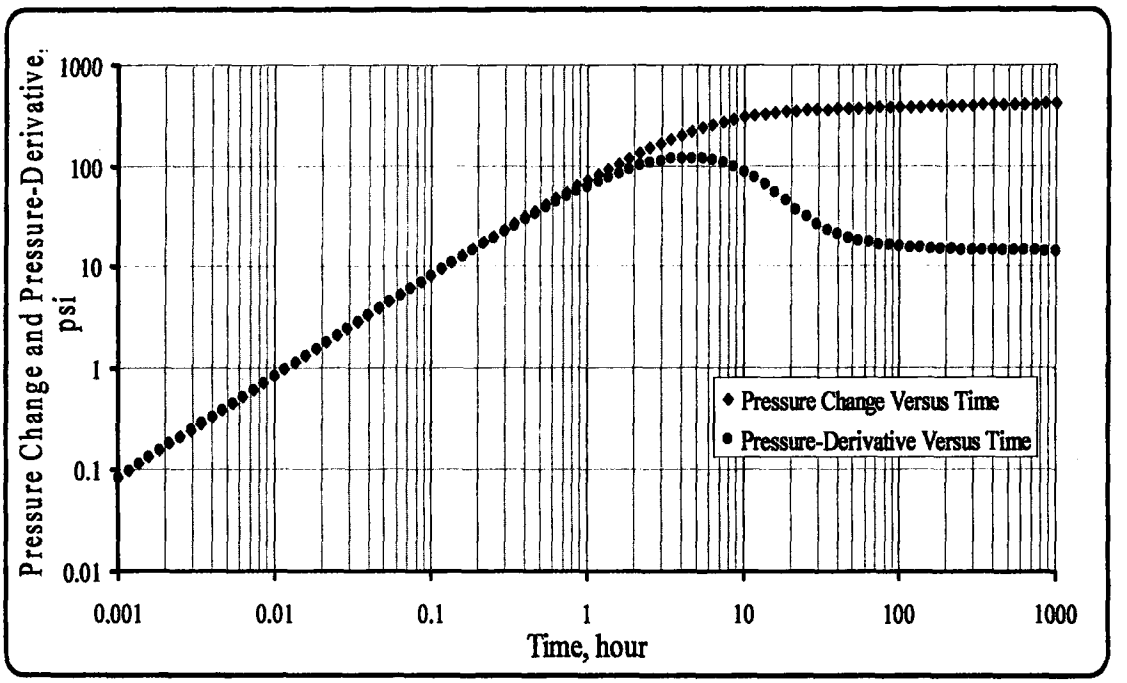

Figure B.9 Pressure change and pressure-derivative versus time at the active well which consists of 15 points on each log cycle.

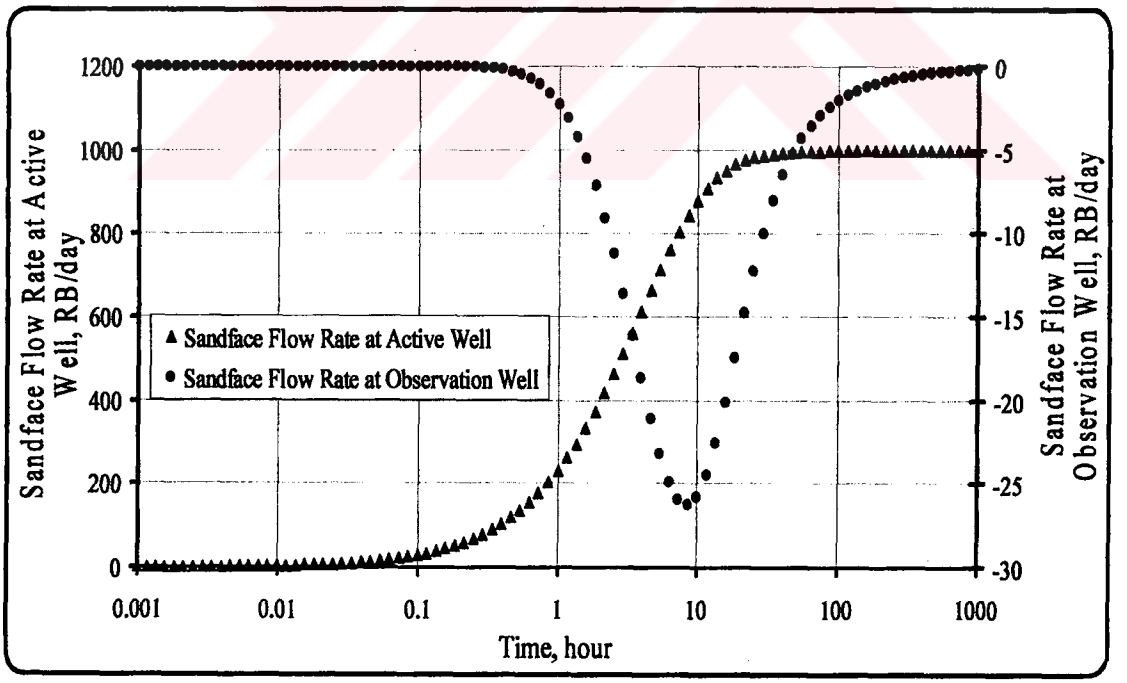

Figure B.10 Sandface flow rates versus time at both wells which consists of 15 points on each log cycle.

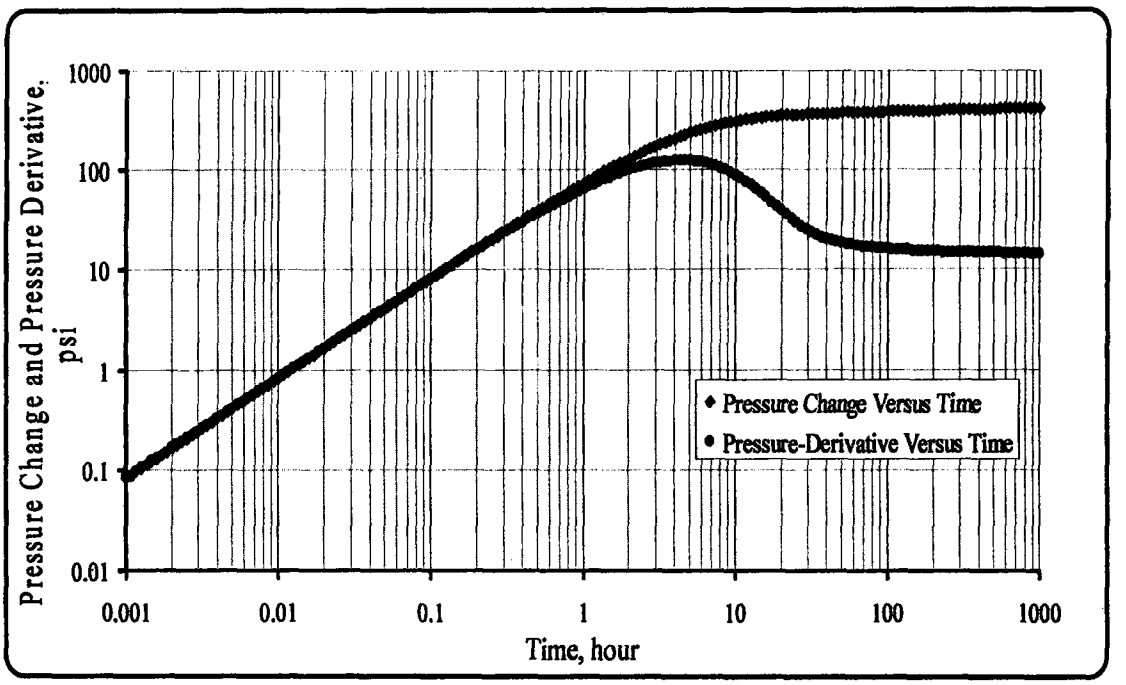

Figure B.11 Pressure change and pressure-derivative versus time at the active well which consists of 30 points on each log cycle.

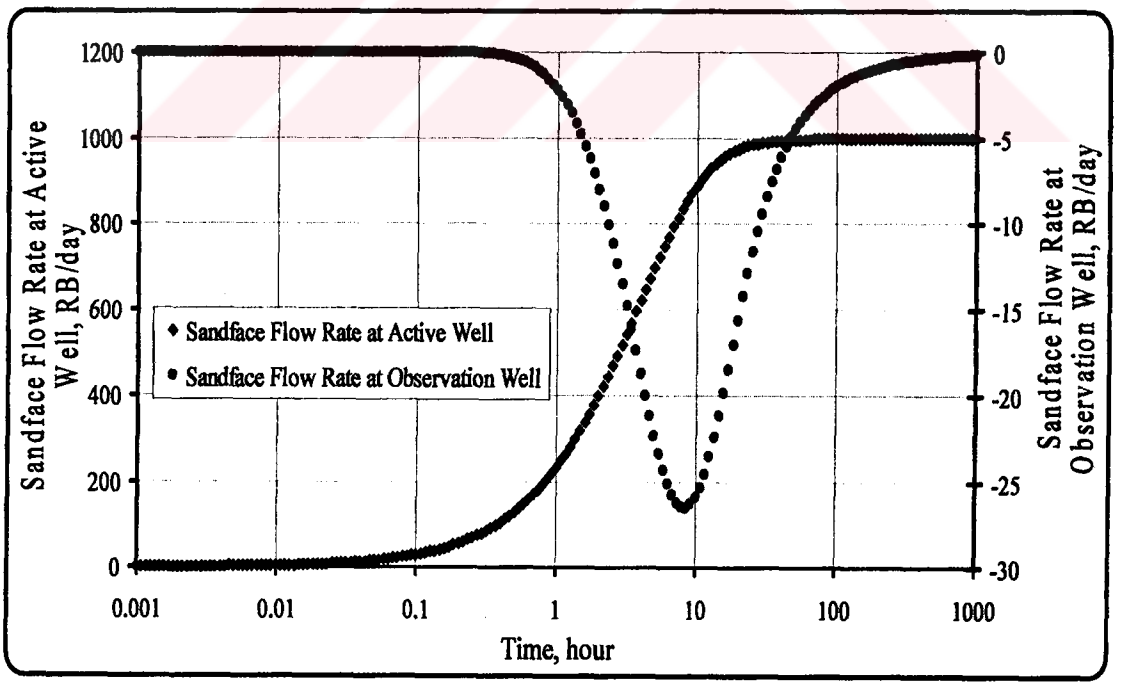

Figure B.12 Sandface flow rates versus time at both wells which consists of 30 points on each log cycle.

Table B.1a Comparison of analytical and numerical solutions; dimensionless layer rate q_{Do2}. ($f_r = 1.0$, $\eta_r = 100$, $r_D = 1000$ *and* $s_{a1} = s_{a2} = s_{o1} = s_{o2} = 0$)

	Onur's Analytical	**This Study**
t_D/r_D^2	q_{Do2}	q_{Do2} (N=10)
0.01	0.0105	0.00976
0.05	0.029757	0.02892
0.08	0.035649	0.03505
0.1	0.038393	0.03792
0.5	0.052672	0.05246
0.7	0.053661	0.05358
1	0.054005	0.05402
2	0.053189	0.05336
6	0.049947	0.05025
10	0.048194	0.04843
20	0.04583	0.04606
50	0.04289	0.04311
80	0.041491	0.04166
100	0.040853	0.04098

Table B.1b Comparison of analytical and numerical solutions in terms of number of time points on each log cycle; dimensionless layer rate q_{Do2}.
($f_r = 1.0$, $\eta_r = 100$, $r_D = 1000$ *and* $s_{a1} = s_{a2} = s_{o1} = s_{o2} = 0$)

This Study % Deviation (N=10)	**This Study % Deviation (N=20)**	**This Study % Deviation (N=30)**	**This Study % Deviation (N=50)**
7.0476	**1.581**	1.173	**0.781**
2.8128	**0.607**	0.451	**0.298**
1.6803	**0.495**	0.372	**0.257**
1.2320	**0.453**	0.344	**0.242**
0.4025	**0.051**	0.030	**0.011**
0.1509	**0.005**	0.000	**0.004**
0.0278	**0.031**	0.022	**0.013**
0.3215	**0.088**	0.060	**0.036**
0.6066	**0.136**	0.098	**0.063**
0.4897	**0.139**	0.100	**0.064**
0.5019	**0.135**	0.096	**0.061**
0.5129	**0.126**	0.092	**0.059**
0.4073	**0.119**	0.085	**0.056**
0.3109	**0.115**	0.083	**0.054**

Table B.2a Comparison of analytical and numerical solutions; dimensionless pressure drop $P_{wD.}$ ($f_r = 1.0$, $\eta_r = 100$, $r_D = 1000$ *and* $s_{a1} = s_{a2} = s_{o1} = s_{o2} = 0$)

	Onur's Analytical	**This Study**
t_D/r_D^2	P_{wD}	P_{wD} (N=10)
0.01	5.594	5.58944
0.05	6.4084	6.40426
0.08	6.6414	6.63704
0.1	6.7502	6.74669
0.5	7.5262	7.52285
0.7	7.6913	7.68944
1	7.8689	7.86779
2	8.221	8.21958
6	8.7861	8.78508
10	9.0502	9.04932
20	9.4082	9.40727
50	9.8802	9.87927
80	10.122	10.12103
100	10.236	10.23573

Table B.2b Comparison of analytical and numerical solutions in terms of number of time points on each log cycle; dimensionless pressure drop, P_{wD}

($f_r = 1.0$, $\eta_r = 100$, $r_D = 1000$ *and* $s_{a1} = s_{a2} = s_{o1} = s_{o2} = 0$)

This Study % Deviation (N=10)	**This Study % Deviation (N=20)**	**This Study % Deviation (N=30)**	**This Study % Deviation (N=50)**
7.0476	**1.581**	1.173	**0.781**
2.8128	**0.607**	0.451	**0.298**
1.6803	**0.495**	0.372	**0.257**
1.2320	**0.453**	0.344	**0.242**
0.4025	**0.051**	0.030	**0.011**
0.1509	**0.005**	0.000	**0.004**
0.0278	**0.031**	0.022	**0.013**
0.3215	**0.088**	0.060	**0.036**
0.6066	**0.136**	0.098	**0.063**
0.4897	**0.139**	0.100	**0.064**
0.5019	**0.135**	0.096	**0.061**
0.5129	**0.126**	0.092	**0.059**
0.4073	**0.119**	0.085	**0.056**
0.3109	**0.115**	0.083	**0.054**

Table B.3a Comparison of analytical and numerical solutions; dimensionless pressure drop $P_{OD.}$ ($f_r = 1.0$, $\eta_r = 100$, $r_D = 1000$ *and* $s_{a1} = s_{a2} = s_{o1} = s_{o2} = 0$)

	Onur's Analytical	**This Study**
t_D/r_D^2	P_{OD}	P_{OD} (N=10)
0.01	0.086441	0.09108
0.05	0.30682	0.31232
0.08	0.38744	0.39169
0.1	0.42783	0.43119
0.5	0.81452	0.81796
0.7	0.93126	0.93334
1	1.0692	1.0705
2	1.37	1.37029
6	1.8985	1.89767
10	2.1546	2.15387
20	2.5065	2.50571
50	2.9748	2.97401
80	3.2155	3.21484
100	3.3297	3.32923

Table B.3b Comparison of analytical and numerical solutions in terms of number of time points on each log cycle; dimensionless pressure drop, $P_{OD.}$

($f_r = 1.0$, $\eta_r = 100$, $r_D = 1000$ *and* $s_{a1} = s_{a2} = s_{o1} = s_{o2} = 0$)

This Study % Deviation (N=10)	**This Study % Deviation (N=20)**	**This Study % Deviation (N=30)**	**This Study % Deviation (N=50)**
5.367	**0.575**	0.415	**0.278**
1.793	**0.246**	0.170	**0.110**
1.097	**0.237**	0.173	**0.119**
0.785	**0.202**	0.142	**0.093**
0.422	**0.076**	0.052	**0.032**
0.223	**0.060**	0.043	**0.028**
0.122	**0.040**	0.028	**0.019**
0.021	**0.008**	0.005	**0.002**
0.044	**0.004**	0.002	**0.000**
0.034	**0.004**	0.002	**0.000**
0.032	**0.004**	0.002	**0.000**
0.027	**0.002**	0.001	**0.002**
0.021	**0.005**	0.003	**0.001**
0.014	**0.003**	0.002	**0.000**

Table B.4a Comparison of analytical and numerical solutions; dimensionless layer rate q_{Da2}. ($f_r = 1.0$, $\eta_r = 100$, $r_D = 1000$ *and* $s_{a1} = 5$, $s_{a2} = 20$, $s_{o1} = 2$, $s_{o2} = 10$)

	Onur's Analytical	**This Study**
t_D/r_D^2	q_{Da2}	q_{Da2} (N=10)
0.01	0.32692	0.32666
0.05	0.33371	0.33351
0.08	0.3355	0.33532
0.1	0.33629	0.33614
0.5	0.34126	0.34107
0.7	0.34215	0.342
1	0.34303	0.34291
2	0.34459	0.34449
6	0.34679	0.34669
10	0.34772	0.34764
20	0.3489	0.34884
50	0.35036	0.35029
80	0.35106	0.35101
100	0.35138	0.35134

Table B.4b Comparison of analytical and numerical solutions in terms of number of time points on each log cycle; dimensionless layer rate q_{Da2}.
($f_r = 1.0$, $\eta_r = 100$, $r_D = 1000$ *and* $s_{a1} = 5$, $s_{a2} = 20$, $s_{o1} = 2$, $s_{o2} = 10$)

This Study % Deviation (N=10)	**This Study % Deviation (N=20)**	**This Study % Deviation (N=30)**	**This Study % Deviation (N=50)**
0.080	**0.009**	0.008	**0.006**
0.060	**0.003**	0.007	**0.010**
0.054	**0.010**	0.008	**0.005**
0.045	**0.012**	0.009	**0.006**
0.056	**0.008**	0.006	**0.003**
0.044	**0.009**	0.007	**0.005**
0.035	**0.009**	0.006	**0.004**
0.029	**0.004**	0.003	**0.002**
0.029	**0.008**	0.005	**0.003**
0.023	**0.006**	0.005	**0.003**
0.017	**0.005**	0.003	**0.001**
0.020	**0.004**	0.004	**0.002**
0.014	**0.006**	0.003	**0.002**
0.011	**0.003**	0.002	**0.001**

Table B.5a Comparison of analytical and numerical solutions; dimensionless layer rate q_{Do2}. ($f_r = 1.0$, $\eta_r = 100$, $r_D = 1000$ *and* $s_{a1} = 5$, $s_{a2} = 20$, $s_{o1} = 2$, $s_{o2} = 10$)

	Onur's Analytical	**This Study**
t_D/r_D^2	q_{Do2}	q_{Do2} (N=10)
0.01	0.0088277	0.00806
0.05	0.024916	0.02435
0.08	0.030038	0.02962
0.1	0.032448	0.03211
0.5	0.047639	0.04723
0.7	0.05	0.04971
1	0.052179	0.05196
2	0.055632	0.05545
6	0.05973	0.05957
10	0.061296	0.06118
20	0.063209	0.0631
50	0.065475	0.06538
80	0.066549	0.06647
100	0.067041	0.06698

Table B.5b Comparison of analytical and numerical solutions in terms of number of time points on each log cycle; dimensionless layer rate q_{Do2}.

($f_r = 1.0$, $\eta_r = 100$, $r_D = 1000$ *and* $s_{a1} = 5$, $s_{a2} = 20$, $s_{o1} = 2$, $s_{o2} = 10$)

This Study % Deviation (N=10)	**This Study % Deviation (N=20)**	**This Study % Deviation (N=30)**	**This Study % Deviation (N=50)**
8.696	**4.284**	4.020	**3.814**
2.272	**0.411**	0.289	**0.187**
1.392	**0.337**	0.246	**0.163**
1.042	**0.335**	0.235	**0.154**
0.859	**0.142**	0.105	**0.065**
0.580	**0.128**	0.090	**0.058**
0.420	**0.114**	0.081	**0.052**
0.327	**0.094**	0.062	**0.041**
0.268	**0.061**	0.042	**0.028**
0.189	**0.059**	0.038	**0.024**
0.172	**0.052**	0.033	**0.020**
0.145	**0.032**	0.027	**0.018**
0.119	**0.034**	0.026	**0.017**
0.091	**0.032**	0.024	**0.016**

Table B.6a Comparison of analytical and numerical solutions; dimensionless pressure drop P_{wD}.

($f_r = 1.0$, $\eta_r = 100$, $r_D = 1000$ *and* $s_{a1} = 5$, $s_{a2} = 20$, $s_{o1} = 2$, $s_{o2} = 10$)

	Onur's Analytical	**This Study**
t_D/r_D^2	P_{wD}	P_{wD} (N=10)
0.01	16.121	16.11615
0.05	16.994	16.98949
0.08	17.243	17.23786
0.1	17.359	17.35464
0.5	18.174	18.16857
0.7	18.343	18.33968
1	18.523	18.52069
2	18.876	18.87338
6	19.438	19.43653
10	19.7	19.69942
20	20.057	20.05596
50	20.528	20.52692
80	20.769	20.76836
100	20.883	20.88296

Table B.6b Comparison of analytical and numerical solutions in terms of number of time points on each log cycle; dimensionless pressure drop, P_{wD}

($f_r = 1.0$, $\eta_r = 100$, $r_D = 1000$ *and* $s_{a1} = 5$, $s_{a2} = 20$, $s_{o1} = 2$, $s_{o2} = 10$)

This Study % Deviation (N=10)	**This Study % Deviation (N=20)**	**This Study % Deviation (N=30)**	**This Study % Deviation (N=50)**
0.030	**0.003**	0.003	**0.002**
0.027	**0.011**	0.012	**0.014**
0.030	**0.004**	0.002	**0.000**
0.025	**0.006**	0.004	**0.002**
0.030	**0.004**	0.003	**0.001**
0.018	**0.003**	0.001	**0.000**
0.012	**0.002**	0.001	**0.000**
0.014	**0.006**	0.006	**0.005**
0.008	**0.002**	0.002	**0.001**
0.003	**0.000**	0.001	**0.001**
0.005	**0.003**	0.002	**0.002**
0.005	**0.003**	0.003	**0.003**
0.003	**0.001**	0.001	**0.001**
0.000	**0.001**	0.001	**0.001**

Table B.7a Comparison of analytical and numerical solutions; dimensionless pressure drop $P_{OD.}$

($f_r = 1.0,\ \eta_r = 100,\ r_D = 1000$ *and* $s_{a1} = 5,\ s_{a2} = 20,\ s_{o1} = 2,\ s_{o2} = 10$)

	Onur's Analytical	**This Study**
t_D/r_D^2	P_{OD}	P_{OD} (N=10)
0.01	0.24065	0.23641
0.05	0.75486	0.7499
0.08	0.92682	0.92318
0.1	1.0099	1.00697
0.5	1.6446	1.64127
0.7	1.7907	1.78847
1	1.9513	1.94965
2	2.2773	2.27601
6	2.8178	2.81686
10	3.0743	3.07361
20	3.4246	3.42409
50	3.8896	3.8892
80	4.1285	4.12814
100	4.2419	4.24161

Table B.7b Comparison of analytical and numerical solutions in terms of number of time points on each log cycle; dimensionless pressure drop, $P_{OD.}$

($f_r = 1.0,\ \eta_r = 100,\ r_D = 1000$ *and* $s_{a1} = 5,\ s_{a2} = 20,\ s_{o1} = 2,\ s_{o2} = 10$)

This Study % Deviation (N=10)	**This Study % Deviation (N=20)**	**This Study % Deviation (N=30)**	**This Study % Deviation (N=50)**
1.762	**0.216**	0.162	**0.109**
0.657	**0.092**	0.064	**0.037**
0.393	**0.076**	0.051	**0.029**
0.290	**0.075**	0.053	**0.032**
0.202	**0.037**	0.027	**0.016**
0.125	**0.030**	0.022	**0.014**
0.085	**0.025**	0.018	**0.012**
0.057	**0.016**	0.012	**0.008**
0.033	**0.009**	0.007	**0.005**
0.022	**0.008**	0.007	**0.005**
0.015	**0.004**	0.004	**0.002**
0.010	**0.002**	0.001	**0.000**
0.009	**0.003**	0.002	**0.002**
0.007	**0.003**	0.002	**0.001**

B.2 Case Study Over Examining of CPU Time of GBAND Matrix Solver

Table B.8 CPU time of GBAND matrix solver to compute pressure drops and sandface flow rates.

Number of Layer	Dimension of Matrix	Total Termination Time For 101 Time Step	CPU Time of GBAND For Each Time Step (for one time step)
1	(4x4)	0,38 sec	≤ 0.05 sec
5	(12x12)	0,39 sec	0.05 sec
10	(22x22)	0,55 sec	0,05 sec
20	(42x42)	0,88 sec	0,06 sec
30	(62x62)	1.6 sec	0,06 sec
40	(82x82)	2.91 sec	0,06 sec
50	(102x102)	5.49 sec	0,06 sec
100	(202x202)	41,53 sec	0,39 sec
200	(402x402)	339,17 sec	3,73 sec

Numbers in first columns show number of layers of which reservoir forms. Expressions in second columns demonstrate sizes of matrix formed in forward computation. Third column displays computation times of a full well test which consists of 101 times matrix solution. Question marks in last four boxes of third column means that author didn't want to wait any more seening results due to time cost. Fourth columns displays run times per each matrix solution. As seen in Table B.8, huge matrices occured in solving our problems are solved by GBAND matrix solver fastly. Computer used to measure CPU times in Table B.8 had a 128 MB RAM and a Celeron 400 Mhz cpu.

APPENDIX C

Dimensionless Expressions

The dimensionless wellbore pressure drops at both the active well and the interference well (observation well) which is shut-in for all times are defined as

$$p_{wD} = \frac{\overline{kh}\Delta p_{wa}}{141.2q\mu} \qquad \text{C.1}$$

and

$$p_{oD} = \frac{\overline{kh}\Delta p_{wo}}{141.2q\mu} \qquad \text{C.2}$$

In Eqs. C.1-C.2, Δp_{wa} *and* Δp_{wo} denote pressure drops at active and the observation wells respectively. q represents surface flow rate.

The dimensionless times are given by the following equations :

$$t_D = \frac{2.637\times10^{-4}\overline{\eta}t}{r_w^2} \qquad \text{C.3}$$

In Eq. C.3, $\overline{\eta}$ denotes the average diffusivity which is defined by

$$\overline{\eta} = \frac{\overline{k}}{\overline{\phi}\,\overline{c}_t\mu} \qquad \text{C.4}$$

The dimensionless sandface flow rate from layer j at the active well is defined by

$$q_{Daj} = \frac{q_{aj}(t)}{q}, \qquad \text{C.5}$$

where we have used the subscript "a" to denote the active well. The analogous dimensionless sandface rate at the observation well is defined by

$$q_{Doj} = \frac{q_{oj}(t)}{q}, \qquad \text{C.6}$$

where the subscript "o" refers to the observation well. In Eqs. C.5-C.6, $q_{aj}(t)$ and $q_{oj}(t)$ represent sandace flow rates in RB/day from layer j at the active well and the observation well, respectively.

The dimensionless radial distances are defined as

$$r_D = \frac{r}{r_w} \qquad \text{C.7}$$

In Eq. C.5, r represents distance between the active and observation wells and r_w represents radius of the active or observation well.

APPENDIX D

Input Page of The Program Designed In This Study

```
**********************************************************************************
************************** INPUT FILE OF THE PROGRAM ***************************
**********************************************************************************
**********************************************************************************
*                                   CARD1
**********************************************************************************
* NLAYER:  NUMBER OF LAYERS
* VIS :    VISCOSITY OF FLUID, cp
* PERM :   PERMEABILITY OF INDIVIDUAL LAYER, md
* POR :    POROSITY OF INDIVIDUAL LAYER
* CT :     COMPRESSIBILITY OF THE ROCK, 1/psi
* THICK :  THICKNESS OF INDIVIDUAL LAYER, ft
* SKINA :  SKIN FACTOR OF INDIVIDUAL LAYER IN ACTIVE WELL REGION, psi
* SKINO :  SKIN FACTOR OF INDIVIDUAL LAYER IN OBSERVATION WELL REGION, psi
* RWA :    RADIUS OF ACTIVE WELL, ft
* RWO :    RADIUS OF OBSERVATION WELL, ft
* R :      DISTANCE BETWEEN ACTIVE AND OBSERAVTION WELLS, ft
* CA :     WELLBORE STORAGE AT ACTIVE WELL
* CO :     WELLBORE STORAGE AT OBSERVATION WELL
**********************************************************************************
*  L       R        RWA       RWO
**********************************************************************************
   3      350.0       0.35      0.35
**********************************************************************************
**********************************************************************************
* TI : INITIAL TIME VALUE, hour
* TF : FINAL TIME VALUE, hour
* NCYCLE : NUMBER OF TIME VALUES AT EACH LOG CYCLE
* RATEA : CONSTANT FLOWRATE AT ACTIVE WELL ON DIFFERENT SCHEDULES
* RATEO : CONSTANT FLOWRATE AT OBSERVATION WELL ON DIFFERENT SCHEDULES
* INDEX : NUMBER OF SCENARIOS
**********************************************************************************
* INDEX     TI
**********************************************************************************
    2      0.001
**********************************************************************************
*  TF      NCYCLE    RATEA     RATEO
**********************************************************************************
  1000.0     20      1000.0      0.0
  2000.0     20       0.0        0.0
  300.0      5       1000.0      0.0
**********************************************************************************
*                                   CARD2
**********************************************************************************
 ICOMP =====> 0 {Program Works in FORWARD Mode}
                //DUHAMEL Principle//
 ICOMP =====> 1 {Program Works in INVERSE Mode and Sensitivities are Computed}
                //LEVENBERG-MARQUARDT Algorithm is used//
 ICOMP =====> 2 {Program Works in INVERSE Mode and it uses Gradient Free Techniqu
                //SIMULATED ANNEALING Algorithm// [Global Optimizer]
 ICOMP =====> 3 {Program Works in INVERSE Mode and it uses Gradient Free Techniqu
                 //POLYTOPE (Non-Linear Simplex) Algorithm// [Local Optimizer]
```

```
*********************************************************************************
***  ICOMP
      0
*********************************************************************************
* OPTIMIZATION PARAMETERS RELATED TO LEVENBERG-MARQUARDT ALGORITHM
*      TOL          MAXIT
*********************************************************************************
     1.0e-6          1200
*********************************************************************************
* OPTIMIZATION PARAMETERS RELATED TO SIMULATED ANNEALING ALGORITHM
*********************************************************************************
 In this description, SP is single precision, DP is double precision,
 INT is integer, L is logical and (N) denotes an array of length n.
 Thus, DP(N) denotes a double precision array of length n.

   RT - The temperature reduction factor. (DP)
   EPS - Error tolerance for termination. If the final function
         values from the last neps temperatures differ from the
         corresponding value at the current temperature by less than
         EPS and the final function value at the current temperature
         differs from the current optimal function value by less than
         EPS, execution terminates and IER = 0 is returned. (EP)
   NS -  Number of cycles.  After NS*N function evaluations, each element of
         VM is adjusted so that approximately half of all function evaluations
         are accepted.  The suggested value is 20. (INT)
   NT -  Number of iterations before temperature reduction. After
         NT*NS*N function evaluations, temperature (T) is changed
        by the factor RT.  Value suggested by Corana et al. is
        MAX(100, 5*N).  See Goffe et al. for further advice. (INT)
   NEPS - Number of final function values used to decide upon termi-
          nation.  See EPS.  Suggested value is 4. (INT)
   MAXEVL - The maximum number of function evaluations.  If it is
            exceeded, IER = 1. (INT)
   C - Vector that controls the step length adjustment.  The suggested
       value for all elements is 2.0. (DP(N))
   IPRINT - controls printing inside SA. (INT)
            Suggested value: 1
            Note: For a given value of IPRINT, the lower valued
                  options (other than 0) are utilized.
 Input/Output Parameters:
   T - On input, the initial temperature. See Goffe et al. for advice.
       On output, the final temperature. (DP)
   VM - The step length vector. On input it should encompass the region of
        interest given the starting value X.  For point X(I), the next
        trial point is selected is from X(I) - VM(I)  to  X(I) + VM(I).
        Since VM is adjusted so that about half of all points are accepted,
        the input value is not very important (i.e. is the value is off,
        SA adjusts VM to the correct value). (DP(N))

*********************************************************************************
  T     RT     NS     NT     NEPS     EPS      MAXEVL      IPRINT     VM
*********************************************************************************
  500   0.95   20     5      4      1.0d-6   500001      1      1.0
*********************************************************************************
```

```
**********************************************************************************
* OPTIMIZATION PARAMETERS RELATED TO POLYTOPE ALGORITHM
**********************************************************************************
      STOPCR        SIMP        IPRINT      IQUAD       MAXF1    MAXF2
**********************************************************************************
     1.0D-6        1.0D-20        1           0          800      24000
**********************************************************************************
**********************************************************************************
* NDATASET: NUMBER OF DATA SET
* STDDEV(NDATASET) : STANDARD DEVIATION
**********************************************************************************
*    NDATASET      IMATCH
                    3
**********************************************************************************
*    STDDEV(NDATASET)
       2.0e100
       0.5
**********************************************************************************
If the number of layers equals to 1, standard deviations are written in 1 row
If the number of layers equals to 2, standard deviations are written in 2 row
       3.897e100       0.2072
       1.9746e100      0.2055
       5.62048      0.00564
**********************************************************************************

*  in this program, we try to estime 10 parameters
*  if you want to estimate parameters, take IOPT=1....
*  if you want to fix the parameters,  take IOPT=0....
**********************************************************************************
REGRESSION PARAMETERS      (1)  CA (IT TAKES ONLY ONE VALUE FOR ALL RESERVOIR SYST
   IN EACH LAYER           (2)  CO (IT TAKES ONLY ONE VALUE FOR ALL RESERVOIR SYST
                           (3)  PERM
                           (4)  POR
                           (5)  CT
                           (6)  THICK
                           (7)  SKINA
                           (8)  SKINO
                           (9)  VIS
**********************************************************************************
*  PARAMETER  IOPT       XINITIAL     LOWERBOUNDARY      UPPERBOUNDARY
**********************************************************************************
       1      1          0.0              0.0          10.0
       2      1          0.0              0.0          10.0
**********************************************************************************
*                          Properties of Layer 1
**********************************************************************************
       3      1          100.0            0.10         10000.0
       4      1          0.15             0.001        0.50
       5      0          1.0e-5           1.0e-8       1.0
       6      0           50              1.0          1000
       7      1           5.0             1.0e-3       100
       8      1           2.0             1.0e-3       100
       9      0           1.0             0.1          20.0
```

```
*********************************************************************************
*                        Properties of Layer 2
*********************************************************************************
      10      1          50.0            0.1             10000.0
      11      1          0.3             0.001           0.50
      12      0          25.0e-5         1.0e-8          1.0
      13      0          100             1.0             1000
      14      1          20.0            1.0e-3          100
      15      1          10.0            1.0e-3          100
      16      0          1.0             0.1             20.0
*********************************************************************************
*                        Properties of Layer 3
*********************************************************************************
      17      1          163.80            0.1             1000.0
      18      1          0.268             0.001           1.0
      19      0          1.0e-4            1.0e-8          1.0
      20      0          30                1.0             1000
      21      1          7.60              1.0e-3          100
      22      1          87.10             1.0e-3          100
      23      0          1.0               0.1             2.0
*********************************************************************************
*                        Properties of Layer 4
*********************************************************************************
```

.....Properties can be added as much as number of layers .....

AUTOBIOGRAPHY

Author was born in Rize on November 30, 1978. He started to his education life in İyidere in 1983. He graduated from Iyidere High School in 1994. Having joined to Petroleum and Natural Gas Engineering Department of Mining Faculty at ITU in 1996, he graduated from this department in June 2000 as a Petroleum and Natural Gas Engineer by being awarded for graduating ranking first from the B.S. After 1 year from graduation year, he decided continuing to study at master program of the same department of Science and Technology Institute at ITU. He was also charged as a research assistant in Department of Petroleum and Natural Gas Engineering at ITU and he has continued studying presently as a research assistant since 2002.